Titre: Title:	Biomechanical Simulator for the Surgical Correction of Sagittal Balance in Adult Spinal Deformity
Auteur: Author:	David Benoit
Date:	2019
Type:	Mémoire ou thèse / Dissertation or Thesis
Référence: Citation:	Benoit, D. (2019). Biomechanical Simulator for the Surgical Correction of Sagittal Balance in Adult Spinal Deformity [Mémoire de maîtrise, Polytechnique Montréal]. PolyPublie. https://publications.polymtl.ca/3906/

URL de PolyPublie: PolyPublie URL:	https://publications.polymtl.ca/3906/
Directeurs de recherche: Advisors:	Carl-Éric Aubin
Programme: Program:	Génie mécanique

UNIVERSITÉ DE MONTRÉAL

BIOMECHANICAL SIMULATOR FOR THE SURGICAL CORRECTION OF SAGITTAL BALANCE IN ADULT SPINAL DEFORMITY

DAVID BENOIT

DÉPARTEMENT DE GÉNIE MÉCANIQUE

ÉCOLE POLYTECHNIQUE DE MONTRÉAL

MÉMOIRE PRÉSENTÉ EN VUE DE L'OBTENTION

DU DIPLÔME DE MAÎTRISE ÈS SCIENCES APPLIQUÉES

(GÉNIE MÉCANIQUE)

MAI 2019

UNIVERSITÉ DE MONTRÉAL

ÉCOLE POLYTECHNIQUE DE MONTRÉAL

Ce mémoire intitulé :

BIOMECHANICAL SIMULATOR FOR THE SURGICAL CORRECTION OF SAGITTAL BALANCE IN ADULT SPINAL DEFORMITY

présenté par : BENOIT David

en vue de l'obtention du diplôme de : Maîtrise ès sciences appliquées

a été dûment accepté par le jury d'examen constitué de :

Mme VILLEMURE Isabelle, Ph. D., présidente

M. AUBIN Carl-Éric, Ph. D., membre et directeur de recherche

M. DAMMAK Maher, Ph. D., membre

DEDICATION

Another brick in the wall

REMERCIEMENTS

Je voudrais remercier en premier lieu mon directeur de recherche, le professeur Carl-Éric Aubin pour m'avoir donné l'opportunité de réaliser ce projet et d'avoir fait preuve d'une grande pédagogie tout au long de celui-ci. Malgré son énorme implication dans le domaine de la recherche, il aura toujours été disponible pour répondre à mes questions et me guider dans mon projet. Merci de m'avoir fait confiance en me donnant autant d'autonomie dès mon premier stage que j'ai complété dans ce laboratoire, alors que j'étais encore au baccalauréat.

Plusieurs personnes ont contribué à l'accomplissement de ce projet d'une manière ou d'une autre. Merci à Christiane Caouette qui a toujours été disponible pour la résolution de problèmes ou pour l'ajout de modules concernant la création du modèle multi-corps flexible. Ses connaissances avancées en Matlab m'auront aussi beaucoup aidé à réaliser l'interface de planification chirurgicale. Merci à Xiaoyu Wang pour son aide à la présentation des résultats ainsi qu'à la rédaction et la révision de l'article scientifique. Merci aux associés de recherche Nathalie Bourassa pour la grande aide à réaliser les reconstructions 3D de patients et Christian Bellefleur pour l'aide à la résolution de problèmes informatiques. Merci à Jeremy Rawlinson pour les nombreux conseils offerts tout au long du projet ainsi qu'à Maher Dammak pour les commentaires sur l'article scientifique.

Merci à Dr Dennis G. Crandall et Jan Ravela de Sonoran Spine d'avoir collaboré au projet en nous fournissant les radiographies de patients.

Merci au Conseil de Recherches en Sciences Naturelles et en Génie du Canada (CRSNG) et à Medtronic qui ont financé ce projet de recherche.

Un grand merci à tous mes collègues du laboratoire, autant pour le support scientifique que pour le support moral. J'aurai développé de belles amitiés que j'espère garder longtemps. Un merci particulier à Maeva Lopez Poncelas, ma collègue de modélisation multi-corps flexible. J'espère t'avoir aidé autant que tu m'as aidé!

Un énorme merci à ma famille qui aura toujours été là pour me soutenir dans tous les projets que j'entreprends. Elle m'aura permis de m'investir dans mon projet à un point que je n'aurais pas pu atteindre sans sa précieuse aide.

RÉSUMÉ

Pour maintenir une posture érigée minimisant les dépenses énergétiques, l'alignement de la colonne vertébrale dans le plan sagittal est d'une grande importance. Dans le contexte des déformations de la colonne vertébrale chez l'adulte, un mauvais alignement dans le plan sagittal demande une dépense énergétique plus élevée et est associé à la douleur et à une perte de fonction. Le maintien d'une posture érigée dans de telles conditions implique une activation accrue des muscles du tronc et l'utilisation de mécanismes compensatoires pour contrebalancer le débalancement antérieur du haut du corps. L'instrumentation chirurgicale est indiquée chez les patients souffrant de grandes douleurs et de handicaps lorsque les traitements non chirurgicaux ne sont plus suffisants. Cette procédure consiste à insérer des vis dans les pédicules des vertèbres et à redresser la colonne vertébrale à l'aide de tiges métalliques, ce qui conduit à la fusion permanente de la colonne vertébrale. Pour la correction de déformations importantes et manquant de flexibilité dans le plan sagittal, l'ostéotomie de soustraction pédiculaire (OSP) est une procédure souvent utilisée pour rétablir le profil sagittal normal de la colonne lombaire. Cette technique implique la résection des éléments postérieurs de la vertèbre ainsi qu'un coin d'os dans le corps vertébral pour créer une forte angulation de la colonne vertébrale. C'est une procédure très exigeante en raison des risques de complications mécaniques. De nombreux facteurs de risque ayant une incidence sur les taux de complications mécaniques après une instrumentation chirurgicale avec OSP ont été identifiés dans le cadre d'études cliniques. Les patients ayant eu des complications mécaniques avaient reçu une correction significativement plus grande de l'axe vertical sagittal, un cintrage plus grand des tiges dans le plan sagittal et une ostéotomie réalisée à un niveau plus caudal. Il a également été démontré que jusqu'à 40% des patients gardaient un alignement sagittal antérieur après une chirurgie avec OSP et qu'un alignement sagittal non neutre était associé à des taux plus élevés de révision chirurgicale. Même si des objectifs chirurgicaux globaux ont été définis avec la classification SRS-Schwab pour la correction du déséquilibre sagittal, la stratégie chirurgicale optimale spécifique au patient reste mal définie. En outre, malgré les études cliniques et biomécaniques, les relations entre les contraintes mécaniques dans l'instrumentation et les différents paramètres de correction dans le plan sagittal (degré de correction sagittale par variation de l'angle de l'OSP et de l'angle de cintrage des tiges, niveau vertébral de l'OSP et nombre de tiges) sont encore mal comprises. Les connaissances biomécaniques sur les facteurs de risque et leurs effets sur les complications mécaniques liées aux OSP telles que le bris des tiges sont encore

limitées et une meilleure compréhension de l'impact biomécanique des OSP pourrait être un excellent outil pour aider les chirurgiens dans leur planification préopératoire de la correction du déséquilibre sagittal.

Ce projet vise donc à répondre à la question de recherche suivante : « *Comment l'angle de résection de l'OSP, le cintrage des tiges, le niveau vertébral de l'OSP et le nombre de tiges impactent-ils biomécaniquement la correction de l'équilibre sagittal et les forces dans l'instrumentation, et comment doivent-ils être ajustés pour réduire les risques de défaillance mécanique dans le contexte des difformités de la colonne vertébrale chez l'adulte?* »

Pour répondre à la question de recherche, les objectifs suivants ont été définis :

- Développer un modèle biomécanique multi-corps personnalisé de la colonne vertébrale intégré dans une plateforme de simulation pour simuler la correction chirurgicale de l'équilibre sagittal chez l'adulte;
- Exploiter le modèle biomécanique pour évaluer les effets des paramètres de la correction dans le plan sagittal sur la distribution des forces et des moments dans la colonne vertébrale et l'instrumentation.

Un modèle biomécanique multi-corps flexible de la colonne vertébrale spécifique au patient a été développé pour simuler la chirurgie d'instrumentation avec OSP pour la correction des déformations dans le plan sagittal chez l'adulte. Les vertèbres et le bassin étaient considérés comme des corps rigides. Ceux-ci étaient reliés par des ressorts à 6 dimensions représentant les disques intervertébraux, les ligaments et les facettes dont les propriétés mécaniques étaient issues de la littérature. Les vis pédiculaires, les tiges et les manœuvres chirurgicales ont finalement été modélisées pour chaque cas.

Le modèle biomécanique a ensuite été intégré à une plateforme de simulation. Cette plateforme de simulation permet de définir graphiquement les principales étapes de la planification chirurgicale telles que différentes configurations d'ostéotomies et de paramètres d'instrumentation. Plusieurs scénarios chirurgicaux ont été simulés afin de comparer relativement les différentes stratégies en termes de correction géométrique et des efforts dans la colonne instrumentée.

Enfin, le modèle biomécanique et la plateforme de simulation ont été utilisés pour simuler les chirurgies d'instrumentation de trois patients adultes ayant un déséquilibre sagittal fixe avec OSP

dans la région lombaire. L'instrumentation réelle a été simulée pour vérifier le modèle, puis trois paramètres ont été simulés en alternance : la quantité de correction sagittale en variant l'angle de résection de l'OSP et l'angle de cintrage des tiges (± 7.5°), le niveau vertébral de l'OSP (± 1 niveau) ainsi que le nombre de tiges (2 vs 4). Les différents scénarios chirurgicaux ont ensuite été comparés sur la base de trois variables biomécaniques : forces axiales dans les vis pédiculaires, moments de flexion dans les tiges et les forces de compression vertébrale. Ces variables ont été plus spécifiquement étudiées près du niveau de l'OSP, où la plupart des complications mécaniques sont rapportées.

Dans les trois cas, la différence maximale entre l'instrumentation chirurgicale simulée et réelle était inférieure à 4° pour les courbes sagittales et coronales et inférieure à 8 mm pour la distance de l'axe vertical sagittal (SVA), valeurs inférieures ou égales au seuil défini par la variabilité intra et inter-observateur. L'augmentation (ou la diminution) de l'angle de résection de l'OSP de 7.5°, concomitamment au cintrage des tiges, a modifié la force axiale moyenne dans les vis de + 38% (-19%) et les moments de flexion des tiges de + 28% (-11%) autour de l'OSP, respectivement. Les moments de flexion dans les tiges étaient inférieurs de 31% au site de l'OSP pour une OSP performée à un niveau supérieur et de 20% supérieurs pour l'OSP à un niveau inférieur. L'ajout de tiges satellites a diminué les moments de flexion dans les tiges de 24% au niveau de l'OSP et les forces axiales moyennes dans les vis de 22% autour de l'OSP. Pour tous les paramètres étudiés, aucune tendance particulière n'a été trouvée pour les forces de compression vertébrale. Enfin, une étude de sensibilité a été réalisée pour évaluer l'effet sur les résultats de cette étude des paramètres dont les valeurs étaient incertaines. L'angle de résection de l'OSP (± 1.5°), la rigidité intervertébrale (± 15%) et la rétroversion pelvienne postopératoire (± 5°) ont été étudiés. La différence de pourcentage relative des efforts dans la colonne vertébrale instrumentée pour différents degrés de correction sagittale a été évaluée pour tous ces paramètres (<6% pour l'angle de résection de l'OSP, <7.8% pour la rigidité intervertébrale et <5% pour la rétroversion pelvienne postopératoire) et il a été constaté que les résultats de cette étude n'étaient pas affectés.

En conclusion, au cours de ce projet de maîtrise, un modèle biomécanique de la colonne vertébrale simulant la chirurgie instrumentée pour la correction de l'alignement sagittal a été développé. Ce modèle biomécanique a ensuite été intégré à une plateforme de simulation afin de planifier les principales étapes de la chirurgie. Enfin, les effets biomécaniques de différents paramètres de correction sagittale et d'instrumentation sur les charges supportées par la colonne vertébrale et

l'instrumentation ont été évalués. Une correction sagittale plus importante grâce à l'angle de résection de l'OSP et au cintrage des tiges a entraîné des forces axiales plus élevées dans les vis et des moments de flexion sagittaux dans les tiges au niveau de l'OSP. L'OSP réalisée à un niveau plus caudal était associée à des moments plus élevés soutenus par les tiges au niveau de l'OSP. L'utilisation d'instrumentation à 4 tiges a permis de réduire les charges exercées sur les vis et les tiges, réduisant ainsi potentiellement les risques de défaillance mécanique. Les connaissances acquises grâce à ce projet peuvent aider à mieux comprendre les différents facteurs de risque de complications mécaniques après une OSP et, éventuellement, aider les chirurgiens dans leur planification préopératoire de la correction du déséquilibre sagittal.

Mots clés : Modélisation biomécanique, Ostéotomie de soustraction pédiculaire, Instrumentation spinale, Déformation de la colonne vertébrale chez l'adulte, Balance sagittale

ABSTRACT

To maintain an erect posture minimizing energy expenditure, the alignment of the spine in the sagittal plane is of great importance. In adult spine deformity (ASD), sagittal misalignment requires higher energy expenditure and is associated with pain and loss of function. Maintaining an erect posture in such conditions involves increased trunk muscles activation and the use of compensatory mechanisms to counter balance the shift of the upper body. Surgical instrumentation is indicated for patients with high pain and disabilities when non-surgical treatments are not sufficient. This procedure consists in inserting screws in the pedicles of the vertebrae and straightening the spine with metal rods connected to the pedicle screws, leading subsequently to the permanent fusion of the spine. For the correction of large and rigid deformities in the sagittal plane, pedicle subtraction osteotomy (PSO) is a procedure used to restore normal sagittal profile of the lumbar spine.

This technique involves a wedge-shaped resection of the vertebral body along with all posterior elements of the vertebra to locally increase the lumbar lordosis. It is a highly demanding procedure due to the risks of mechanical complications. Patients with mechanical complications after PSO had a significantly greater correction of the sagittal vertical axis, higher sagittal contour of the rods, and osteotomy performed at a more caudal level.

It was also reported that up to 40% of patients kept an anterior sagittal alignment after surgery with PSO and a non-neutral sagittal alignment is associated with higher rates of revision surgery. Even though global surgical objectives have been defined through the SRS-Schwab ASD classification for the correction of sagittal imbalance, patient-specific optimal surgical strategy is still poorly defined. Also, despite clinical and biomechanical investigations, relations between stresses in the instrumentation and different sagittal correction parameters (amount of sagittal correction through varying PSO wedge angle and rod sagittal contouring angle, vertebral level of the PSO and number of rods) is still not well understood. Biomechanical knowledge of the reported risk factors and their effects on mechanical complications related to PSO such as rod breakage are still limited and a better understanding of the PSO's biomechanical impact could be a great tool to assist surgeons in their preoperative planning of sagittal imbalance correction.

Therefore, this project aims to address the following research question: « *How do PSO resection angle, rod curvature, vertebral level of the PSO, and number of rods biomechanically impact the*

correction of sagittal balance and loads in the construct, and how should they be adjusted to reduce the risks of mechanical failure in adult spinal deformity? »

To answer the research question, the following objectives were defined:

- Develop a personalized multi-body biomechanical model integrated in a simulation platform to simulate the surgical correction of sagittal balance with osteotomy for adult spinal deformity.
- Exploit the biomechanical model to evaluate the effects of the tested sagittal correction parameters on the distribution of forces and moments in the instrumented spine.

A patient-specific multi-body biomechanical model of the spine was developed to simulate the instrumentation surgery for sagittal correction of ASD with PSO. The vertebrae and pelvis were considered as rigid bodies. They were connected by 6-dimensional springs representing intervertebral discs, ligaments and facets and mechanical properties were derived from the literature. The pedicle screws, rods and surgical maneuvers were finally modeled for each case.

The biomechanical model was then integrated into a simulation platform. This simulation platform allowed us to graphically define the main steps of surgical planning such as different configurations of osteotomies and instrumentation parameters. Multiple surgical scenarios may be simulated with the help of the biomechanical model to relatively compare different strategies in terms of geometrical and biomechanical outputs.

Finally, the biomechanical model and simulation platform were used to simulate three adult patient surgeries for fixed sagittal imbalance with PSO at L2 or L3. The actual instrumentation was simulated to verify the model, and then three parameters were alternately simulated: amount of sagittal correction through varying the PSO wedge angle and rod sagittal contouring angle (± 7.5°), vertebral level of the PSO (± 1 level) and number of rods (2 vs. 4). The different surgical scenarios were then compared on the basis of three biomechanical variables: axial forces in the pedicle screws, bending moments in the rods and vertebral compressive forces. These variables were more specifically studied near the PSO level, where most of the mechanical complications have been shown to happen.

For the three cases, the maximum difference between simulated and actual surgical instrumentation was below 4° for sagittal and coronal curves and below 8 mm for SVA, which are under or equal

to the threshold defined by the intra- and inter-observer variability. Increasing (or decreasing) the PSO wedge angle by 7.5°, concomitantly to the sagittal rod contour, modified the average screw axial force by +38% (-19%) and the rods bending moments by +28% (-11%) around the PSO, respectively. The bending moments in the rods were 31% lower at the PSO site for a PSO done one level above, and 20% higher for a level below. The addition of satellite rods lowered the bending moments in the rods by 24% at PSO level and lowered the average screw axial force around the PSO by 22%. For all the sagittal correction parameters, no particular trend was found for the vertebral compressive forces. Finally, a sensitivity study was performed to assess the effect of parameters whose values were uncertain on the findings of this study. PSO wedge angle (±1.5°), intervertebral stiffness (±15%) and postoperative pelvic tilt (PT) (±5°) were investigated. Relative percentage difference of the loads in the instrumented spine for different degrees of sagittal correction was evaluated for all those parameters (<6% for PSO wedge angle, <7.8% for intervertebral stiffness and <5% for postoperative PT) and it was found that the conclusions of this study were not affected.

In conclusion, during this master's project, a biomechanical model of the spine to simulate the instrumentation surgery for the correction of sagittal alignment was developed. This biomechanical model was then integrated into a simulation platform to easily plan the major steps of the surgery. Finally, the biomechanical effects of different sagittal correction and instrumentation parameters on the loads sustained by the spine and instrumentation was assessed. Larger sagittal correction through PSO wedge angle and sagittal rod contour resulted in higher screw axial forces and sagittal bending moments in the rods at the level of the PSO. PSO performed at a more caudal level was associated with higher moments sustained by the rods at the PSO level. Using 4-rod constructs reduced the loads sustained by the implants and the rods, thus potentially reducing the risks of mechanical failure. The knowledge acquired from this project may help better understand the different risk factors of mechanical complications after PSO and eventually help to assist surgeons in their preoperative planning of sagittal imbalance correction.

Keywords: Biomechanical modeling, Pedicle subtraction osteotomy, Spinal instrumentation, Adult spinal deformity, Sagittal balance

TABLE OF CONTENTS

LIST OF TABLES

LIST OF FIGURES

LIST OF SYMBOLS AND ABBREVIATIONS

2D	Two Dimensions
3D	Three Dimensions
ASD	Adult Spinal Deformity
CRSNG	Conseil de Recherches en Sciences Naturelles et en Génie du Canada
k	Stiffness
LAT	Lateral
LL	Lumbar Lordosis
Max	Maximum
mm	Millimeter
N	Newton
PA	Posteroanterior
PI	Pelvic Incidence
PT	Pelvic Tilt
PSO	Pedicle Subtraction Osteotomy
RoM	Range of Motion
SPO	Smith-Petersen Osteotomy
SRS	Scoliosis Research Society
SS	Sacral Slope
SVA	Sagittal Vertical Axis
TK	Thoracic Kyphosis
UIV	Upper Instrumented Vertebra

LIST OF ANNEXES

CHAPTER 1 INTRODUCTION

The ideal alignment of the spine in the sagittal plane maintains the center of gravity between the feet and minimizes energy expenditure. Sagittal malalignment with loss of lumbar lordosis is often associated with pain and loss of function and maintaining an erect posture in such conditions involves increased activation of trunk muscles and use of compensatory mechanisms to counter balance the upper body. Surgical instrumentation with pedicle screws and rods is indicated for patients with high pain and disabilities when other treatments are not sufficient.

The SRS-Schwab classification was established to define the overall objectives of surgical correction (Schwab, Ungar, et al., 2012). Based on the correlations between spinopelvic parameters and health-related quality of life scores, deformity thresholds have been defined to predict disability. Radiographic parameters most correlated with pain and disability were a relationship between pelvic incidence (PI) and lumbar lordosis (LL), pelvic tilt (PT) and sagittal vertical axis (SVA).

Pedicle subtraction osteotomy (PSO) is a procedure commonly used to restore normal sagittal profile of the lumbar spine and is indicated for the correction of large and rigid deformities in the sagittal plane. This type of osteotomy involves resection of all posterior elements and removal of the pedicles at the chosen vertebral level, as well as a wedge in the vertebral body, offering a correction of up to 35° on a single level (Schwab et al., 2014).

However, it was reported that up to 40% of patients were under-corrected after surgery with PSO (Blondel et al., 2013) and poorer sagittal alignment is associated with higher rates of revision surgery (Maier et al., 2014). It is also a highly demanding procedure due to the high loads and risk of mechanical complications. Multiple risk factors impacting the rates of mechanical complications after surgical instrumentation with PSO have been identified in clinical studies, such as greater sagittal alignment correction (Smith et al., 2016), highly contoured rods (Barton et al., 2015; Smith et al., 2017; Tang et al., 2013) and osteotomy performed at a more caudal level (Ferrero et al., 2017).

Despite clinical and biomechanical investigations, the relationships between stresses in the instrumentation and the degree of sagittal correction, the level of the osteotomy, and the use of different instrumentation constructs are not yet well understood. Biomechanical knowledge of the

reported risk factors and their effects on mechanical complications related to PSO are still limited to assist surgeons in their preoperative planning of sagittal imbalance correction.

This master's project first aimed at developing a personalized biomechanical model integrated in a simulation platform to simulate the surgical correction of sagittal balance with PSO for adult spinal deformity (ASD). Then, the biomechanical model was exploited to evaluate the effects of sagittal correction parameters on the distribution of forces and moments in the instrumented spine.

Chapter 1 presents a detailed review of knowledge, which aims to define the scientific framework of the research project. Chapter 2 presents the rationale and objectives of the project. The developed biomechanical model to simulate the surgical correction of sagittal balance, the scientific article, and the complementary results are presented in Chapter 3. A general discussion of the project and a conclusion are presented in Chapters 4 and 5, respectively. The numerical platform for surgical planning of sagittal balance with osteotomy is presented in Appendix A.

CHAPTER 2 LITERATURE REVIEW

2.1 Descriptive and functional anatomy of the spine

The spine is a complex structure made of multiple vertebrae stacked on top of each other, maintained together by muscles, tendons and ligaments. It provides support for the upper body and allows to stand upright or perform functional movements such as flexion, extension, lateral bending and axial rotation. The spine also protects the spinal cord, which goes down along the back of the body of the vertebrae.

2.1.1 Anatomical landmarks

Three orthogonal planes have been defined in order to study the anatomy of the spine (Figure 2.1):

- The coronal or frontal plane vertically divides the body in an anterior ventral part and a posterior dorsal part.
- The sagittal or lateral plane vertically divides the body in a left half part and a right half part.
- The transverse or axial plane horizontally divides the body in a cranial (upper) part and a caudal (lower) part.

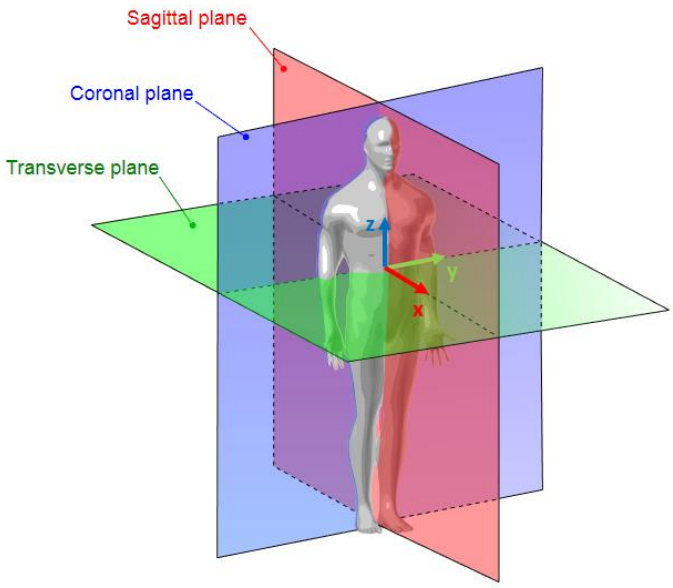

Figure 2.1: Anatomical planes (adapted from Wikimedia Commons, copyright free image)

The orthogonal reference frame is defined so that the sagittal axis (x) is headed towards the dorsoventral direction, the coronal axis (y) is headed towards the left and the longitudinal axis (z) is headed towards the caudocranial direction.

2.1.2 Anatomy of the spine

This section contains essential notions to understand the descriptive and functional anatomy of the spine. The concepts presented mostly come from : (Kim et al., 2013; Steinmetz & Benzel, 2016).

The vertebral column is composed of 24 mobile vertebrae divided into three spinal segments, and between 8 and 10 fixed vertebrae into the sacrum and coccyx (Figure 2.2):

- The cervical segment is composed of seven vertebrae (C1 to C7), forming the neck;
- The thoracic segment is composed of twelve vertebrae (T1 to T12), forming the upper part of the back;
- The lumbar section is composed of five vertebrae (L1 to L5), forming the lower part of the back;
- The sacrum is composed of five fused vertebrae (S1 to S5) linking the spine to the pelvis and the coccyx is composed of three to five fused vertebrae (Co1 to Co3/Co5).

When viewed in the coronal plane, the healthy spine is straight. On the other hand, when viewed in the sagittal plane, the spine has four natural curves: the cervical region with a lordosis curve (posterior concavity), the thoracic region with a kyphosis curve (posterior convexity), the lumbar region with a lordosis curve and the sacrum with a kyphosis curve. Those curves allow to maintain a stable and energetically efficient erect posture by keeping the gravity line over the feet and avoiding buckling of the spine under mechanical loads.

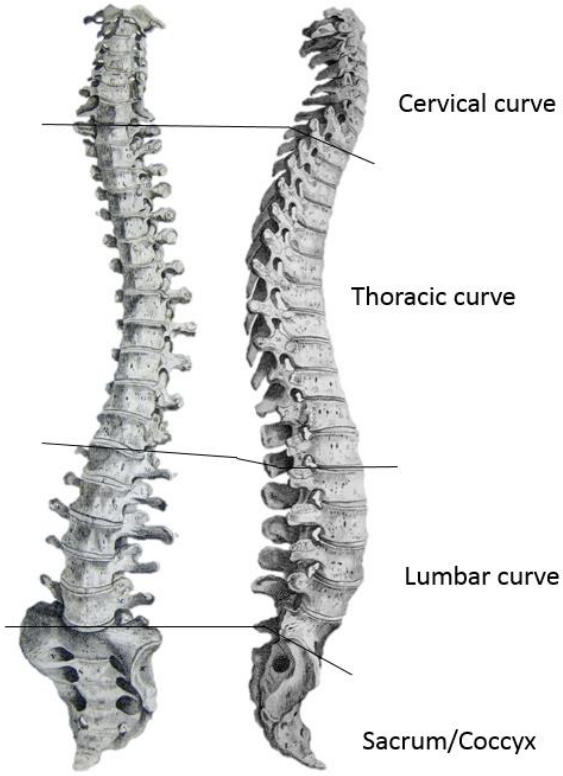

Figure 2.2: Vertebral column and its different regions (adapted from Flickr LiverPoolHLS, copyright free image)

To understand the anatomy and functions of the vertebral column, it is necessary to describe its major components. The spine is divided into rigid components (vertebrae) allowing to support the upper body, and the flexible elements (intervertebral discs, muscles and ligaments) allowing functional movements and stability.

Vertebrae

The anatomy of the vertebrae differs depending on the region of the spine in which they are located. The cervical vertebrae are the smallest, and their size gradually increases to the lumbar region to sustain the increased weight corresponding to the anatomical structures above the respective vertebra. The outer layer of the vertebrae is composed of dense and compact cortical bone and the interior is composed of cancellous trabecular bone.

They are all composed of two major sections: the vertebral body and the neural arch, which includes the posterior elements and the vertebral canal (Figure 2.3).

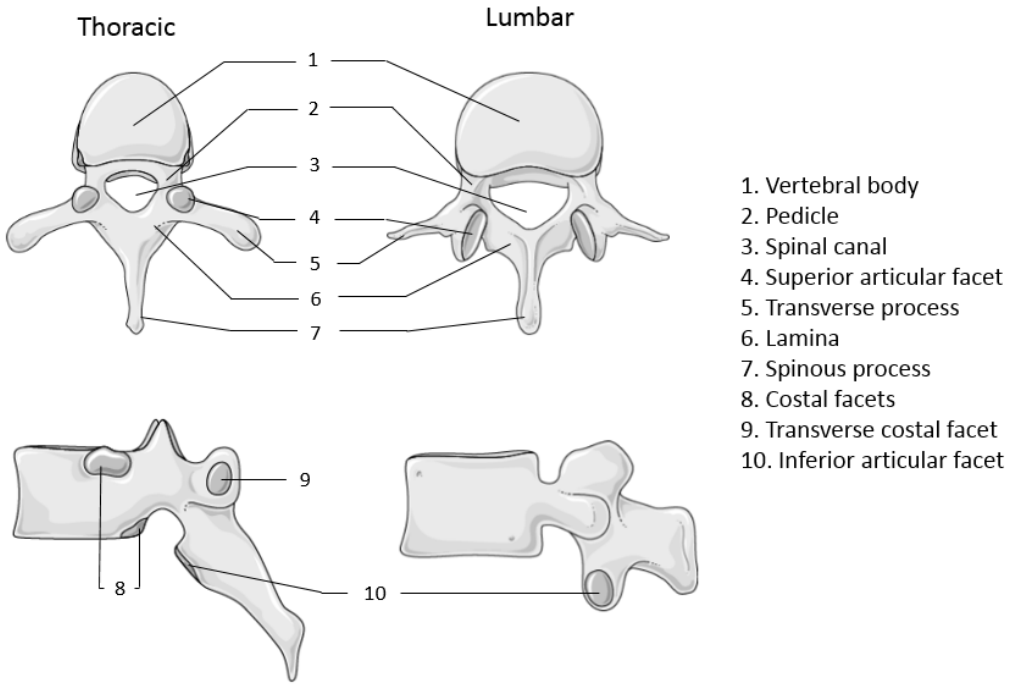

Figure 2.3: Anatomy of the thoracic and lumbar vertebrae (adapted from Servier Medical Art, copyright free image)

The vertebral body is positioned anteriorly to the spine and its function is mainly to support the weight of the upper body. The neural arc has several functions while allowing to protect the spinal cord. The pedicles link the posterior to the anterior part. The superior and inferior articular facets prevent certain movements and ensure a good connection with the other vertebrae. The transverse and spinous process allow muscle and ligament attachment. The thoracic vertebrae also have costal and transverse costal facets, which allow to fix the ribs.

The pelvis links the vertebral column to the lower limbs. It is formed with three main parts (Figure 2.4): the sacrum containing S1 to S5 fused vertebrae, the iliac bones, and the coccyx, which contains three to five fused vertebrae. The fused vertebrae of the sacrum provide strength and stability to the pelvis while the coccyx serves as a site of attachment for the muscles located in the pelvic area.

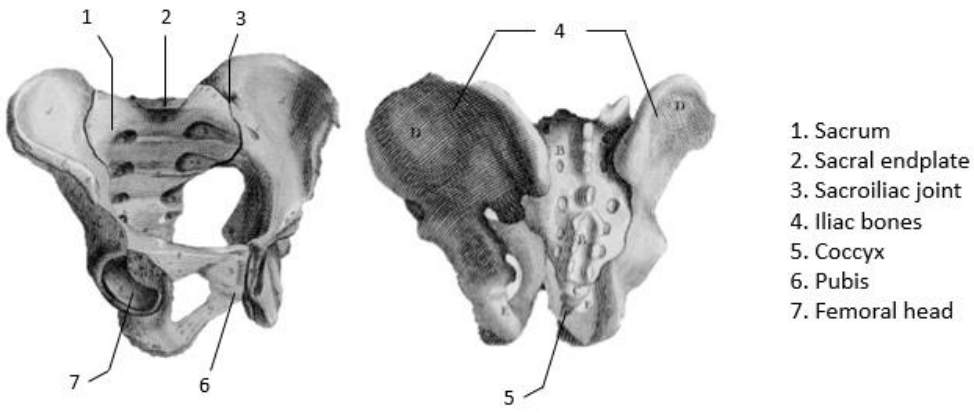

Figure 2.4: Anatomy of the pelvis (adapted from Flickr LiverPoolHLS, copyright free image)

Intervertebral joint

The components of the intervertebral joint, presented in the following paragraphs, allow the vertebrae to articulate with each other to achieve different functional movements (Figure 2.5).

The intervertebral discs are located between each pair of adjacent vertebrae. It is composed of a fibrous outer ring, called the annulus fibrosus, connecting the vertebrae above and below it. An incompressible gel-like substance, called the nucleus pulposus, is located inside the annulus. While separating the vertebrae, the intervertebral disc transmits the mechanical loads between them, absorbs shocks, and restricts intervertebral range of motion (RoM).

Multiple ligaments are included in the intervertebral joint. The ligaments are strong fibrous bands, linking every pair of vertebrae. Their functions are to hold the vertebrae together and stabilize the spine. The anterior and posterior longitudinal ligaments span the entire spine, attaching themselves to the anterior or posterior part of the vertebral body. The ligamentum flavum binds to the lamina between each vertebra. The interspinous and supraspinous ligaments bind the spinous processes together. Finally, the intertransverse ligaments bind the transverse processes together.

Between each pair of vertebrae are facet joints, covered by lubricated cartilages. These facet joints guide and limit the movement between pairs of vertebrae. The facets have different orientation depending on whether they are located in the thoracic or lumbar region. In the thoracic region, they limit the flexion and extension movement and in the lumbar region, they limit the axial rotation.

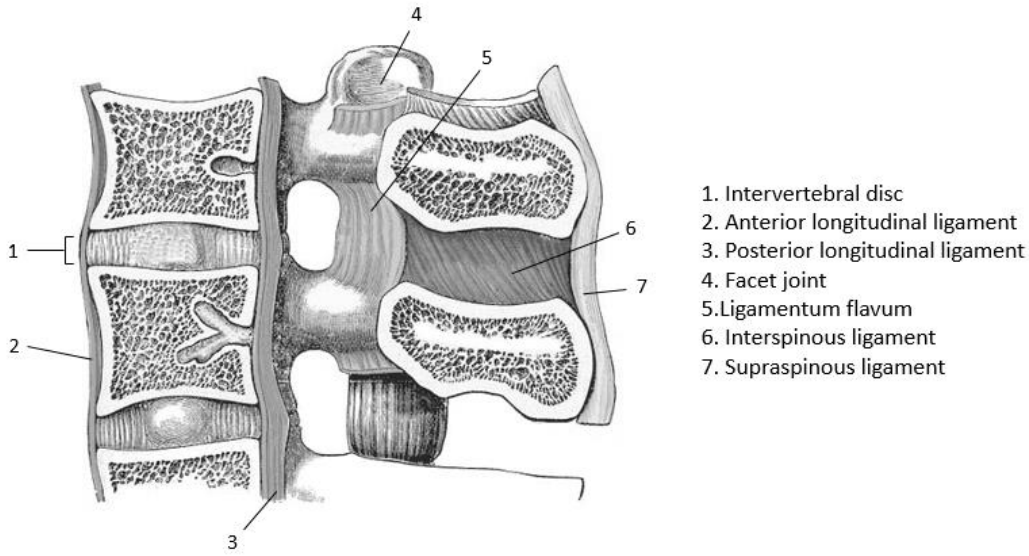

Figure 2.5: Intervertebral joint (adapted from Wikimedia Commons, copyright free image)

2.2 Adult spinal deformity

Adult spinal deformity (ASD) is a complex pathology of the musculoskeletal system that covers various clinical presentations. The aging of the spine can lead to an altered spinal alignment (V. Lafage et al., 2008) and deformity can be present in both sagittal and coronal planes. Indeed, ASD includes scoliosis, sagittal malalignment, kyphosis, spondylolisthesis, rotatory subluxation and axial plane deformity (Ames et al., 2016). The prevalence has been reported to be higher than 60% in the older population (Schwab et al., 2005). In the current section, spinal alignment and deformities will be described with a focus on the sagittal plane for adult population. Cases of altered sagittal alignment are often due to a kyphotic deformity of the lumbar or thoracic region following inflammatory, degenerative or post traumatic disorders (Roussouly & Nnadi, 2010). Individuals suffering from ASD demonstrate functional limitations, pain, and disability. As the magnitude of the deformity increases, health related quality of life measures were also shown to worsen (Glassman, Berven, et al., 2005; V. Lafage et al., 2009; Schwab et al., 2006). To understand sagittal malalignment and its effects, it is first necessary to understand sagittal alignment and its evaluation methods.

2.2.1 Sagittal alignment

For the maintenance of an upright posture while minimizing energy expenditure, normal spinal alignment in the sagittal plane is of great importance. The cone of economy (Dubousset, 1994), a concept on the fundamentals of standing balance, describes a conical zone surrounding an individual from the ground to the head (Figure 2.6). As the body deviates from the center and approaches the side of the cone, higher energy expenditure is required to maintain an erect position. A study using force plate analysis revealed that the center of gravity of the upper body passes through the sacrum and lies in-between a small area around the feet, offering quantitative support to the cone of economy concept (Schwab et al., 2006).

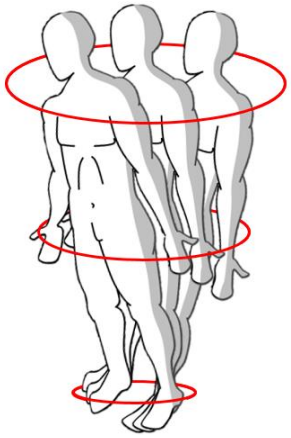

Figure 2.6 : Cone of economy of Dubousset

Normal spinal alignment in the sagittal plane is obtained by a complex relationship between the physiologic curvatures of the spine (cervical, thoracic, lumbar) and the morphology of the pelvis (Savage & Patel, 2014). The different spinal curves allow efficient mechanical loads distribution while increasing efficiency of the spinal muscles.

The main radiographical measurements used to analyze the sagittal spinal alignment are the lumbar lordosis (LL), the thoracic kyphosis (TK) and the sagittal vertical axis (SVA) (Figure 2.7). The LL is the angle between L1 superior vertebral endplate and L5 inferior endplate and TK is the angle between T4 superior vertebral endplate and T12 inferior endplate, but variants also exist (LL between L1 and S1, TK between T2 and T12). The SVA, a parameter to describe the global spine alignment, is the sagittal offset of a plumb line from the vertebral body of C7 and the posterior corner of S1 endplate. The cervical lordosis, the angle between C2 inferior vertebral endplate and

C7 inferior endplate, is also important to maintain a balanced upright posture and horizontal gaze of the head.

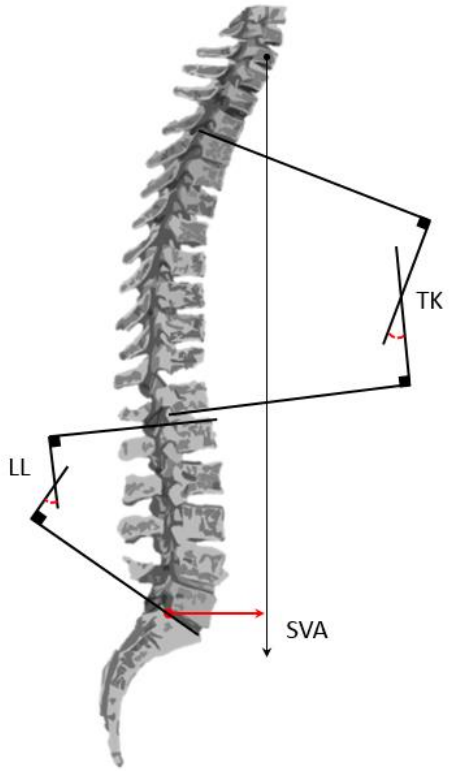

Figure 2.7 : Main sagittal plane spinal measurements (adapted from Wikimedia commons, copyright free image)

In more recent years, multiple authors have highlighted the importance of assessing pelvic parameters in the context of sagittal plane alignment. The main pelvic parameters are pelvic incidence (PI), pelvic tilt (PT), and sacral slope (SS) (Figure 2.8). The PI is the angle measured between the line connecting the center of the femoral head and the middle of the S1 endplate and the line orthogonal to this endplate. PI is a morphological parameter since it does not vary depending on the posture of the patient and is considered to be constant in the evaluation of sagittal alignment (Le Huec et al., 2011). The PT is the angle between a vertical line and the line connecting the center of the femoral head and the middle of the S1 endplate. SS is the angle between the sagittal projection of S1 endplate and a horizontal line. PT and SS are not morphological parameters since they depend on the orientation of the pelvis. They are both interdependent and their sum is equal to the PI (Legaye et al., 1998): $PI = PT + SS$.

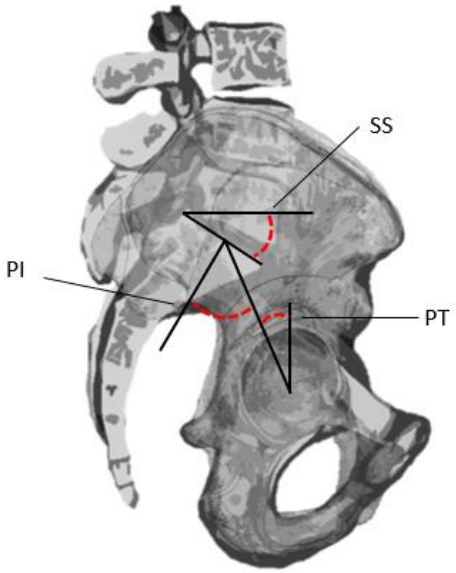

Figure 2.8: Main pelvic measurements (adapted from Wikimedia commons and LiverPoolHLS, copyright free image)

Contrary to the coronal plane, where the normal shape of the spine is in a straight line, there is no unique arrangement of the sagittal alignment in the physiological erect posture. The sagittal plane indices may be affected by multiple variables: age, gender, weight, and the pelvic morphology of the patient (Vialle et al., 2005). Lafage et al. later demonstrated, based on health-related quality of life questionnaires, that normal spino-pelvic parameters vary with age (R. Lafage et al., 2016). In this study, older patients were more likely to have higher positive SVA, compared to the original spino-pelvic parameters. A study analyzed the radiographic indices of 300 asymptomatic subjects aged from 20 to 70 years in order to determine the normal range of sagittal parameters (Vialle et al., 2005). The results are summarized in Table 2-1.

Table 2-1: Mean sagittal radiographic features of asymptomatic subjects

Radiographic measures	Mean (°)	Range (°)	Standard deviation (°)
TK (T4-T12)	41	0 to 69	10
LL (L1-L5)	43	14 to 69	11
SS	41	17 to 63	8
PI	55	33 to 82	11

2.2.2 Sagittal malalignment

As the body ages, changes in the normal spinal alignment can occur after inflammatory, degenerative or post traumatic disorders. These disorders often lead to a loss of LL or thoracic hyperkyphosis, inducing a forward shift of the upper body. To maintain an upright posture, the body needs to use increased activation of the trunk muscles and adapt its posture.

In order to counteract the anterior shift of the upper body, compensatory mechanisms will often occur in the spine, pelvis and lower limbs (Barrey et al., 2011). The goal of the compensation is to keep a balanced erect posture. A more regional compensation is the reduction of the TK through muscle activation, which can be observed in cases with flexible spine. Global compensation, such as retroversion of the pelvis (an increase of PT), results in a backward shift of the upper body and allows to translate posteriorly the anterior gravity line. For more severe spine deformity and when pelvic retroversion is not enough to compensate, recruitment of the lower limbs through knee flexion is observed (Obeid et al., 2011). Ambulatory function may be greatly affected by those compensatory mechanisms.

Global alignment (measured by the SVA) may be used to describe the sagittal spinal alignment. However, SVA is not a morphologic parameter and is dependent on the posture and the extent of compensatory mechanisms. Patients may develop pelvic retroversion in order to correct the anterior global alignment. In cases where there are no soft tissues issues or hip anteversion, pelvic retroversion may be enough to bring the head back over the pelvis and hide any underlying spinal malalignment. For this reason, it is important to consider all the major spinopelvic parameters while assessing the degree of the deformity.

Patients with sagittal malalignment may suffer from back or leg pain from increased trunk muscles activation and usage of compensatory mechanisms. Symptoms also include leg weakness and numbness, difficulty standing upright, and general disability in daily tasks. As the deformity progresses, health related quality of life measures worsen (Glassman, Bridwell, et al., 2005; V. Lafage et al., 2009; Schwab et al., 2006). The radiographic parameters most correlated with pain and disability are sagittal parameters and thresholds of deformity have been defined to predict the disability, based on correlations between spinopelvic parameters and health-related quality of life scores (Schwab et al., 2013) (Figure 2.9). These radiographic parameters are SVA, PT, and mismatch between PI and LL.

Global alignment (SVA)	PI-LL mismatch	Pelvic tilt
No deformity : <4 cm Medium deformity : 4-9.5 cm High deformity : >9.5 cm	No deformity : <10 ° Medium deformity : 10-20 ° High deformity : >20 °	No deformity : <20° Medium deformity : 20-30° High deformity : >30°

Figure 2.9: SRS – Schwab ASD classification system

For cases with small or medium deformity and limited pain and disability, the management of sagittal deformities may start with medical and interventional treatments (Ames et al., 2016). However, most studies in the literature are small cases series and expert opinion and the efficacy of those treatments has not been yet demonstrated (Berven et al., 2018; Everett & Patel, 2007). Surgical management may be considered when cases suffer from deformity progression, pain and functional limitations after medical and interventional treatments have not shown significant improvements (Fu et al., 2014).

2.2.3 Adult scoliosis

Scoliosis is a three dimensional deformity of the spine (Stokes, 1994), comprising a major curvature in the coronal plane (Figure 2.10).

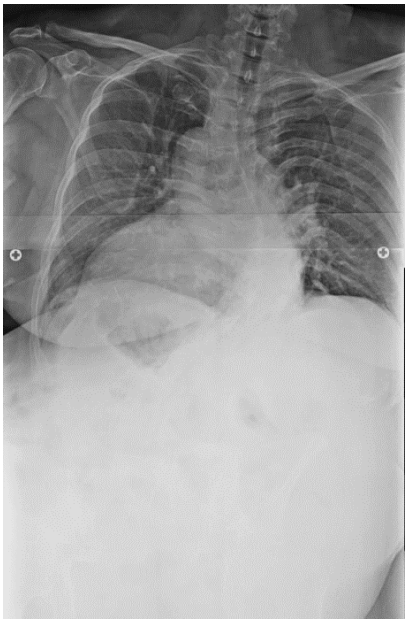

Figure 2.10 : Example of adult idiopathic kyphoscoliosis

Adult scoliosis may present itself under different forms. It can be present since childhood and progress into adult life or may appear in adult life without any preceding deformity. Multiple types of scoliosis exist: primary degenerative scoliosis (de novo), progressive idiopathic scoliosis in adult life, or secondary degenerative scoliosis following metabolic bone disease with asymmetric arthritic disease or vertebral fractures (Aebi, 2005).

A classification of the curve type determined on the basis of maximal coronal angle measured with the standard Cobb technique was done by Schwab et al. (Schwab, Ungar, et al., 2012):

- Type T: Thoracic major curve of more than 30°
- Type L: Lumbar or thoracolumbar major curve of more than 30°
- Type D: Double major curve of more than 30°

Contrary to adolescent scoliosis, where treatment is mainly guided by the deformity, older patients with adult scoliosis rather seek treatment for pain and disability (Bess et al., 2009).

2.3 Surgical correction of sagittal alignment by posterior instrumentation

ASD surgeries are complex and lead to an important cost and resource allocation (Waldrop et al., 2015). Between the years 2000 and 2014 in the US, data documented by the Healthcare Costs and Utilization Project show an increase of 280% in number of discharges reporting one or more diagnosis of abnormal spinal curvature for adults (Healthcare Costs, Utilization Project) and recent evaluation of annual cost of spine care is estimated to be over $86 billion (Arutyunyan et al., 2018). The complexity of the surgeries for ASD has also increased since the years 2000s, as data show an increase in complicated wedge osteotomies performed to treat severe and rigid spinal deformities (Ames et al., 2016).

The goals of the surgical correction of sagittal alignment are radiographic correction of the deformities, prevention of the progression, neural decompression and improvement of health-related quality of life scores (such as reduction of pain and functional limitations and improvement of mental health) (Berven et al., 2018). Sagittal plane deformities are the main driver of disability; the most important improvement brought by surgical procedure is the reduction of pain and disability by correcting those deformities (Fujishiro et al., 2018; Schwab et al., 2013). Biplanar radiographs of the standing posture are mandatory for the analysis of the spinal alignment and

preoperative planning of the surgical correction. Radiographic measures, such as PI, SVA, LL, TK and PT, are used to evaluate the posture and the extent of compensatory mechanisms. A proper restoration of sagittal alignment through surgical instrumentation should probably consider the previously mentioned SRS-Schwab ASD classification parameters.

The surgery may be performed by a posterior approach or more recently by a minimally invasive surgery. There are advantages and disadvantages for both type of surgeries but minimally invasive surgery has been reported to result in suboptimal correction in the sagittal plane in cases with more severe deformities (Mummaneni et al., 2014). In this work, focus will be placed on surgery by posterior instrumentation of the spine.

2.3.1 Posterior instrumentation surgery: biomechanical principles and instrumentation used

Evolution of the instrumentation

The instrumentation used for posterior surgery has evolved considerably since the 1960s. The first type of instrumentation, called Harrington's instrumentation, used a concave-distraction and a convex-compression stainless steel rod. Those rods had a ratchet and a collar end and were fixed to the spine with hooks at the top and bottom ends. This instrumentation led to frequent revisions for reasons such as pseudarthrosis, implant corrosion and breakage and hook dislodgements. Unidirectional distraction also often led to flattening of the back in the sagittal plane (Hasler, 2013). In the 1970s, Luque introduced the segmental spinal instrumentation with fixation on multiple vertebrae (Hasler, 2013; Luque, 1982). Sublaminar wires were used to connect the custom contoured rods to the vertebrae. This technique provides a better stability because of the multiple fixation sites on the vertebrae and the improved prevention of deformity within the instrumented levels (Wenger et al., 1982). Cotrel-Dubousset instrumentation, which aimed at correcting deformities in 3D with the concept of rod derotation maneuver, appeared in the 1980s. This maneuver consists of rotating the rod from the frontal to the sagittal plane, and was first introduced during this period (Hasler, 2013). This type of instrumentation provided more flexibility to create custom-made constructs by incorporating laminar hooks, pedicle hooks and pedicle screws. The rods were also contoured to match the deformity. This maneuver improved the correction obtained in the coronal and sagittal planes but 3D retrospective analysis later showed that there were no notable differences found for the correction in the transverse plane (Kadoury et al., 2009).

Instrumentation with pedicle screws became more and more popular in the 1990s and 2000s (Suk et al., 2001), and still is the most utilized technique. The screws allow for stable and safe manipulation of vertebral bodies by their resistance to pullout (Liljenqvist et al., 2001) and provide superior 3D correction, compared to previous fixation methods (Asghar et al., 2009).

Contemporary instrumentations

Nowadays, a few types of pedicle screws can be used for surgery of spinal deformities. Monoaxial screws have the head of the screw rigidly fixed to the shaft, uniaxial screws have a head that can freely rotate in one plane and multiaxial screws have a spherical link between the head and shaft, allowing rotation in all planes (Figure 2.11). The screws are generally inserted through the pedicles and into the vertebral body.

Figure 2.11: Multiaxial pedicle screws (from Wikimedia commons, copyright free image)

The choice of which type of pedicle screw to use is left to the surgeon. It was shown that using multiaxial over monoaxial pedicle screws greatly reduced loads at the implant-vertebra interface, reducing the odds of screw pullout (X. Wang et al., 2011; X. Wang et al., 2012) and can also facilitate rod seating into the screw head saddle. However, monoaxial screws might still be the preferred choice in some cases for their lower cost. Lower implant density may also be used to lower the cost. A study found significant heterogeneity in number of screws, rods wires and cages used between different centers for ASD (Hostin et al., 2016). Another study found significant variability in implant distributions used to treat adolescent idiopathic scoliosis and proposed best regions for planned screw dropout (Le Naveaux et al., 2015).

Metal rods are used to connect same sided screws that were inserted into vertebral bodies. The rods stabilize the spinal segments, prevent motion, and eventually allow fusion of the disc space. To offer different stiffness, they can be made of different materials (stainless steel, titanium, and cobalt

chrome) and diameters (usually between 5 mm and 6.35 mm). The contour of the rod can be modified to fit the desired postoperative spinal curvature.

To restore LL angle and offer immediate postoperative stability to a vertebral segment, a prosthesis called a cage can be placed in the disc space. Cages are usually cylindrical or rectangular-shaped and their surface is porous to allow bone graft from the vertebrae to fuse with it. Cages geometry can vary in height, lordotic angle, and footprint.

2.3.2 Use of osteotomies for the posterior instrumentation surgery

In cases with flexible spinal curves, instrumentation alone may be sufficient to achieve proper correction of sagittal alignment. However, for severe and rigid curves, osteotomies of the spine may be needed in order to properly restore sagittal alignment (Diebo et al., 2014; Savage & Patel, 2014). Accordingly, assessment of the flexibility of the deformity is an important step of the preoperative planning and can be done by evaluating supine radiographs of the spine with fulcrums or bolsters, CT scans, or MRI scans (Ottardi et al., 2018).

Over the years, a wide variety of osteotomies have been developed. Amongst the most common techniques described in the literature to treat ASD are the Smith Petersen osteotomy (SPO), pedicle subtraction osteotomy (PSO) and vertebral column resections (Bridwell, 2006; Takahashi et al., 2017). In the literature, Smith Petersen (partial facet joint resection) and Ponte (complete facet joint resection) osteotomies are often described as the same technique or used interchangeably and confusion surrounds the nomenclature (Dorward & Lenke, 2010).

A classification of spinal osteotomies based on the extent of bone resection was developed to standardize the descriptions of techniques and interpretation (Schwab et al., 2014). Six grades of osteotomies are defined in the classification:

- Partial (1) and complete (2) facet joint removal;
- Partial (3) and complete (4) pedicle and body resection;
- Vertebra and discs (5) and multiple vertebrae and discs (6) resection.

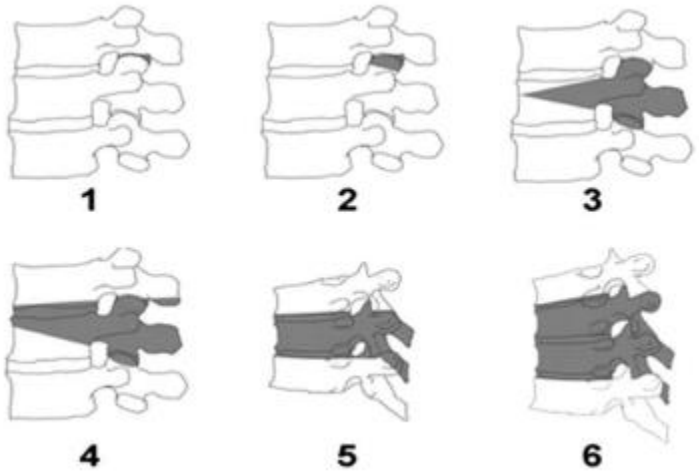

Figure 2.12 : Osteotomy classification grades 1 to 6 (Image reused with permission of: F. Schwab, B. Blondel, E. Chay et al. The comprehensive anatomical spinal osteotomy classification. Neurosurgery. 2014; 74[1]:112-120)

A description of SPO and PSO are presented in the next sections. Publications have shown that both of those osteotomy techniques may provide satisfactory correction (Liu et al., 2015), but indications are different. In this work, focus is put on pedicle subtraction osteotomy, which is the most commonly used technique for the treatment of fixed sagittal imbalance (Ottardi et al., 2018).

2.3.2.1 Smith Petersen osteotomy (SPO)

SPO (Smith-Petersen et al., 1945) is a grade 1 osteotomy and a commonly used technique originally used to treat ankylosing spondylitis. It is associated with the resection of the inferior facets, joint capsules, laminae, and posterior ligaments of a certain spinal level. The osteotomy site is then closed, shortening the posterior column and lengthening the anterior column. This technique often involves multiple levels and can achieve 5° to 10° of correction per level (Cho et al., 2005; Schwab et al., 2014). Limited deformity correction and prerequisite anterior column mobility make this type of osteotomy suitable for mild to moderate and flexible deformities of the spine. Best indications for using SPO technique were described as having a long, rounded and smooth kyphosis (Bridwell, 2006) or lack of lordosis.

2.3.2.2 Pedicle subtraction osteotomy (PSO)

PSO (Thomasen, 1985) is a grade 3 osteotomy and is the most commonly used technique to treat fixed sagittal imbalance. It involves a wedge-shaped resection of the vertebral body along with all

posterior elements of the vertebra (Figure 2.13). The osteotomy site is then closed, shortening the posterior column with no anterior column lengthening. The large contact area of the superior and inferior parts of the vertebra helps the fusion of the PSO body (Dorward & Lenke, 2010). It is possible to achieve between 25° and 35° of correction at the osteotomy level (Bridwell, 2006). The PSO is most often performed to increase LL in cases of ASD but may also be performed in the thoracic curve (Bakaloudis et al., 2011). Indications for using PSO technique were described as having degenerative changes in the spine and a sharp and severe deformity with little or no flexibility (Barrey et al., 2014; Berjano & Aebi, 2015).

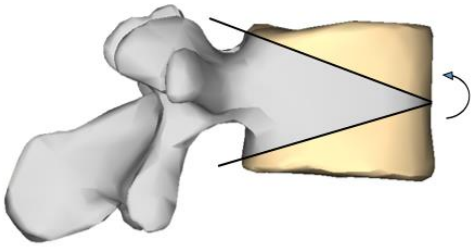

Figure 2.13 : PSO (adapted from Wikimedia commons, copyright free image)

2.3.2.3 Clinical and biomechanical studies of ASD surgery with osteotomies

Osteotomies are an effective technique used to restore normal sagittal profile of the spine. However, they are highly demanding procedures due to the risk of complications, especially for the pedicle subtraction osteotomy. A retrospective study (Smith et al., 2011) on 578 patients who underwent surgical treatment of thoracolumbar fixed sagittal deformity showed that a higher complication rate was present for procedures including an osteotomy, compared to cases not including an osteotomy (34.8% vs 17%). Between the 215 cases that underwent an osteotomy, cases with a PSO had higher complication rate (39.1%) than cases with a SPO (28.1%). Another study compared the results of executing three SPO and one PSO for the correction of fixed sagittal imbalance (Cho et al., 2005). They found that the correction in kyphosis between the two methods was nearly identical but there was a significantly greater risk of decompensation with SPO, whereas there was substantially greater blood loss with the PSO technique. Another study documented a 19% reoperation rate for patients treated with PSO and a 16% rate for patients not treated with this procedure (Scheer et al., 2013). The authors reported that the most common indications for reoperation were instrumentation complications and radiographic failure.

The rate of mechanical complication after surgical correction of ASD with an osteotomy is relatively high. Barton et al. (Barton et al., 2017) investigated the rate of mechanical complication on a cohort of 88 patients and found an incidence of 43.6%. The prevalence of pseudarthrosis after lumbar PSO was assessed on a retrospective cohort of 171 patients (Dickson et al., 2014). The authors found that the overall prevalence of pseudarthrosis was 10.5%. Of those, 61% occurred at the PSO site and the most common radiographic finding was rod breakage. Smith et al. (Smith, Shaffrey, et al., 2012) evaluated symptomatic rod fracture for ASD on a cohort of 442 patients. It was found that rod fracture occurred in 6.8% of all cases, while it occurred in 15.8% of cases with a PSO. Failure occurred at the PSO site in 89% of those cases. Furthermore, the rate of rod fracture in patients with a PSO based on rod material was lower for cobalt chrome (7%), compared to stainless steel (17%) and titanium (25%). A prospective assessment of the rates for rod fracture following surgery for ASD was conducted on a cohort of 287 patients (Smith et al., 2014). They found a rate of rod fracture of 9% for all patients and a rate of 22% for patients with a PSO with a minimum of 1-year follow-up. 91% of the failures were adjacent to the PSO level. Patients with rod fracture were older, had greater BMI and a greater baseline sagittal malalignment. In a later study by the same author (Smith et al., 2017) on complication rates associated with 3 column osteotomies (3CO), 82 patients with a 2-year follow-up were included. The most common complication was rod breakage (32%) and the most common indication for reoperation was also rod breakage (n=14). The authors, in accordance with a biomechanical study on the fatigue life of the rods after PSO (Tang et al., 2013), suggested that the risk of rod breakage may derive from the severity of rod contour across the 3CO level. Another study on 75 patients reported an incidence rate of rod breakage of 16.2% when PSO was performed (Barton et al., 2015). Factors significantly associated with rod fracture were: fusion construct crossing thoracolumbar and lumbosacral junctions, sagittal rod contour >60°, the presence of dominos and/or parallel connectors, and pseudarthrosis at ≥1-year follow-up.

Multiple authors have proposed using 4-rod constructs in order to reduced rod breakage and pseudarthrosis (S. Gupta et al., 2017; Hyun et al., 2014; Luca et al., 2014; Smith et al., 2014) (Figure 2.14). A study investigated effects of a 4-rod construct on motion and surface rod strain of a PSO model to reduce incidence of rod fracture (Hallager et al., 2016). The authors found that addition of accessory rods significantly reduced flexion-extension motion at the PSO level and use of cobalt-chrome material significantly reduced rod strain. Similarly, La Barbera et al. (La Barbera

et al., 2018) conducted tests on six human cadaveric spine segments to compare constructs of 2, 3 and 4 rods and measured strains on the primary rods with strain gauge rosettes. The authors found that adding two accessory rods after PSO was an effective strategy to significantly reduce rod strains. A finite element model was used to investigate the biomechanical performance of different hardware constructs and found that using satellite rods was a good method to reduce stresses on the spinal fixators, near the site of the PSO (Luca et al., 2017). In a similar study, Januszewski et al. studied rod stress after PSO for different surgical constructs (Januszewski et al., 2017). The authors found that 4-rod constructs were effective at reducing stress in the rods near the zone of the PSO by up to 50%.

Figure 2.14 : 4-rod construct covering the zone of the PSO

Although the risks associated with osteotomies are high, a recent study investigated if the performance of surgeries including a 3CO improves with years of surgical practice (Diebo et al., 2017). The authors found that despite being performed on a more disabled population and offering a greater correction at the site of the osteotomy, surgical revisions and complication rate are decreasing.

2.3.3 Preoperative planning of the surgery

Preoperative planning in the context of ASD is critical.

To help define surgical objectives, two major classifications have been developed. These classifications may help surgeons to consistently characterize the deformities and the associated surgical treatment. The SRS-Schwab classification is the most recognized one. It relies on studies correlating health-related quality of life scores and radiographical outcomes to define thresholds of correction during surgical procedures (Schwab, Ungar, et al., 2012). In the sagittal plane, three parameters have been defined to help define surgical objectives: PI-LL < 10°, SVA < 4cm, and PT < 20°. Roussouly's classification has been developed from the geometrical analysis of the variation of sagittal curvatures of asymptomatic population (Roussouly et al., 2005). This classification initially included four patterns of sagittal alignment and was defined based on the SS and spinal shape:

- Type 1 SS smaller to 35° and apex of the lumbar lordosis located at the center of L5
- Type 2 SS smaller to 35° and apex of the lumbar lordosis located at the base of L4
- Type 3 SS between 35° and 45° and apex of the lumbar lordosis located at the center of L4
- Type 4 SS greater than 45° and apex of the lumbar lordosis located at the base of L3

Roussouly's classification was later completed to include type 3 anteverted (Laouissat et al., 2018). Differently from the SRS-Schwab classification which is based on the magnitude of the restauration of lumbar lordosis, Roussouly's classification also considers the geometrical shape of the spinal curves.

However, an important proportion of patients do not report a clinically significant change in health care related quality of life and/or still have poor sagittal alignment after surgery. Moal et al. analyzed the radiographic outcomes of ASD correction of 161 patients and found that only 23% of patients had a complete radiographic correction in both sagittal and coronal planes (Moal et al., 2014). Sagittal deformity with pathological SVA or PI-LL was corrected in 50% of the cases whereas pathological PT was only corrected in 24% of the cases. Another study reported failed realignment after ASD surgery with PSO in 23% of the cases (Schwab, Patel, et al., 2012). Patients with failed realignment had significantly larger preoperative deformity but received a similar amount of correction as the patients with successful realignment. An important factor to consider while planning the surgery is postoperative alignment changes through spinal segments that are not included inside the instrumentation construct. A clinical study evaluated how the compensatory

changes in the unfused part of the thoracic spine after PSO impacted global spinal alignment (V. Lafage, Ames, et al., 2012).The authors found that for patients with reciprocal changes, the majority was unfavorable and risk factors were larger PI, inadequate postoperative LL and older age. To illustrate the importance of preoperative planning, a study assessed the ability of surgeons to predict postoperative alignment of the spine after being shown preoperative radiographs and surgical plan (Ailon et al., 2016). The authors found that one-third of the time, surgeons were not able to predict the adequacy of the surgical plan.

The first steps of surgical planning of sagittal imbalance consists of finding the drivers of deformity (loss of LL being the most common one) and how the patient adapted to the deformity through compensatory mechanisms. After finding the amount of correction needed to obtain a good postoperative alignment, surgical technique can be selected depending on the etiology of the deformity. For more rigid deformities, PSO is the preferable technique. Different tools have been developed in order to help the preoperative planning of the surgery.

Predictive mathematical formulas

Mathematical formulas have been developed to help preoperative planning of sagittal correction with PSO and predict postoperative radiographic parameters (Y. J. Kim et al., 2006; V. Lafage et al., 2011; Ondra et al., 2006; Rose et al., 2009; Schwab et al., 2009) but are not all equally accurate. Smith et al. (Smith, Bess, et al., 2012) evaluated the ability of those formulas to predict SVA after PSO and found that formulas incorporating pelvic alignment were better at predicting SVA. Formulas that do not account for PT and expected changes in the unfused segments did not accurately predict sagittal correction and may predispose to residual postoperative deformity. Based on the preoperative variables PI, age, max LL and max TK, the Lafage formulas used to calculate the postoperative PT and SVA had the greatest accuracy (89%) in predicting postoperative SVA.

Computer assisted predictive methods

Current computer assisted methods used to predict postoperative alignment first require identification of anatomical landmarks. The surgical objectives are defined by the user and the objectives are then simulated to predict final alignment (R. Lafage et al., 2018).

Surgimap is a computer program integrating spinal measurements and tools for surgical planning through a graphical method with radiographs (Akbar et al., 2013). Surgeons may rotate the

radiographs to evaluate the amount of correction needed by considering the pelvic compensation. It is possible to graphically trace osteotomies or cages on the radiographic image to locally tilt the radiograph and simulate the geometric correction.

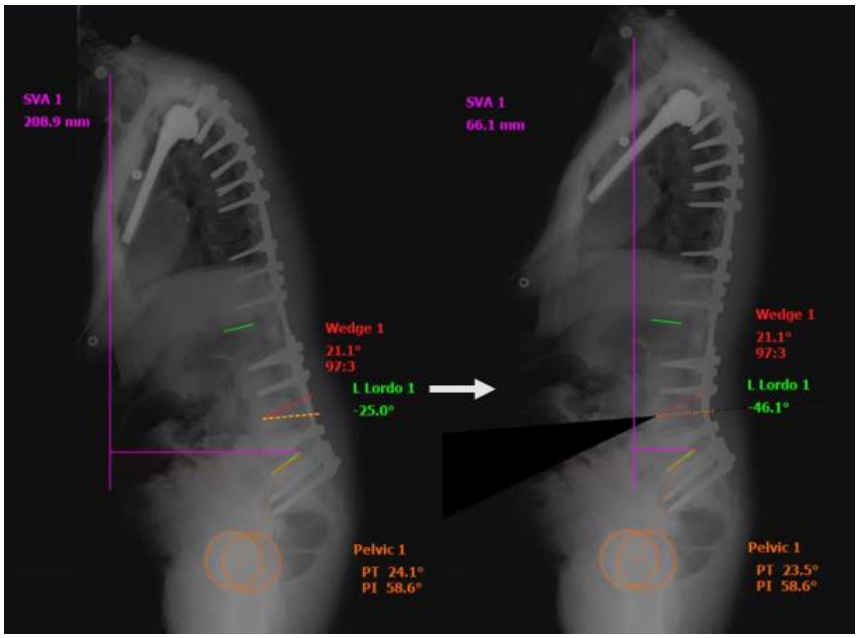

Figure 2.15 : Simulation of a PSO with Surgimap

Another method reported using machine learning algorithms to predict postoperative spinal alignment (Moal et al., 2017). The authors used a probabilistic principal component analysis based on 250 patients to predict postoperative alignment including the pelvis and the unfused segments. The model provided good PT prediction but was less effective at predicting change in the unfused segments.

2.4 Biomechanical simulation of posterior instrumented spinal surgery

2.4.1 3D reconstruction techniques

The 3D reconstruction of the spine allows to simultaneously analyze the deformities in the sagittal, coronal and axial planes, and is done from biplanar radiographs of the patient. From the 3D reconstruction, it is also possible to create computational biomechanical models of the spine to simulate surgical instrumentation.

One method of 3D reconstruction is done with two standard radiographs (coronal and sagittal). An explicit calibration algorithm to estimate the geometrical parameters of the radiographic setup is

used to reconstruct the spine in 3D (Cheriet et al., 2007). To calibrate the images, a calibration belt with markers whose position is known is worn by the patient during the acquisition (Kadoury et al., 2007). Corresponding vertebra landmarks are identified in both radiographs by the user and the 3D position of the vertebra landmarks are iteratively updated until the solution converges to a stable state. The anatomical markers identification error of good quality X-ray images has a standard deviation of about 1 mm, and results in a 1.8 mm reconstruction error for this reconstruction technique.

Another method of 3D reconstruction is by using the EOS imaging system (EOS Imaging, Paris, France). The EOS system allows to simultaneously acquire coronal and sagittal X-rays by scanning the X-ray source up and down in a cabin. This technique removes any chance of postural change that might occur in the spine when taking coronal and sagittal X-rays one after the other. The image quality from EOS system was shown to be significantly better than standard radiography while reducing radiation dose 6 to 9 times (Deschênes et al., 2010). A 3D reconstruction method using biplanar EOS X-rays was proposed by Humbert et al. (Humbert et al., 2009). The precision for this 3D reconstruction method is 1.8 mm for the position of the vertebra and between 2.3° and 3.9° for the orientation.

After obtaining the 3D coordinates of the vertebrae, it is possible to obtain a 3D geometric model of each vertebra with a kriging method (Delorme et al., 2003). This method allows to deform a reference geometry of a vertebra so that it coincides with the identified anatomical markers.

Other medical imaging methods may be used for the 3D reconstruction of the spine like CT-scan and MRI. However, these methods are incompatible with postoperative evaluation after instrumentation with metallic rods and pedicle screws.

2.4.2 Biomechanical models of the human spine for surgical instrumentation

Computerized models allow to study the biomechanical aspects of the surgical instrumentation of the spine. Mechanical properties of the different components of the spine and instrumentation may be modeled to represent real mechanical behavior. For the same patient, multiple different surgical strategies may be compared, which would be impossible for *in vivo* or *in vitro* experiments. Two major approaches have been developed to model mechanical behavior of the spine with instrumentation: multibody modeling and finite element modeling (Figure 2.16).

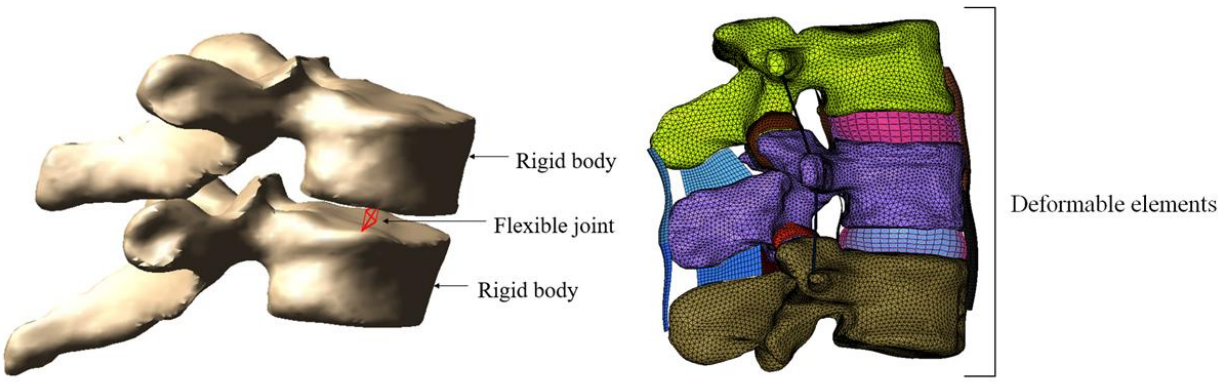

Figure 2.16 : ADAMS multibody model (left) and SM2S finite element model (right)

2.4.2.1 Flexible multibody modeling

Flexible multibody modeling is a method of computerized simulation in which the components of the system are composed of rigid and flexible bodies. The connections between the rigid bodies are modeled as kinematic constraints (joints) or force elements (flexible elements such as a stiffness matrix), which allow to establish differential equations and to solve them using iterative mathematical methods. Boundary conditions must be defined in the model and forces or displacements may be applied on the system to assess resulting displacements and joint reaction forces. To describe the entire configuration of the system, a number of variables proportional to the number of degrees of freedom are necessary. The number of degrees of freedom depends on the number of independent coordinates necessary to describe the whole system. Kinematics and dynamics of the system may be studied using this kind of modeling. However, as opposed to finite element analysis, the study of stresses and local deformations is not possible.

In the context of the spine, the bony parts (vertebrae, pelvis and ribs) are modeled as rigid bodies and soft tissues (intervertebral discs, ligaments and muscles) are modeled as flexible elements, which properties are defined in the literature (Panjabi & Brand, 1976; Panjabi et al., 1994). The model allows to study the biomechanical response of the spine subject to the instrumented surgery for different configurations of boundary conditions, surgical maneuvers and postoperative functional loadings. The different configurations may be compared in terms of correction and in terms of loads sustained by the spine and instrumentation.

Many modeling parameters may affect the simulation time but compared to finite element method, the number of degrees of freedom in multibody modeling is much smaller. This makes this modeling method adequate to be used in a clinical context (Aubin et al., 2008). This type of model is particularly interesting for the analysis of the whole spinal structure behavior during instrumentation maneuvers.

Among the first to develop a multibody biomechanical model for the instrumentation of the spine with ADAMS (MSC Software) was Poulin et al. (Poulin et al., 1998). The thoracic and lumbar vertebrae were modeled as rigid bodies while the intervertebral discs, ligaments and facet joints were modeled as flexible elements. The implants were modeled as rigid bodies and were fixed to the vertebrae and the rods consisted of multiple rigid segments. After simulation of surgical instrumentation for scoliosis correction, 80% adequacy was found for the Cobb angle correction in the coronal plane, demonstrating the feasibility of this approach to model the instrumentation surgery of the spine.

This model was later exploited to simulate Cotrel-Dubousset instrumentation (Aubin et al., 2003). The geometric representation of each vertebra was improved using a detailed geometry of the vertebrae which was adjusted to the patients with a kriging method. Three steps representing the surgical procedure were simulated: translation of hooks and screws to the first rod, rotation of the rod by 90° and look-up of the hooks and screws on the rod. Implant-vertebra forces as high as 1000N were found, which could be explained by the use of monoaxial screws rigidly connected to the vertebrae and the fact that the rods were considered as rigid bodies.

Petit at al. proposed a method to characterize patient specific mechanical properties of the spine using the flexible multi-body model (Petit et al., 2004). The original mechanical properties of the intervertebral segments, which were defined from *in vitro* experiments, were adjusted using an optimization algorithm which aimed at reducing the difference between the real measured angles and the results of the simulation of different spine segments in lateral bending. Then, the modeling of the intervertebral link and implant/vertebra complex was improved (Luce, 2004). The intervertebral spherical joint was replaced by a 6X6 rigidity matrix, which allowed to consider the intrinsic coupling movements between vertebrae. The bone-screw connections were modeled as non-linear general springs and their load-displacement behaviour was defined from experimental tests conducted on cadaveric vertebrae. The new mechanical properties did not significantly

influence the correction of the spine, but highly reduced intervertebral and implant/vertebra forces induced by the surgery. Stirbu et al. then modeled the rods while considering the elastic behavior of the material (Stirbu, 2004). The rods had 20 segments linked by flexible elements whose mechanical properties were adapted for different materials and geometries.

The model was later used to develop a Spine Surgery Simulator (S3) (Aubin et al., 2008). The simulator was developed to predict the correction of the scoliotic spine for a specific patient and instrumentation. It can be used to simulate different surgical strategies for the same patient before the real surgery. The technical feasibility was demonstrated after simulating 10 scoliotic cases, which agreed well with the actual postoperative results (mean difference less than 5° with respect to the clinical indices).

Wang et al. modeled four types of pedicle screws presenting different kinematic characteristics and types of connection to the rods (monoaxial, uniaxial, polyaxial and dorsoaxial screws) (X. Wang et al., 2012). The four types of pedicle screws were simulated on 10 scoliotic patients and the authors found that the bone-screw loads were significantly different. The bone-screw loads were smaller for pedicle screws presenting more degrees of freedom. Wang et al. later studied the effect of differential rod contouring on 3D correction and forces at the bone-screw interface (X. Wang et al., 2016). The authors found that the transverse plane correction improved when increasing the concave rod contouring angle and diameter compared to the convex rod. However, there was a significant increase of screw pullout forces. Wang et al. (2016) also added to the model the posterior and anterior longitudinal ligaments, ligamentum flavum, supraspinous and interspinous ligaments, intertransverse ligaments and facet joints. The ligaments were modeled using a translational spring while the facet joints were modeled using a 6X6 stiffness matrix.

Martino et al. used the model to study vertebral derotation maneuvers with different types and density of implants to maximize the tridimensional correction of scoliosis and minimize the implant-vertebra forces (Martino et al., 2013). A sensitivity analysis on surgical variables (implant type and density, number of derotation levels, vertebral derotation angle and the force applied during the maneuver) was conducted to analyze the 3D correction and loads on the instrumentation. The parameters that influenced the most the scoliosis correction were implant type and density, and vertebral derotation angle. Later, Boyer et al. studied the biomechanical effect of different derotation maneuvers on the 3D correction of idiopathic scoliosis and the loads sustained at the

implants (Boyer, 2017). Different surgical scenarios were modeled: no vertebral derotation, « en bloc » derotation and segmental derotation. The simulated vertebral derotations improved the transverse plane correction. Compared to « en bloc » derotation, segmental derotation improved the correction of the scoliotic spine but increased the loads sustained by the implants. To validate the forces applied on the derotators in the model, a tool equipped with a sensor able to measure intra-operative forces applied by the surgeon on the derotators and to record derotation angle was developed.

Cammarata et al. adapted the model to study the effects of four surgical variables on the risks of developing proximal junctional kyphosis (PJK) (Cammarata et al., 2014). The erect posture of the spine was modeled, including gravitational loads (Kiefer et al., 1997; Pearsall et al., 1996). The models of 6 adult patients with scoliosis were developed to analyze the effect of four surgical variables and found that preserving more posterior intervertebral elements, using transition rods, using transverse process hooks at UIV and smaller sagittal rod curvature decreased the risks of developing PJK.

Desrochers-Perrault et al. adapted the model to study the iliac screw fixation for the correction of neuromuscular scoliosis (Desrochers-Perrault et al., 2014). Sacroiliac connections were modeled on the pelvis by adding two 6X6 stiffness matrices connecting the iliac crest to the sacrum. Six patients were simulated to assess the loads on the iliac screw during and after surgery as functions of different instrumentation variables (combined use of sacral screws, use of lateral offset connectors, use of cross-rod connectors, and iliac screw insertion point and trajectory). Use of lateral connectors and sacral screws, and iliac screw insertion points had significant effects on loads at iliac screws.

Le Navéaux et al. created patient-specific spine models of 9 Lenke 1 patients who underwent posterior instrumentation to study how implant distribution impacts 3D correction and forces at the implant-bone interface (Le Naveaux et al., 2016). From each of those patients, 128 virtual implant configurations were generated from existing implant patterns used in clinical practice and found that increasing the number of implants allowed for a limited 3D correction improvement while over constraining the instrumentation, resulting in increased forces at the implant bone interface.

Salvi, Wang et al. modeled different types of osteotomies for the correction of hyperkyphotic patients to study the loads sustained by the spine and the instrumentation (Salvi et al., 2016). The

Ponte and pedicle subtraction osteotomies were performed in the thoracic region of the spine to treat hyperkyphotic deformities of young patients (12-19 years old). Ponte osteotomy and PSO were modeled by reducing the intervertebral stiffness representing the removal of posterior elements such as supraspinous and interspinous ligaments, ligamentum flavum and facet joints. In the case of Ponte osteotomy, the intervertebral stiffness was modified in one functional spinal unit while in the case of the PSO, both the superior and inferior functional spinal units' stiffness were modified. To represent the geometric change of performing the osteotomies, the Ponte osteotomy allowed a RoM of 10° in flexion while the PSO allowed a flexion motion of 30° at the anterior midpoint of the vertebral body. In the case of the PSO, a 6X6 stiffness matrix was defined between the upper and lower parts of the vertebra at the anterior midpoint of the vertebral body which represented the stabilizing effect of the surrounding anatomical structures. No relative translational motion was allowed in the caudocranial direction. This modeling choice represents a PSO without fusion at the osteotomy site and the loads sustained by the instrumentation may be higher in this case as the instability generated by the unfused segments will be bigger compared to a PSO with proper fusion. Multi-level Ponte osteotomy allowed similar kyphotic correction to 1-level PSO. No significant difference was found in upright position for the loads sustained by the instrumentation between the Ponte osteotomy and the PSO but in simulations of 30° flexion, the rod bending moments increased by 2% to 8% for the multi-level Ponte osteotomies and by 38% for the PSO. However, PSO are most commonly performed in the lumbar section of the spine for the treatment of rigid deformities in the context of adult spinal deformity whereas this study compared different types of osteotomies in the thoracic region for adolescent cases. Different sagittal correction parameters related to PSO and reported to impact the risks of mechanical failure of the instrumentation such as level of the PSO or amount of sagittal correction were not assessed.

2.4.2.2 Finite element models

Finite element modeling is a numerical method used to analyze problems with complex geometries and material properties subject to different loadings where analytical solutions can not be obtained. This method allows to divide a complex geometry into a finite number of simple interconnected elements to obtain an approximate solution of the real solution. The behavior of each element is described by constitutive equations and their properties depend on their assigned material. Contrary to flexible multibody modeling, finite element modeling allows to study the local deformations and

stresses of the components of the model. Modeling of a system as complex as the spine requires multiple simplifications such as how the mechanical properties are defined, or the way boundary conditions and loads are applied to represent adequate mechanical behavior. After the definition of boundary conditions and loads or displacements, the system is iteratively solved to reach equilibrium. The finite element method allows to solve implicit (time-independent) or explicit (time-dependent) problems. For cases where loads are slowly applied to the model and acceleration effects are negligible, the implicit approach is adequate. The explicit approach is required when the effects of acceleration cannot be neglected. The higher the number of degrees of freedom, the longer the computational time.

A personalized geometric model of the spine was developed using a stereo-radiographic 3D reconstruction technique (Aubin et al., 1995). This model was later used to simulate correction of scoliosis with Cotrel-Dubousset instrumentation (Leborgne et al., 1999) on a patient specific case. The results demonstrated the feasibility to analyze different surgical strategies. The model was later used by Lafage et al. to simulate the surgical instrumentation of 10 scoliotic cases (V. Lafage et al., 2004). Lateral bending films were used to personalize the model properties and each step of the surgery were simulated. Differences between simulations and postoperative measurements were on average 5° for vertebral rotation and 6 mm for linear position.

Using a comprehensive finite element model of an L3 vertebra, Bianco et al. analyzed different pedicle screw diameters, lengths, threads, and insertion trajectories on anchorage performance (Bianco et al., 2017). The model included elastoplastic bone properties and contact interactions with the screws. The trabecular and cortical bone with realistic regional thickness were modeled according to their respective mechanical properties. All independent variables had a significant effect on maximum pullout force of the screws. The screw diameter was the parameter that affected the most the pullout force.

Using a finite element model of the spine from L1 to the sacrum, Charosky et al. studied the biomechanical instability after a PSO and compared different rod contours (Charosky et al., 2014). The PSO was modeled by removing all posterior elements and the posterior 2/3 of the vertebra to simulate a 30° wedge. The authors modified the model to simulate a PSO with healthy, highly dehydrated or completely degenerated discs and with mono axial or multi axial pedicle screws. The instability of the PSO was rotational and was greatly increased when discs were degenerated. The

rods sustained higher stresses located at the apex of the rods with mono axial screws and sharp contoured rods.

Ottardi et al. analyzed the destabilization of a 30° PSO at L3 and L4 with a non-linear finite element model of a L1-S1 spine (Ottardi et al., 2016). They found that the PSO consistently increased the RoMs and the largest variation was in axial rotation (58%) for PSO at L3 and in lateral bending (43%) for PSO at L4. PSO induced an instability at both L3 and L4 but L4 had greater influence on the RoM. However, the posterior instrumentation was not modeled. The same model was later used by Luca et al. to investigate different constructs (Ti6Al4V and CoCr rod materials, 2 vs. 4 rod constructs and 5 and 6 mm rod diameter) for the surgical instrumentation with a PSO (Luca et al., 2017). The CoCr rods sustained up to 39% higher stresses than Ti rods and rods with a diameter of 5 mm sustained up to 17% higher stresses compared to rods of 6 mm. Stress reduction of up to 50% was reported when using 4-rod constructs.

Januszewski et al. used a nonlinear finite element model of a T12-S1 spine segment to compare different techniques of surgical instrumentation after PSO, as well as to compare the stresses in the rods for a PSO with different configurations of interbody cages, accessory rods or satellite rods (Januszewski et al., 2017). They found that the stress in the rods was higher for a PSO with standard 2-rod construct and lower when adding interbody support and satellite rods.

Vosoughi et al. used an osseoligamentous finite element model of a T10-pelvis spinal segment to assess the RoM and stress distribution near the site of the PSO for different configurations of satellite rod constructs (Vosoughi et al., 2018). To model the L3 PSO, all posterior elements were removed along with a 30° wedge in the vertebral body and a friction coefficient of 0.46 was defined at the PSO interface. Posteriorly affixed satellite rods had the greatest reduction of RoM compared to instrumentation with standard bilateral rods (36% in flexion/extension, 17% in lateral bending and 10% in axial rotation). After the application of a follower load representing the erect posture, stresses in the rods near the site of the PSO decreased for all configurations when adding satellite rods. Recessed short-rod technique had the highest reduction of the maximum stress values in the rods with a safety factor of 4.1 compared to 2.7 for standard bilateral rods.

2.4.2.3 Multibody and finite element hybrid models

To evaluate the effects of proximal implants, tissue dissection, and LL restoration on the risk of developing proximal junctional failure, Fradet et al. used a patient-specific multibody and finite

element hybrid model of the spine (Fradet et al., 2018). The multibody model was first used to simulate the instrumentation correction and physiological loads to estimate forces and moments within the proximal junctional spinal segment for different postoperative functional loadings. The finite element model was then used to investigate local stresses and failure in the implants and spinal components on a T10-T12 segment by implementing the resultant proximal junctional loads from the multibody model. The authors found that the risk of PJF increased with the level of resection of posterior elements as stress levels were found to be higher. When using screws at UIV, the resulting stresses were higher and more concentrated locally compared to transverse process hooks, also increasing the risk of PJF.

CHAPTER 3 RATIONALE, OBJECTIVES AND RESEARCH QUESTION

2.1 Summary of the problem

The critical review of knowledge identified the following issues related to the sagittal alignment in surgical instrumentation of ASD:

- The optimal organization of spino-pelvic parameters to have a balanced sagittal spine after surgical instrumentation for the treatment of ASD is mostly conceived in terms of geometrical considerations and is not fully biomechanically understood.
- Patient-specific optimal surgical strategy is still poorly defined and suboptimal sagittal alignment after surgical instrumentation is associated with higher rates of revision surgery.
- PSO is a highly demanding procedure due to high risk of mechanical complications such as rod breakage, screw pullout, and pseudarthrosis. Multiple risk factors impacting the rates of mechanical complications after surgical instrumentation with PSO have been identified in clinical studies. Those are greater sagittal alignment correction through varying the resection angle of the PSO and rod curvature, vertebral level of the PSO and number of rods but biomechanical knowledge of the reported risk factors is still limited.
- To assist surgeons in their preoperative planning of surgical instrumentation for the correction of sagittal imbalance with PSO, biomechanical modeling may help to reduce the rates of mechanical complications. Current preoperative planning techniques do not include prediction of postoperative alignment based on biomechanical simulations of the surgery.

3.1.1 Research question

Previous findings allow to formulate the following research question:

« *How do PSO resection angle, rod curvature, vertebral level of the PSO, and number of rods biomechanically impact the correction of sagittal balance and loads in the construct, and how should they be adjusted to reduce the risks of mechanical failure in adult spinal deformity?* »

3.1.2 Specific objectives

To answer the research question, the following objectives were defined:

First objective: Develop a personalized multi-body biomechanical model integrated in a simulation platform to simulate the surgical correction of sagittal balance with osteotomy for adult spinal deformity.

Second objective: Exploit the biomechanical model to evaluate the effects of the tested sagittal correction parameters on the distribution of forces and moments in the instrumented spine.

This thesis is built on the basis of an article in Chapter 4 that presents the key elements of the two previously described objectives. The chapter is completed by additional methodological aspects and complementary results. A general discussion as well as a conclusion and recommendations are presented in Chapter 5 and Chapter 6, respectively. The simulation platform for the surgical planning of sagittal correction with osteotomy is presented in Appendix A.

CHAPTER 4 BIOMECHANICS OF THE SURGICAL CORRECTION OF SAGITTAL BALANCE

4.1 Situation and decription of article 1

The title of the scientific article is « Biomechanical analysis of sagittal correction parameters for surgical instrumentation with pedicle subtraction osteotomy in adult spinal deformity » and was submitted to Clinical Biomechanics on March 8, 2019. The objective of this article was to assess the mechanical loads along the instrumented spine with respect to sagittal correction parameters (PSO resection angle, rod curvature, vertebral level of the PSO, and number of rods). Patient-specific biomechanical computer models of the spine were created for 3 adult cases who underwent surgery with PSO in the lumbar spine. After simulating the actual instrumentation to verify the model, the different sagittal correction parameters were alternately simulated. PSO resection angle and rod curvature were simultaneously increased or decreased by 7.5°, vertebral level of the PSO was performed one level above and one level below the actual level and different numbers of rods were simulated (2 vs. 4-rod constructs). The contribution of the first author for the preparation and writing of the article is estimated at 75%.

4.2 Article 1: Biomechanical analysis of sagittal correction parameters for surgical instrumentation with pedicle subtraction osteotomy in adult spinal deformity

David Benoit[a,b]; Xiaoyu Wang[a,b]; Dennis G. Crandall[c]; Carl-Éric Aubin[a,b]

a - Research Center, Sainte-Justine University Hospital Center, 3175, Côte Sainte-Catherine Road, Montréal, Québec H3T 1C5, Canada

b - Polytechnique Montréal, Department of Mechanical Engineering, P.O. Box 6079, Downtown Station, Montréal, Québec H3C 3A7, Canada

c - Sonoran Spine, 1255 W Rio Salado Parkway, Suite 107, Tempe, AZ 85281, USA

Original manuscript submitted to Clinical Biomechanics on March 8, 2019

4.2.1 Abstract

Background: Important rates of mechanical failures have been reported in patients who have undergone instrumentation with pedicle subtraction osteotomy (PSO). The objective was to assess the mechanical loads along the instrumented spine as functions of sagittal correction parameters.

Methods: Patient-specific biomechanical computer models of the spine were created for 3 adult cases who underwent surgery with PSO at L2 or L3. The actual instrumentation was simulated to verify the model, and then three parameters were alternately simulated: amount of sagittal correction through varying PSO wedge angle and rod sagittal contouring angle, vertebral level of the PSO and number of rods (2 vs. 4).

Findings: Increasing (or decreasing) the amount of sagittal correction by 7.5° modified the average screw axial force by +38% (-19%) and the rods bending moments by +28% (-11%) around the PSO, respectively. The bending moments in the rods were 31% lower at the PSO site for a PSO done one level above, and 20% higher for a level below. Addition of satellite rods lowered the bending moments in the rods by 24% at PSO level and lowered the average screw axial force around the PSO by 22%.

Interpretation: The amount of sagittal correction was linked to higher loads sustained by the screws and rods. Rods are subject to higher bending moments at the PSO site for a PSO done at a lower level. A 4-rod construct is an effective way to reduce the risk of rod breakage by reducing the loads sustained by the rods around the PSO level.

Highlights:

- Greater simulated subtraction pedicle osteotomy wedge angle and rod sagittal contouring in the lumbar region for sagittal plane correction of adult spinal deformity resulted in higher loads on the screws and the rods around the osteotomy level.
- A more caudally simulated pedicle subtraction osteotomy was associated with higher loads in the rods around the osteotomy level.
- Using 4-rod constructs (vs. 2 rods) reduced the loads on the screws and rods around the osteotomy level, thus the risks of mechanical failure.

Keywords: Biomechanical modeling, Pedicle subtraction osteotomy, Spinal instrumentation, Adult spinal deformity, Sagittal balance

4.2.2 Introduction

Spinal sagittal malalignment with loss of lumbar lordosis (LL) is often associated with pain and loss of function. Maintaining an erect posture in such conditions may involve increased trunk muscles activation and the use of compensatory mechanisms, such as pelvic retroversion and knee flexion. These actions are often unconsciously utilized by patients, which can lead to a compensatory thoracic hypokyphosis (Diebo et al., 2015). Health related quality of life measures worsen with the progression of the sagittal plane deformity (Glassman, Bridwell, et al., 2005; V. Lafage et al., 2009; Schwab et al., 2006). Surgical instrumentation with rods and pedicle screws is the main treatment option for cases with major disability.

In cases of rigid sagittal malalignment, pedicle subtraction osteotomy (PSO) is an effective technique to restore normal sagittal profile of the lumbar spine. This type of osteotomy extends through all three vertebral columns of the spine (Bridwell et al., 2003). It involves the resection of all posterior elements and the removal of the pedicles at the chosen vertebral level, as well as the resection of a wedge from the vertebral body. The wedge is then closed, offering a correction of up to 35° on a single level (Bridwell et al., 2003; Schwab et al., 2014).

However, the PSO is a highly demanding procedure in part due to the high loads and risk of mechanical complications such as rod breakage and pseudarthrosis (15.8 - 22%) (Smith, Shaffrey, et al., 2012; Smith et al., 2014). Common problems after 2-year follow-up can involve implant-related loosening or failures in the area of the 3-column osteotomy (3CO), which includes PSO and vertebral column resection (Smith et al., 2016). Multiple risk factors have been identified as impacting the rates of mechanical complications following surgery with PSO, such as greater sagittal alignment correction (Smith et al., 2014), rod contour angle (Barton et al., 2015; Smith et al., 2017; Tang et al., 2013) and 3CO performed at a more caudal level (Ferrero et al., 2017).

Use of a 4-rod construct is one of the solutions proposed to reduce the risk of rod fracture and to provide improved stability across the PSO site (Barrey et al., 2014). The 4-rod constructs comprise two primary rods and two auxiliary (satellite) rods over the PSO site with the later rigidly connected to the former. Hyun et al. compared radiographic outcomes for standard 2-rod constructs to multi-

rod constructs and found significant differences in the occurrence of rod breakage (17% vs. 3%) and revision surgery for pseudarthrosis at the osteotomy site (9% vs. 0%) (Hyun et al., 2014). Similarly, Gupta et al. compared outcomes for 2-rod constructs and 4-rod constructs and found a significant difference in the rates of rod breakage (25% vs. 0%) and pseudarthrosis (25% vs. 3%) (S. Gupta et al., 2017). Two *in vitro* studies investigated the effect of adding satellite rods on primary rods strain and stability at PSO level and found a significant reduction of primary rods strain and motion near the level of the osteotomy in flexion-extension (Hallager et al., 2016; La Barbera et al., 2018). Luca et al. compared different constructs following PSO using a finite element (FE) model of the lumbar spine (L1-S1) and found that 4-rod constructs reduced the maximal stress on primary rods by up to 50% (Luca et al., 2017). Using a FE model of a T12-S1 spine segment, Januszewski et al. also studied different instrumentations with PSO and found that adding additional rods reduced the stress by 29% to 50% in the primary rods (Januszewski et al., 2017).

Despite the above clinical and biomechanical investigations, stresses in the instrumentation constructs have not yet been assessed as functions of surgical maneuvers and surgeon-specified instrumentation parameters. Biomechanical knowledge of the reported risk factors and their effects on mechanical complications related to PSO are still limited to assist surgeons in their preoperative planning of sagittal imbalance correction. The objective of this study was to computationally evaluate the postoperative mechanical loads sustained by the instrumentation constructs and the spine as functions of the sagittal plane correction through varying the PSO wedge angle and rod sagittal plane contouring angle at the apex of the lumbar curve, vertebral level of the PSO, and the number of rods (standard 2-rod vs. 4-rod constructs).

4.2.3 Methods

Numerical simulations were conducted using patient-specific biomechanical models of patients operated for adult spinal deformities (ASD) in order to assess the impact of sagittal correction and instrumentation parameters (PSO wedge angle and rod sagittal plane contouring angle at the apex of the lumbar curve, vertebral level of the PSO and the number of rods) on the loads sustained by the instrumentation and the spine. Based on the actual spinal instrumentations, alternative surgical scenarios were also simulated and evaluated. Patient-specific modeling and simulation details are presented in the following subsections.

Patient-specific numerical spine models

Three ASD patients who underwent spinal instrumentation with PSO for sagittal imbalance were selected from a single medical center (Table 4-1). The inclusion criteria were preoperative sagittal vertical axis (SVA) > 5 cm and/or pelvic tilt (PT) > 25°, long instrumentation (5+ levels) and PSO performed at L2 or L3. Cases with neuromuscular or neurological conditions, tumors, inflammatory arthritis or traumatic failure were not included in the study. Pre and postoperative radiographs and surgical documentation, such as instrumentation construct details and surgical maneuvers, were retrieved. Case 1 had a revision surgery in which previous instrumentation constructs were removed and a PSO with posterior fixation was performed. Cases 2 and 3 had no revision surgery.

Table 4-1: Patient demographic data, geometric indices and instrumentation specifications

Case	Age at surgery	Sex	Weight (Kg)	Diagnosis	PREOP L1-L5 lordosis	PREOP PT	PREOP SVA (mm)	Pelvic incidence	Instrumented levels	PSO level	PSO wedge angle
1	68	M	103	Revision surgery for fixed sagittal imbalance and non-union	10°	43°	105	49°	T5-S1	L3	21°
2	78	M	89	Fixed sagittal imbalance and degenerative kyphoscoliosis	24°	34°	180	67°	T10-S1	L2	28°
3	52	F	88	Fixed sagittal imbalance and idiopathic kyphoscoliosis	39°	46°	120	55°	T5-S1	L3	33°

Using preoperative postero-anterior (PA) and lateral (LAT) radiographs, a 3-dimensional (3D) geometric model of the spine (C7-Pelvis) was built using previously developed 3D reconstruction techniques (Cheriet et al., 2007; Kadoury et al., 2007). For each vertebra, anatomical bony landmarks were identified on both radiographs, and their 2D coordinates were first computed and then used to determine their 3D coordinates in space using self-calibration and optimization algorithms (Cheriet et al., 2007; Kadoury et al., 2007). The 3D coordinates of these landmarks were used to register detailed geometric models of the vertebrae and pelvis (Cheriet et al., 2007; Kadoury et al., 2007).

The biomechanical model of the spine was implemented on the engineering platform Adams/View, (Version MD Adams 2017, MSC Software Corporation, Santa Ana, CA, USA) (Aubin et al., 2008). The vertebrae and pelvis were modeled as rigid bodies based with the assumption that their deformation would be negligible during the simulated surgery compared to the intervertebral displacement and the deformation of the intervertebral discs and ligaments. The intervertebral discs, facet joints and ligaments were modeled as flexible elements (six-dimensional springs) and their stiffness was defined using experimental data reported in the literature (Panjabi & Brand, 1976; Panjabi et al., 1994).

Modeling of instrumentation and postoperative functional loading

Multi-axial screws were simulated with the screw head and shank modeled as rigid bodies connected through a spherical kinematic joint. The screw models were aligned to their corresponding vertebra following the straight forward trajectory approach (Lehman Jr et al., 2003). The bone-screw connection was modeled as nonlinear general springs to restrain their relative motion. The nonlinear general springs were defined using load displacement relationship from in-house experimental data on cadaveric instrumented vertebrae (Aubin et al., 2008). The rods were modeled as flexible beams whose mechanical properties were based on the rod materials and geometries. The rod pre-insertion shapes were based on their 3D reconstruction from postoperative PA and LAT radiographs, with a modified contour to take into account their deformation during the surgery.

The intraoperative prone position of the patient during the surgery was modeled by applying boundary conditions to the spine model, more specifically by fixing the pelvis in space and constraining the motion of the C7 vertebra on a craniocaudal axis with three degrees of freedom in rotation. The surgical maneuvers were simulated as follows:

- Insertion of the rods in the implants above the PSO: Progressive forces were modeled between the rods and their corresponding implants until the rods were fully seated into all screw heads, for all the implants proximal to the PSO level (Figure 4.1a).
- Simulation of the PSO (Figure 4.1b):
    - Modification of the stiffness of the flexible elements representing the intervertebral discs, facet joints, and ligaments of the superior and inferior functional spinal unit,

to represent the removal of all posterior elements of the vertebral body (Salvi et al., 2016).

- Resection of a bony wedge in the vertebra.
- Closure of the PSO by simulating a modification of the posture of the patient on the operating table.
- Definition of a joint between the upper and lower part of the wedges of the PSO so that both remaining parts of the vertebral body would stay in contact during the insertion of the rods in the implants inferior to the PSO, representing the effect of the surgical compressor tool to prevent any motion.

- Insertion of the rods in the implants below the PSO: Progressive forces were modeled between the rods and their corresponding implants until the rods were fully seated into all screw heads (Figure 4.1c).
- Screw tightening: Fixed joints were modeled between all the implants and the corresponding rods.

Kinematic constraints on the C7 vertebra were removed and replaced with a flexible joint before the simulation of the PSO closure to allow sagittal plane correction and maintain global sagittal alignment.

To assess the forces sustained by the instrumentation and the spine under gravitational loading while the patient is in an upright position, the pelvis as well as the whole spine were positioned to reflect the actual postoperative PT. To maintain the postoperative SVA under gravitational loading, C7 translations in the transverse plane were blocked again and the C7 translational spring was removed.

A follower load was then applied to each vertebra (Figure 4.1d), with a magnitude proportional to the body weight of their respective body section at each vertebral level (Duval-Beaupere & Robain, 1987). The application point coincided with the flexible elements representing the discs and ligaments and their orientation was perpendicular to their respective vertebral endplate. The follower load also represents back muscles activation needed to maintain an upright posture under gravitational loading (Patwardhan et al., 1999). This loading mode was shown to have the best agreement with *in vivo* data available in the literature (Rohlmann et al., 2009).

Rods, implants and instrumentation maneuvers variables were simulated, and the results verified so that the simulated correction was close to the actual surgical result for sagittal (difference of LL, thoracic kyphosis (TK) < 5° and SVA < 1cm) and coronal (main Cobb angles < 5°, if applicable) parameters.

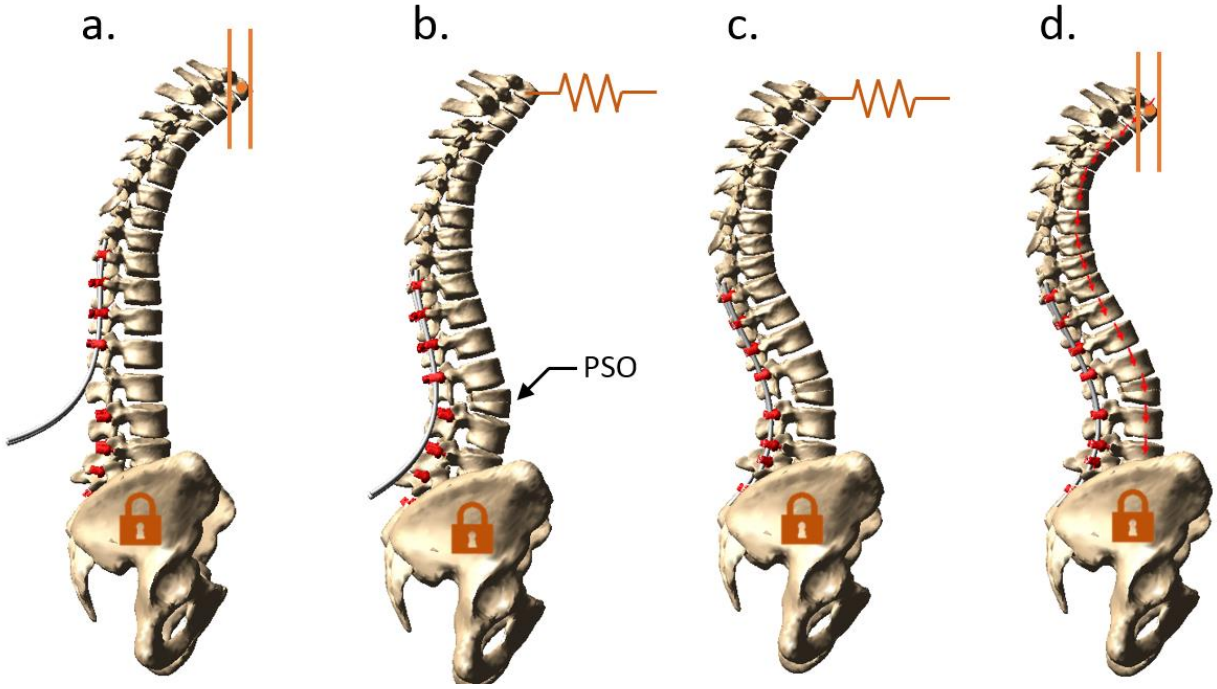

Figure 4.1: Main steps of the simulated instrumentation (case #2). (a) Insertion of the pedicle screws, and connection to the rods above the PSO. The pelvis is blocked and an inline vertical constraint is defined at C7. (b) Simulation of the PSO at L2, with a linear spring at C7 to simulate the compensatory forces to keep the posture balanced. (c) Connection of the rods to the remaining screws below the PSO. (d) Rotation of the pelvis to reach the actual postoperative PT and application of a follower load, with an inline vertical constraint at C7.

Simulation of alternative surgical strategies

The actual instrumentation was first simulated to verify the model, by comparing the simulated to the actual correction. Each case was then subject to 5 additional simulations with different surgical strategies to evaluate mechanical loads sustained by the instrumented spine. First, the sagittal correction was studied by increasing or decreasing the PSO wedge angle and the rod sagittal contouring angle at the PSO level by 7.5°. Then, the PSO was performed one level above and one level below the actual level. The sagittal contour angle of the rods was kept the same but the

location of the apex of the rods curvature was modified to be at the PSO site. Finally, different numbers of rods were simulated; the loads sustained by the conventional 2-rod constructs were compared to 4-rod constructs. The additional auxiliary rods were fixed to the primary rods one level above and one level below the PSO. The conventional 2-rod constructs were used in the actual instrumentation of the first two patients while 4-rod constructs were used for the third patient. Alternative instrumentation scenarios were therefore 4-rod constructs for the first two cases and conventional 2-rod constructs for the third case.

For alternative values of sagittal corrections, the variation in postoperative PT was estimated as a function of the regional change in LL (through PSO) and TK (through instrumentation and postoperative reciprocal changes) using a predictive linear equation reported by Lafage et al. (V. Lafage et al., 2011) (PT = 1.14 + 0.71 PI – 0.52 LL – 0.19 TK). The equation was adapted to estimate the variation of PT from the real postoperative measure: $\Delta PT = -0.52\,\Delta LL - 0.19\,\Delta TK$ (ΔPT: pelvic tilt change [°], ΔLL: lumbar lordosis change [°], ΔTK: thoracic kyphosis change [°]).

All other instrumentation parameters remained unchanged while the different surgical strategies were simulated for the three patients.

4.2.4 Results

Preoperative and postoperative standing lateral full-length spinal radiographs as well as the simulated instrumented spine are presented in Figure 4.2. The difference between the simulated and actual surgical instrumentation was below 4° for the sagittal and coronal curves and below 9 mm for SVA, which is within the measurement accuracy and a difference considered clinically unimportant (M. Gupta et al., 2016).

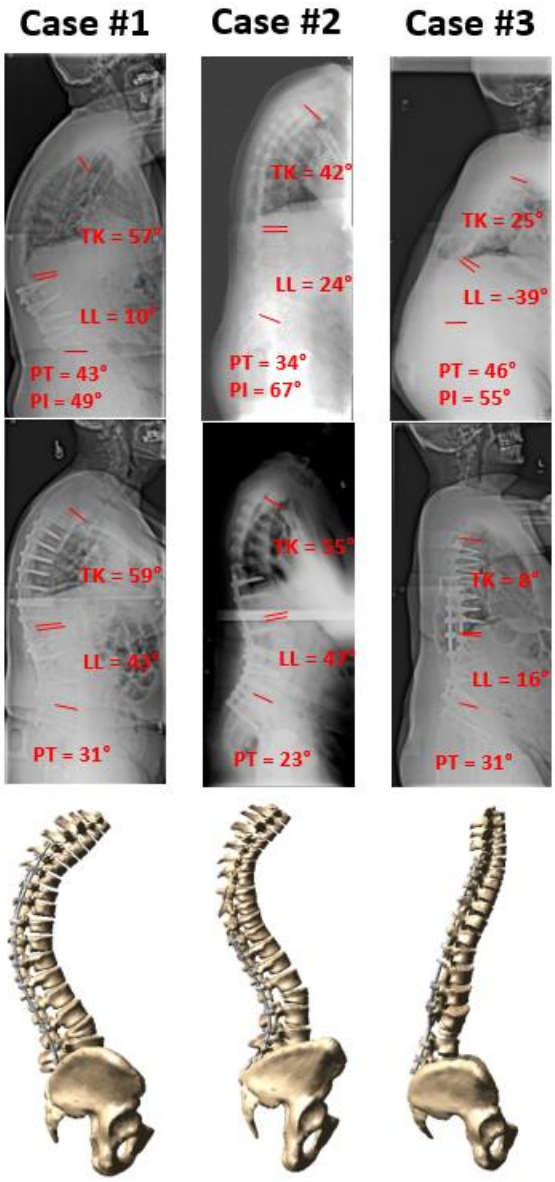

Figure 4.2: Preoperative (1st row) and postoperative (2nd row) lateral radiographs and simulated instrumented spine (3rd row)

The average axial forces for the pedicle screws directly adjacent to the PSO site were 118, 146, and 201 N for -7.5°, actual, and +7.5° sagittal correction, respectively. The average sagittal bending moments in the rods covering the PSO level were 5.9, 6.6, and 8.6 Nm, respectively (Figure 4.3). The +7.5° correction of sagittal alignment for the same cases increased screw axial forces by a mean of 38% and bending moments in the rods by 27% while -7.5° correction reduced axial forces by 19% and bending moments in the rods by 11%. For the three cases, no tendency was found for the average spinal compressive force in the intervertebral discs.

The average sagittal bending moments in the rods at the PSO level were 4.5, 6.6, and 7.9 Nm, for the PSO performed at the more cranial level, the actual level, and at the more caudal level, respectively (Figure 4.3). The bending moments in the rods at the PSO level were 31% lower for the most cranial PSO while they were 20% higher for the most caudal PSO. Local peak bending moments in the rods were located at or near the PSO site, regardless of the PSO vertebral level. For the three cases, no tendency was found for the vertebra-implant axial forces or the spinal compressive forces in the intervertebral discs.

The average screw axial forces adjacent to the PSO were 193 N for the conventional 2-rod constructs and 152 N for the 4-rod constructs, while the average bending moments in the rods at the PSO level were 7.2 and 5.4 Nm, respectively (Figure 4.3). Adding two auxiliary rods reduced average screw axial forces by 22% and the average bending moments in the rods by 24%. Figure 4.4 shows how the bending moment peak in the rods at the PSO level was reduced after adding two auxiliary rods for case #2 of the study.

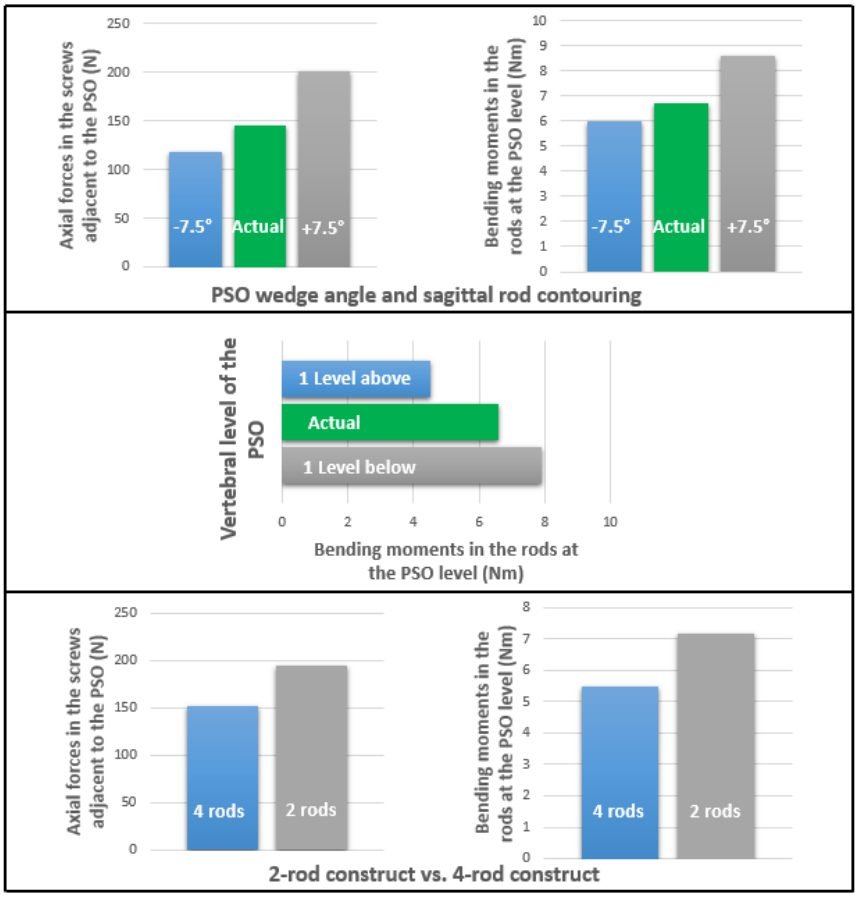

Figure 4.3: Average results for the three cases and for the different parameters tested.

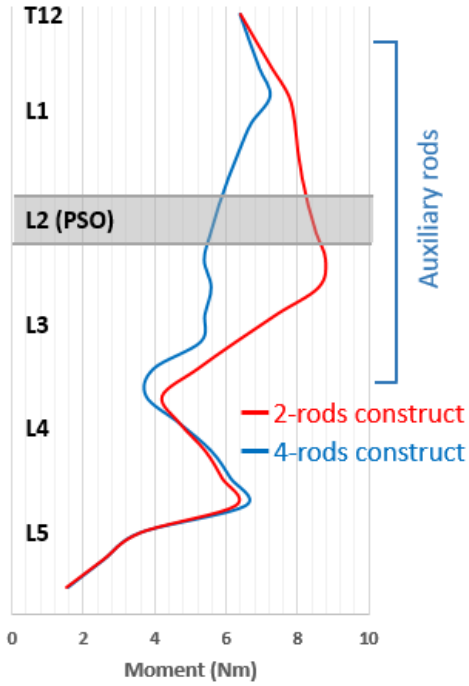

Figure 4.4: Comparison of the sagittal bending moments in the rods in the lumbar region for the 2-rod constructs and 4-rod constructs (case #2). The auxiliary rods were attached to the primary rods between T12 and L1 to between L3 and L4.

4.2.5 Discussion

The developed biomechanical model allowed to simulate spinal instrumentation with PSO for 3 adult deformity cases with sagittal malalignment, and to quantitatively evaluate the effects of sagittal correction, PSO vertebral level and different rod configurations on the loads sustained by the spine and the instrumentation constructs. Through simulations of different instrumentation scenarios derived from real surgical cases, it was found that there were between 19% and 38% differences in forces at the bone-screw connections and between 11% and 27% differences in the rod bending moments between the different degrees of sagittal correction. For all cases, screw axial forces and sagittal bending moments in the rods at the level of the PSO were higher for a larger PSO wedge angle and sagittal rod contour. This is in agreement with previous clinical studies, which demonstrated that higher rates of rod fracture (Barton et al., 2017; Smith et al., 2014) or

implant related complications (Soroceanu et al., 2015) were significantly linked to a greater magnitude of sagittal alignment correction during surgery.

Highest bending moments were always found close to the PSO site, which concurred with clinical studies reporting that rod breakages occurred mostly at this location (Smith, Shaffrey, et al., 2012; Smith et al., 2014). For the tested cases, PSO at a more distal level resulted in higher bending moments in the rod segment facing the PSO site. This could be explained by the fact that the rod segment facing the PSO supports of a greater portion of the body weight. The lever arm of the body weight above the PSO, which is supported by the rods, also increases the bending loads in the rods. Finally, performing the PSO at a more distal level required the rods to be more contoured at the more distal portion of the lumbar spine, where most of the lordotic curve is located (Le Huec et al., 2015), which results in higher bending loads in the rods. Those findings are in line with clinical studies concluding that there is a significantly greater risk of revision for instrumentation failure when 3CO is performed at a more caudal level (Ferrero et al., 2017). However, the level of the osteotomy needs to be planned based on the curve characteristics of the spine and location of previous fusion masses or pseudarthrosis (Bergin et al., 2010).

Adding auxiliary rods allowed a reduction in the bending loads in the primary rods, thus lowering risks of mechanical failure. While screw breakage or loosening is not as common as rod breakage in adult spinal instrumentation, several authors have reported rates ranging from 4% to 20% (Barton et al., 2017; Smith et al., 2016; Smith et al., 2017; Soroceanu et al., 2015). In this study, adding auxiliary rods also reduced screw axial forces and therefore the risks of implant pullout. From a structural mechanical point of view, auxiliary rods augment the instrumentation construct stiffness and reduce the range of motion at the PSO level (Hallager et al., 2016), which could reduce the loads supported by the implants. 4-rod constructs have been proposed to reduce the risks of mechanical failure near the osteotomy site (S. Gupta et al., 2017; Hyun et al., 2014), and is supported by *in-vitro* studies (Hallager et al., 2016; La Barbera et al., 2018). To achieve adequate sagittal correction, it is important to properly plan the instrumentation parameters such as PSO wedge angle, rod contouring and PSO location. Those surgical parameters can impact the risks of mechanical failure. The use of 4-rod constructs is an option that can help achieve primary surgical objectives while controlling the risks associated with this procedure.

This study focused on the effects of surgeon-specified surgical parameters; therefore, other parameters such as the fusion quality at the PSO interface were not investigated. The instability due to a poor fusion may make the instrumentation constructs subject to higher stresses and strains, and thus further reduces their fatigue life, resulting in a higher rate of rod breakage and fixation failure.

The study was performed on three adult spinal instrumentation cases with different baseline deformities (different sagittal modifiers and presence or not of coronal deformities). It revealed the effects of key mechanical risk factors common in instrumentations with PSO. The developed model could be further used to test other instrumentation constructs such as those with cages and different types of rods. Further work needs to be done to acquire comprehensive data essential for surgeons to optimize their surgical strategies and instrumentation parameters to reduce the risk of mechanical failure in adult instrumentations involving PSO.

4.2.6 Conclusions

This study assessed the biomechanical effects of different sagittal correction and instrumentation parameters on the loads sustained by the spine and instrumentation. Larger sagittal correction through PSO wedge angle and sagittal rod contour resulted in higher vertebra-implant axial forces and sagittal bending moments in the rods at the level of the PSO. PSO performed at a more caudal level was associated with higher moments sustained by the rods at the PSO level. Using 4-rod constructs reduced the loads sustained by the implants and the rods, thus potentially reducing the risks of mechanical failure. The knowledge acquired from the biomechanical simulations may help better understand the different risk factors of mechanical complications after PSO.

Acknowledgements

Thanks to Dr Maher Dammak for reading and suggesting improvements to the article.

Funding

This study was financially supported by Medtronic and the Natural Sciences and Engineering Research Council of Canada (Industrial Research Chair program with Medtronic of Canada).

4.2.7 References

1. Diebo, B.G., et al., *Sagittal alignment of the spine: What do you need to know?* Clin Neurol Neurosurg, 2015. **139**: p. 295-301.
2. Glassman, S.D., et al., *The impact of positive sagittal balance in adult spinal deformity.* Spine, 2005. **30**(18): p. 2024-2029.
3. Lafage, V., et al., *Pelvic tilt and truncal inclination: two key radiographic parameters in the setting of adults with spinal deformity.* Spine, 2009. **34**(17): p. E599-E606.
4. Schwab, F., et al., *Gravity line analysis in adult volunteers: age-related correlation with spinal parameters, pelvic parameters, and foot position.* Spine (Phila Pa 1976), 2006. **31**(25): p. E959-67.
5. Bridwell, K.H., et al., *Pedicle subtraction osteotomy for the treatment of fixed sagittal imbalance.* J Bone Joint Surg Am, 2003. **85**(3): p. 454-463.
6. Schwab, F., et al., *The comprehensive anatomical spinal osteotomy classification.* Neurosurgery, 2014. **76**: p. S33-S41.
7. Smith, J.S., et al., *Assessment of Symptomatic Rod Fracture After Posterior Instrumented Fusion for Adult Spinal Deformity.* Neurosurgery, 2012. **71**(4): p. 862-868.
8. Smith, J.S., et al., *Prospective multicenter assessment of risk factors for rod fracture following surgery for adult spinal deformity: Clinical article.* Journal of Neurosurgery: Spine, 2014. **21**(6): p. 994-1003.
9. Smith, J.S., et al., *Prospective multicenter assessment of perioperative and minimum 2-year postoperative complication rates associated with adult spinal deformity surgery.* J Neurosurg Spine, 2016. **25**(1): p. 1-14.
10. Smith, J.S., et al., *Complication rates associated with 3-column osteotomy in 82 adult spinal deformity patients: retrospective review of a prospectively collected multicenter consecutive series with 2-year follow-up.* J Neurosurg Spine, 2017. **27**(4): p. 1-14.
11. Tang, J.A., et al., *Effect of severity of rod contour on posterior rod failure in the setting of lumbar pedicle subtraction osteotomy (PSO): a biomechanical study.* Neurosurgery, 2013. **72**(2): p. 276-282; discussion 283.
12. Barton, C., et al., *Risk factors for rod fracture after posterior correction of adult spinal deformity with osteotomy: a retrospective case-series.* Scoliosis, 2015. **10**: p. 30.
13. Ferrero, E., et al., *Sagittal alignment and complications following lumbar 3-column osteotomy: does the level of resection matter?* J Neurosurg Spine, 2017. **27**(5): p. 560-569.
14. Barrey, C., et al., *Pedicle subtraction osteotomy in the lumbar spine: indications, technical aspects, results and complications.* Eur J Orthop Surg Traumatol, 2014. **24**(1): p. 21-30.
15. Hyun, S.J., et al., *Comparison of standard 2-rod constructs to multiple-rod constructs for fixation across 3-column spinal osteotomies.* Spine (Phila Pa 1976), 2014. **39**(22): p. 1899-1904.

16. Gupta, S., et al., *A novel 4-Rod technique offers potential to reduce rod breakage and pseudarthrosis in pedicle subtraction osteotomies for adult spinal deformity correction.* Operative Neurosurgery, 2017. **14**(4): p. 449-456.

17. Hallager, D.W., et al., *Use of Supplemental Short Pre-Contoured Accessory Rods and Cobalt Chrome Alloy Posterior Rods Reduces Primary Rod Strain and Range of Motion Across the Pedicle Subtraction Osteotomy Level: An In Vitro Biomechanical Study.* Spine (Phila Pa 1976), 2016. **41**(7): p. E388-395.

18. La Barbera, L., et al., *Biomechanical advantages of supplemental accessory and satellite rods with and without interbody cages implantation for the stabilization of pedicle subtraction osteotomy.* Eur Spine J, 2018. **27**(9): p. 2357-2366.

19. Luca, A., et al., *Instrumentation failure following pedicle subtraction osteotomy: the role of rod material, diameter, and multi-rod constructs.* Eur Spine J, 2017. **26**(3): p. 764-770.

20. Januszewski, J., et al., *Biomechanical study of rod stress after pedicle subtraction osteotomy versus anterior column reconstruction: A finite element study.* Surgical neurology international, 2017. **8**. 207

21. Kadoury, S., et al., *A versatile 3D reconstruction system of the spine and pelvis for clinical assessment of spinal deformities.* Med Biol Eng Comput, 2007. **45**(6): p. 591-602.

22. Cheriet, F., et al., *A novel system for the 3-D reconstruction of the human spine and rib cage from biplanar X-ray images.* IEEE Trans Biomed Eng, 2007. **54**(7): p. 1356-1358.

23. Aubin, C.E., et al., *Preoperative planning simulator for spinal deformity surgeries.* Spine, 2008. **33**(20): p. 2143-2152.

24. Panjabi, M.M. and J.R. Brand, *Mechanical properties of the human thoracic spine as shown by three-dimensional load-displacement curves.* The Journal of bone and joint surgery. American volume, 1976. **58**(5): p. 642-652.

25. Panjabi, M.M., et al., *Mechanical behavior of the human lumbar and lumbosacral spine as shown by three-dimensional load-displacement curves.* JBJS, 1994. **76**(3): p. 413-424.

26. Lehman Jr, R.A., et al., *Straight-forward versus anatomic trajectory technique of thoracic pedicle screw fixation: a biomechanical analysis.* Spine, 2003. **28**(18): p. 2058-2065.

27. Salvi, G., et al., *Biomechanical analysis of Ponte and pedicle subtraction osteotomies for the surgical correction of kyphotic deformities.* Eur Spine J, 2016. **25**(8): p. 2452-2460.

28. Duval-Beaupere, G. and G. Robain, *Visualization on full spine radiographs of the anatomical connections of the centres of the segmental body mass supported by each vertebra and measured in vivo.* International orthopaedics, 1987. **11**(3): p. 261-269.

29. Patwardhan, A.G., et al., *A follower load increases the load-carrying capacity of the lumbar spine in compression.* Spine, 1999. **24**(10): p. 1003-1009.

30. Rohlmann, A., et al., *Applying a follower load delivers realistic results for simulating standing.* J Biomech, 2009. **42**(10): p. 1520-1526.

31. Lafage, V., et al., *Spino-pelvic parameters after surgery can be predicted: a preliminary formula and validation of standing alignment.* Spine (Phila Pa 1976), 2011. **36**(13): p. 1037-1045.

32. Gupta, M., et al., *Dedicated Spine Measurement Software Quantifies Key Spino-Pelvic Parameters More Reliably Than Traditional Picture Archiving and Communication Systems Tools.* Spine (Phila Pa 1976), 2016. **41**(1): p. E22-E27.

33. Barton, C., et al., *Different types of mechanical complications after surgical correction of adult spine deformity with osteotomy.* World Journal of Meta-Analysis, 2017. **5**(6): p. 132-149.

34. Soroceanu, A., et al., *Radiographical and Implant-Related Complications in Adult Spinal Deformity Surgery: Incidence, Patient Risk Factors, and Impact on Health-Related Quality of Life.* Spine (Phila Pa 1976), 2015. **40**(18): p. 1414-1421.

35. Le Huec, J.C., et al., *Evidence showing the relationship between sagittal balance and clinical outcomes in surgical treatment of degenerative spinal diseases: a literature review.* Int Orthop, 2015. **39**(1): p. 87-95.

36. Bergin, P.F., et al., *The use of spinal osteotomy in the treatment of spinal deformity.* Orthopedics, 2010. **33**(8): p. 586-594.

37. Daniels, A.H., et al., *Rod Fracture After Apparently Solid Radiographic Fusion in Adult Spinal Deformity Patients.* World Neurosurg, 2018. **117**: p. e530-e537.

4.3 Complementary methodological aspects

4.3.1 Biomechanical model of the spine

The personalized biomechanical multi-body model developed with Adams/View, (Version MD Adams 2017, MSC Software Corporation, Santa Ana, CA, USA) software and presented in the manuscript (section 4.2) is here further described.

The vertebrae (C7 to L5) and pelvis were modeled as rigid bodies with the assumption that their deformation was unimportant compared to the intervertebral displacement and the deformation of the intervertebral discs and ligaments. The vertebrae and pelvis were successively connected by flexible elements representing the intervertebral discs, facet joints and ligaments. Those flexible elements were connected to the center of mass of adjacent vertebrae (Figure 4.5) and their stiffness matrix was defined using data from experimental tests conducted on thoracic and lumbar vertebral units (Gardner-Morse & Stokes, 2004; Panjabi & Brand, 1976) (Equations 1 and 2).

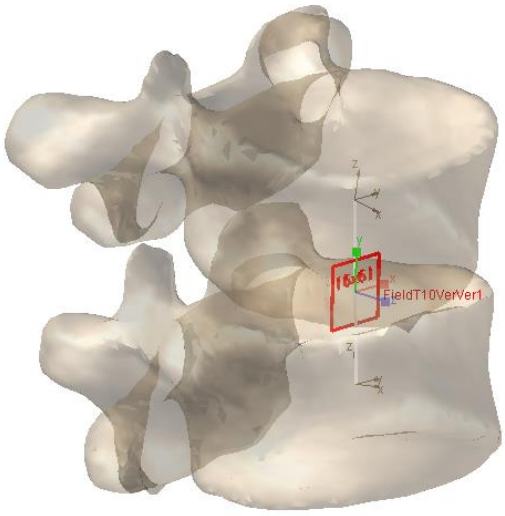

Figure 4.5: Flexible element connected to the center of mass of adjacent vertebrae along with their respective axis system

Equation 1: Stiffness matrix of the thoracic vertebral units (Panjabi & Brand, 1976)

$$k_{thoracic} = \begin{bmatrix} 100 & 0 & 50 & 0 & -1640 & 0 \\ 0 & 110 & 0 & 150 & 0 & 580 \\ 50 & 0 & 780 & 0 & -760 & 0 \\ 0 & 150 & 0 & 148000 & 0 & -8040 \\ -1640 & 0 & -760 & 0 & 152000 & 0 \\ 0 & 580 & 0 & -8040 & 0 & 153000 \end{bmatrix}$$

Equation 2: Stiffness matrix of the lumbar vertebral units (Gardner-Morse & Stokes, 2004)

$$k_{lumbar} = \begin{bmatrix} 251 & 0 & 0 & 0 & -6510 & 0 \\ 0 & 332 & 0 & 6960 & 0 & -11000 \\ 0 & 0 & 438 & 0 & 1370 & 0 \\ 0 & 6960 & 0 & 174000 & 0 & -235000 \\ -6510 & 0 & 1370 & 0 & 241000 & 0 \\ 0 & -11000 & 0 & -235000 & 0 & 564000 \end{bmatrix}$$

4.3.2 Modeling of instrumentation maneuvers and postoperative functional loading

To model the instrumentation maneuvers and postoperative functional loading, a quasi-static approach was used. This approach allows to reduce simulation time since the dynamic effects of the surgical maneuvers are negligible.

Initial boundary conditions

To simulate the intraoperative prone position of the patient, a fixed joint was defined on the pelvis and motion of the C7 vertebra was constrained so that only translation on a craniocaudal axis and rotation in all planes were allowed (Figure 4.6).

Figure 4.6: Initial boundary conditions

Insertion of the rods in the implants proximal to the PSO level

Rods were inserted in the most proximal implants at the UIV and a fixed kinematic joint was modeled between the screw head and the inserted rod segment for both sides. The rods were then inserted in all implants proximal to the PSO level using progressive forces between the rods and their corresponding implants, until the rods were fully seated into all screw heads. Cylindrical joints were modeled between all screw heads and their respective rod segments to only allow translation and rotation along the main axis of the rod segments (Figure 4.7).

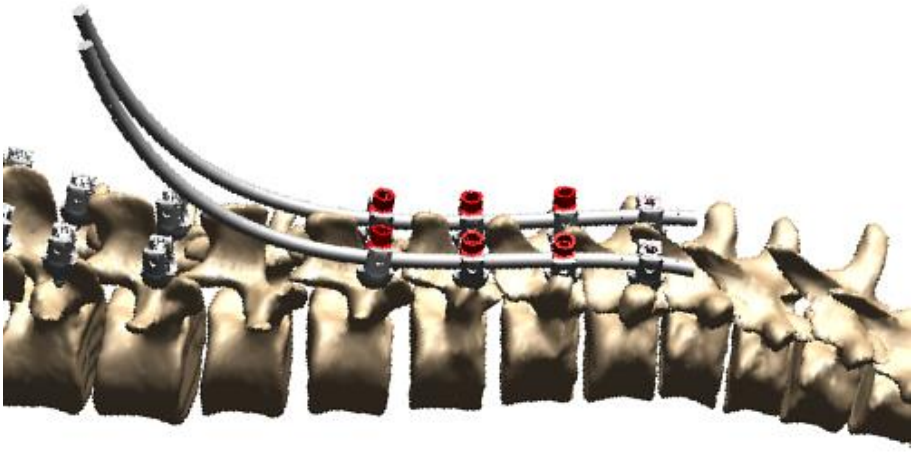

Figure 4.7: Insertion of the rods in the implants proximal to the PSO

Pedicle subtraction osteotomy

Stiffness of the superior and inferior vertebral units were reduced to account for the removal of all posterior ligaments and the geometry of the vertebra was modified to represent the removal of a wedge in the vertebral body and closure of the two remaining vertebral segments (Salvi, 2014). The reduction of stiffness from the removal of all posterior ligaments was modeled by multiplying coefficients to the rotational terms (k_{44}, k_{55} and k_{66}) of the vertebral units stiffness matrices presented in section 4.3.1. Those coefficients were obtained from cadaveric experimental tests (Gardner-Morse & Stokes, 2004) (Equation 3).

Equation 3: Stiffness matrix of lumbar vertebral units with reduced rotational terms to model removal of posterior elements (Gardner-Morse & Stokes, 2004)

$$k_{lumbar} = \begin{bmatrix} 251 & 0 & 0 & 0 & -6510 & 0 \\ 0 & 332 & 0 & 6960 & 0 & -11000 \\ 0 & 0 & 438 & 0 & 1370 & 0 \\ 0 & 6960 & 0 & A*174000 & 0 & -235000 \\ -6510 & 0 & 1370 & 0 & B*241000 & 0 \\ 0 & -11000 & 0 & -235000 & 0 & C*564000 \end{bmatrix} \quad where \quad \begin{matrix} A = 0.302 \\ B = 0.208 \\ C = 0.086 \end{matrix}$$

The model's anatomical markers belonging to the vertebral body were then divided into two separate rigid bodies, connected by a revolute kinematic joint located on the most anterior part of the vertebra, at an equal distance between the superior and inferior vertebral end plates. The superior part of the vertebra was then rotated with respect to the lower part by the specified wedge angle. A fixed joint was then defined between the superior and inferior parts of the vertebral body to simulate the effect of a surgical compressor tool attached to the pedicles of the vertebrae directly adjacent to the PSO, locking both vertebral bodies of the PSO together (Singh et al., 2015) (Figure 4.8).

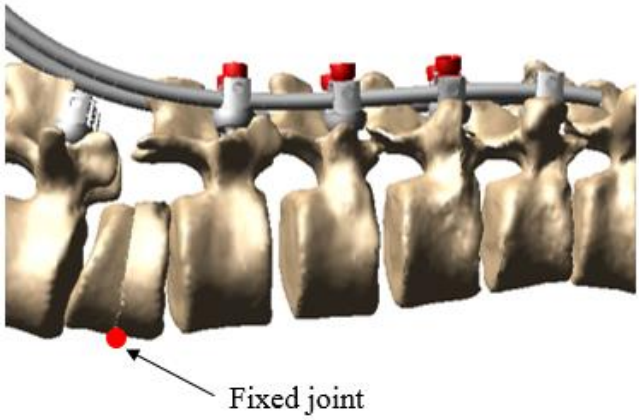

Figure 4.8: Simulation of the PSO

To allow sagittal plane correction during the closure of the PSO, the initial kinematic constraint defined on C7 vertebra was removed. Reciprocal changes in the unfused thoracic spinal segment (V. Lafage, Ames, et al., 2012) were simulated by adding a sagittal translational spring attached to C7 and exerting a postero-anterior force on the upper segment of the spine (Figure 4.9). Stiffness coefficient of the spring was iteratively adjusted until actual postoperative SVA was reached.

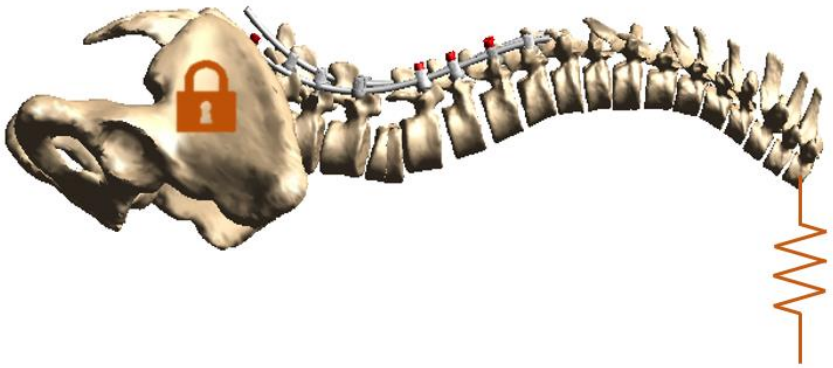

Figure 4.9: Boundary conditions for the closure of the PSO

After closure of the PSO, the translational spring on C7 was replaced by the initial boundary condition at the new position of C7, only allowing translation on a craniocaudal axis and rotation in all planes.

Insertion of the rods in the implants distal to PSO level

The rods were then inserted in all implants distal to PSO level by applying progressive forces between the rods and implants. Cylindrical joints were modeled between all screw heads and their respective rod segments.

Tightening of all screws

Fixed joints were modeled between all screw heads and their respective rod segments to simulate tightening of the screws.

Attachment of auxiliary rods

For cases with 4-rod constructs, auxiliary rods were added at the last step of surgery. The auxiliary rods were made of the same material and had the same diameter as the main rods. They were positioned laterally to the main rods, at a distance of 15 mm. Fixed constraints were defined between the ends of the auxiliary rods and their respective adjacent segments of the main rods to model auxiliary rods connectors, based on the assumption that their deformation was negligible compared to the deformation of the rods. Auxiliary rods covered the zone of the PSO, as well as the vertebral levels directly adjacent to the PSO (Figure 4.10).

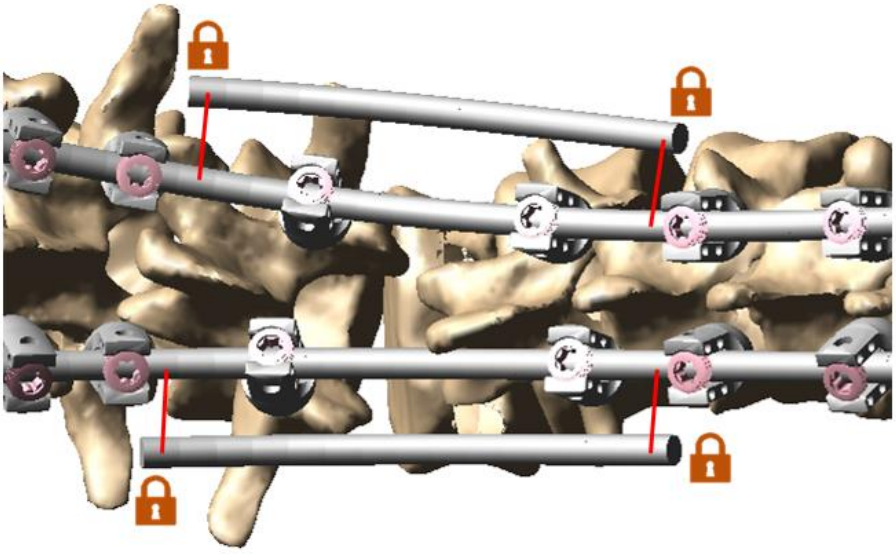

Figure 4.10: Auxiliary rods covering the segment of the PSO

Application of gravitational loads

After all surgical maneuvers were simulated, gravitational loads were added to the spinal construct to represent a postoperative erect posture. The magnitude of the forces applied on each vertebra was proportional to the body weight of their corresponding transverse vertebral section (Duval-Beaupere & Robain, 1987) (Table 4-2).

All gravitational forces were perpendicular to their respective superior vertebral endplate and located at the center of mass of their vertebra. The gravitational axial forces allowed to simulate a follower load representing the activation of back muscles needed to maintain an upright posture under gravitational loading. The follower load was shown to considerably increase load-carrying capacity of the lumbar spine when the application point of the forces was near the center of rotation of the vertebral segments, which provides an explanation of how the lumbar spine can resist large compressive loads (Patwardhan et al., 1999). This loading mode was also shown to agree with *in vivo* data for calculated values of intervertebral rotations and intradiscal pressures (Rohlmann et al., 2009).

Table 4-2: % of body weight applied on each vertebra

Vertebral level	Body weight of transverse vertebral section (%)
C7	8.24
T1	1.12
T2	3.02
T3	7.09
T4	1.97
T5	1.78
T6	1.81
T7	1.63
T8	1.75
T9	1.71
T10	1.86
T11	2.25
T12	2.47
L1	2.54
L2	2.43
L3	2.42
L4	2.40
L5	2.77

4.4 Verification, validation and uncertainty quantification

Verification, validation and uncertainty quantification of the biomechanical model aimed at establishing the credibility of the model and its outputs and was done following the ASME standard « V&V 40 - 2018 » (ASME V&V 40, 2018). Verification of the model allows to assess if the underlying mathematical model was solved correctly while validation of the model allows to assess if the underlying mathematical model correctly represents the reality of interest. Uncertainty quantification allows to define the uncertainty of the inputs of the model and assess how the studied outputs are affected by those uncertainties.

Establishing the model's credibility is essential to build confidence in its ability to predict results for the investigated parameters. In this study, the context of use of the model was the simulation of surgical instrumentation for the correction of sagittal alignment for adult spinal deformity and the reality of interest was more specifically the PSO. The model was used to assess how PSO resection

angle, rod curvature, vertebral level of the PSO, and number of rods biomechanically impact the correction of sagittal balance and loads in the instrumentation. To demonstrate the credibility of the model, different steps were undertaken.

Retrospective data such as pre and postoperative radiographs and surgical documentation were used to reconstruct the preoperative spine and the rods in 3D and simulate the surgical maneuvers. The simulated results were compared to the actual surgery using sagittal (SVA, TK, LL, PT) and coronal (Cobb angles) geometrical indices measured on postoperative radiographs. The model was considered adequate if the difference between the geometrical indices of the simulated and the actual correction were below the reported variability for intra- and inter-observer measurement (M. Gupta et al., 2016; Polly Jr et al., 1996), and below what is considered clinically important difference by many authors for the angle measurements (5°) (Shea et al., 1998). This calibration allowed to ensure that the model can adequately replicate baseline data. Results are presented in section 4.4.1.

The credibility of the model was then further assessed by comparing the simulations to relevant data available in the literature. The axial forces in the model at the implant-vertebra interface were compared to the pull-out forces reported by Liljenqvist to confirm that the loads sustained by the screws were below failure (Liljenqvist et al., 2001).

Finally, an evaluation was conducted to assess how sensitive the simulation results (loads in the instrumentation) were to uncertainties of some input parameters. A quantification of the uncertainties for the three studied parameters is presented below. The first evaluated parameter is the PSO wedge angle. In the study presented in section 4.1, PSO wedge angle and sagittal rod contouring angle were simultaneously modified by ± 7.5°. A sensitivity analysis was conducted to study the effects of a possible mismatch between the adjusted rod sagittal contour and curve of the LL after PSO. The initial rod sagittal contour was defined using postoperative radiographs and was adjusted using an automatic script for the different degrees of sagittal correction, limiting the possible mismatch. Three different PSO wedge angles were tested: the reference PSO wedge angle (28°), PSO wedge angle increased by 1.5° (ref +1.5°) and PSO wedge angle decreased by 1.5° (ref -1.5°). The second evaluated parameter is the intervertebral stiffness and the test was conducted to assess how the selected intervertebral stiffness affected the loads supported by the instrumentation. The spine may be more or less stiff for different patients and surgeons may

practice osteotomies to make the spine more flexible, in turn allowing to achieve adequate correction. Removal of the facets and resection of the interspinous ligament, spinous process and ligamentum flavum have been reported to increase displacements by 15% when inducing lordosis (C. Wang et al., 2015). Three intervertebral stiffness levels were tested: reference intervertebral stiffness presented in section 4.3.1, reference stiffness increased by 15% (ref +15%) and reference stiffness decreased by 15% (ref -15%). Impact of this parameter on the loads supported by the instrumented spine was investigated with simulations of variable degrees of sagittal correction. The last evaluated parameter is the postoperative PT. In the study reported in section 4.1, the simulated PT was estimated using a predictive linear equation reported by Lafage et al. (V. Lafage, Bharucha, et al., 2012) when alternative degrees of sagittal corrections (through rod contour and PSO wedge angle) were simulated. Authors reported a median absolute error of 4.1° between formula predicted PT and actual postoperative PT. To study the effect of this parameter, simulated postoperative PT (23°) was therefore modified by ±5°. The pelvis as well as the whole spine were rotated around the pelvis. Three different PT values were tested: the reference PT, PT increased by 5° (ref +5°) and PT decreased by 5° (ref -5°). Impact of this parameter on the loads supported by the instrumented spine was investigated with simulations of different degrees of sagittal correction. Simulations were conducted for different degrees of sagittal correction to assess the relative percentage difference in the loads supported by the instrumented spine and quantification of the sensitivity of those three parameters is presented in section 4.4.2.

4.4.1 Comparison of the simulated results to the actual surgery

The simulated results for the three cases of the study are compared to the actual surgery and are presented in Table 4-3,Table 4-4 and Table 4-5. The developed model allowed to adequately represent actual surgical instrumentation with a difference of less than 4° for sagittal and coronal curves and 8 mm or less for SVA which are below the reported variability for intra- and inter-observer measurements (M. Gupta et al., 2016; Polly Jr et al., 1996) and below the clinically important difference for the angle measurements (Shea et al., 1998).

Table 4-3: Comparison of the geometrical indices for the actual surgery and the simulated results for case #1

Geometrical indices		Actual surgery	Simulated results	Delta
Sagittal	TK	59°	63°	4°
	LL	43°	47°	4°
	PT	31°	31°	0°
	SVA	105 mm	106 mm	1 mm
Coronal	T1-T5	3°	4°	1°
	T6-T12	5°	2°	3°
	L1-L5	2°	0°	2°

Table 4-4: Comparison of the geometrical indices for the actual surgery and the simulated results for case #2

Geometrical indices		Actual surgery	Simulated results	Delta
Sagittal	TK	55°	59°	4°
	LL	47°	44°	3°
	PT	23°	23°	0°
	SVA	65 mm	62 mm	3 mm
Coronal	T1-T5	2°	4°	2°
	T6-T12	1°	2°	1°
	L1-L5	7°	4°	3°

Table 4-5: Comparison of the geometrical indices for the actual surgery and the simulated results for case #3

Geometrical indices		Actual surgery	Simulated results	Delta
Sagittal	TK	8°	5°	3°
	LL	16°	12°	4°
	PT	31°	31°	0°
	SVA	27 mm	35 mm	8 mm
Coronal	T1-T5	20°	19°	1°
	T6-T12	45°	44°	1°
	L1-L5	35°	31°	4°

4.4.2 Sensitivity analyses

Sensitivity analyses were conducted on modeling parameters that were difficult to precisely measure in order to assess how the simulation results were impacted. Impact of modeling parameters on loads supported by the instrumented spine was investigated for case #2 presented in the scientific article.

PSO wedge angle

Results for the loads supported by the rods and screws adjacent to PSO level are reported in Table 4-6 and Table 4-7. A 1.5° variation of the PSO wedge angle impacted the vertebra-implant axial forces on average by 8.5 N with the maximum relative difference for the tested PSO wedge angles being 9 N (8.2%). The relative percentage difference of screw axial forces for different degrees of sagittal correction was smaller than 5%. The impact of this parameter on the bending moment in the rods was on average 0.4 Nm with the maximum relative difference for the tested PSO wedge angles being 0.6 Nm (10%). The relative percentage difference of bending moments in the rods for different degrees of sagittal correction was smaller than 6%.

Table 4-6: Vertebra-implant axial forces (N) adjacent to PSO level for different degrees of sagittal correction when varying the reference PSO wedge angle (28°) by ±1.5° (% increase or decrease from Reference)

	Sagittal correction angle		
	-7.5°	**Actual**	**+7.5°**
Reference PSO wedge angle (28°)	104 N	139 N	193 N
Ref +1.5°	113 N (+8.2%)	149 N (+7.0%)	202 N (+4.3%)
Ref -1.5°	101 N (-3.1%)	130 N (-6.3%)	182 N (-5.9%)

Table 4-7: Bending moments (Nm) in the rods adjacent to PSO level for different degrees of sagittal correction when varying PSO wedge angle (28°) by ±1.5° (% increase or decrease from Reference)

	Sagittal correction angle		
	-7.5°	**Actual**	**+7.5°**
Reference PSO wedge angle (28°)	5.8 Nm	6.7 Nm	7.2 Nm
Ref +1.5°	6.3 Nm (+8.7%)	7.1Nm (+7.0%)	7.5 Nm (+4.2%)
Ref -1.5°	5.2 Nm (-10.0%)	6.4 Nm (-4.2%)	6.8 Nm (-6.2%)

Intervertebral stiffness

The loads supported by the rods and screws adjacent to the PSO level are reported in Table 4-8 and Table 4-9. The impact of the variation of the intervertebral stiffness by 15% on vertebra-implant axial forces was on average 5 N, with the maximum relative difference for the tested PSO wedge angles being 5 N (4.9%). Relative percentage difference of screw axial forces for different degrees of sagittal correction was smaller than 5%. The bending moments in the rods were impacted on average by 0.4 Nm, with the maximum relative difference for the tested PSO wedge angles being 0.7 Nm (9.4%). Relative percentage difference of bending moments in the rods for different degrees of sagittal correction was up to 7.8%. Results of the simulations can be exploited having such effects in mind when interpreting the results of the comparative study to assess loads on the instrumentation.

Table 4-8: Vertebra-implant axial forces (N) adjacent to PSO level for different variations of the degrees of sagittal correction when varying intervertebral stiffness by ±15% (% increase or decrease from Reference)

	Sagittal correction angle		
	-7.5°	**Actual**	**+7.5°**
Reference	104 N	139 N	193 N
Ref +15%	109 N (+4.9%)	142 N (+1.8%)	198 N (+2.6%)
Ref -15%	100 N (-3.9%)	142 N (+2.4%)	203 N (+4.8%)

Table 4-9: Bending moments in the rods (Nm) adjacent to PSO level for different variations of the degrees of sagittal correction when varying intervertebral stiffness by ±15% (% increase or decrease from Reference)

	Sagittal correction angle		
	-7.5°	**Actual**	**+7.5°**
Reference	5.8 Nm	6.7 Nm	7.2 Nm
Ref +15%	6.3 Nm (+7.9%)	7.2 Nm (+8.4%)	7.9 Nm (+9.4%)
Ref -15%	5.4 Nm (-7.4%)	6.1 Nm (-9.2%)	7.1 Nm (-1.4%)

Postoperative PT

The loads supported by the rods and screws adjacent to PSO level are reported in Table 4-10 and

Table 4-11. The impact of the variation of postoperative PT by 5° on the vertebra-implant axial forces was on average 3.5 N, with the maximum relative difference for the tested PSO wedge angles being 11 N (5.5%). The relative percentage difference of screw axial forces for different degrees of sagittal correction was smaller than 5%. For the impact on the bending moments in the rods, difference was on average 0.2 Nm, with the maximum relative difference for the tested PSO wedge angles being 0.4 Nm (5.5%). Relative percentage difference of bending moments in the rods for different degrees of sagittal correction was smaller than 5%.

Table 4-10: Vertebra-implant axial forces (N) adjacent to PSO level for different degrees of sagittal correction when varying postoperative PT (23°) by ±5° (% increase or decrease from Reference)

	Sagittal correction angle		
	-7,5°	**Actual**	**+7,5°**
Reference	104 N	139 N	193 N
Ref +5°	103 N (-1.1%)	140 N (+0.5%)	204 N (+5.5%)
Ref -5°	108 N (+3.5%)	139 N (-0.4%)	197 N (+1.7%)

Table 4-11: Bending moments in the rods (Nm) adjacent to the PSO level for different degrees of sagittal correction when varying postoperative PT (23°) by ±5° (% increase or decrease from Reference)

	Sagittal correction angle		
	-7,5°	**Actual**	**+7,5°**
Reference	5.8 Nm	6.7 Nm	7.2 Nm
Ref +5°	6.0 Nm (+3.2%)	6.9 Nm (+3.4%)	7.6 Nm (+5.5%)
Ref -5°	5.6 Nm (-2.8%)	6.5 Nm (-3.3%)	7.3 Nm (+0.6%)

4.5 Complementary studies

4.5.1 Sagittal moment on the pelvis

Table 4-12 presents the sagittal plane moments on the pelvis after the simultaneous variation of the PSO wedge angle and rod contour, complementary to the results already reported in section 3.1.1. The sagittal plane moments on the pelvis on average are 6.0, 2.6 and -3.2 Nm for the -7.5°, actual, and +7.5° sagittal correction, respectively.

Table 4-12: Sagittal moment on the pelvis in relation to the simulated sagittal correction (simultaneous variation of the PSO wedge angle and rod contour)

Case	- 7.5° Sagittal correction (Nm)	Actual sagittal correction (Nm)	+ 7.5° Sagittal correction (Nm)
1	10.5	3.7	-3.6
2	3.9	0.0	-2.6
3	3.5	4.2	-3.5
Mean	6.0	2.6	-3.2

CHAPTER 5 GENERAL DISCUSSION

The work presented in this master's thesis aimed at assessing the biomechanical impact of different sagittal correction parameters on the correction of sagittal balance and loads in the spine and instrumentation. A personalized multi-body biomechanical model was adapted to simulate surgical correction of ASD with PSO. The biomechanical model was exploited to evaluate the effects of PSO wedge angle, sagittal rod contouring, level of the PSO and number of rods used on the distribution of forces and moments in the spine and instrumentation. A simulation platform integrating the biomechanical model was developed as an interface to help planning and defining the surgical correction steps through Matlab. This biomechanical simulator allows to plan the major steps of the surgery, conduct a biomechanical simulation of the surgery, and analyze results on the basis of sagittal correction and loads in the instrumented spine.

5.1 Interpretation of the biomechanical simulations and of the parametric study

Simulations of the spinal instrumentation with PSO for the treatment of sagittal malalignment was conducted with three surgical cases. A more pronounced (7.5°) correction of the lumbar sagittal curve increased vertebra-implant axial forces and bending moments in the rods near the level of the PSO, which is inferred as higher risks of mechanical failure, in agreement with multiple clinical studies reporting higher rates of mechanical failures for greater sagittal alignment correction (Barton et al., 2017; Smith et al., 2014; Soroceanu et al., 2015). Inversely, the loads supported by the instrumentation decreased for a smaller (-7.5°) sagittal correction. The loads supported by the instrumentation and spine are shared differently as rod contour increases. Under gravitational loading, more bended rods are subject to higher bending moments in the sagittal plane. Higher bending moments resulted in higher stress, which could be interpreted as decreasing fatigue life and increasing chances of mechanical failure.

Bending moments in the rods at the PSO level were higher for a more caudal PSO, in agreement with a clinical study that similarly assessed instrumentation failure (Ferrero et al., 2017). Local peak bending moments in the rods were located at or near the PSO site, regardless of PSO vertebral level, which could be explained by the fact that the apex of the curvature of the rods were adjusted to be at PSO level for all different scenarios evaluated. Furthermore, the absence of fixation at the

PSO level creates a longer lever arm in the rods between the adjacent upper and lower vertebral levels to the PSO, in turn leading to a greater bending moment.

Adding auxiliary rods reduced average and peak vertebra-implant axial forces and bending moments in the rods through a load sharing mechanism, which would increase fatigue life of the main rods at their most vulnerable location. To attain proper postoperative sagittal alignment of the spine, surgical strategies associated with higher risks of instrumentation failures (such as performing a PSO with a larger wedge angle or at a more caudal level) are sometimes necessary. However, using an instrumentation construct with auxiliary rods may help to lower such risks.

Higher vertebral compression forces as opposed to higher loads sustained by the instrumentation may help to reduce the risks of instrumentation failure and improve the stability of the spine, particularly near the level of the PSO. For the different sagittal correction parameters tested in this study, no difference was found for the vertebral compression loads. Postoperative gravitational loads and stabilization of the spine by back muscles, which were modeled using the follower load method, may be a limiting factor to fully assess vertebral compression loads. The magnitude and orientation of the loads supported by the intervertebral discs may be affected by the alignment of the spine. However, the follower forces were always perpendicular to their respective superior vertebral endplate in the model.

The computed sagittal plane moment at the pelvis could be interpreted to estimate the muscular effort necessary to postoperatively maintain the posture and pelvic orientation. For the smaller simulated correction of sagittal alignment (-7.5°) the sagittal moments were always positive, indicating that an extension compensation is necessary to maintain the specified standing posture, and therefore supplementary forces are required to achieve postural stability. Inversely, for the greater sagittal correction simulations (+7.5°), moments always were negative, indicating the necessity of flexion compensation mechanism to maintain the specified standing posture. An equilibrated moment should be the target to minimize the compensation mechanisms to stabilize the spine. Minimal compensation was observed for case #2 while a slight extension compensation was necessary to maintain the specified standing posture for cases #1 and #3. By offering a quantitative assessment of the efforts necessary to balance a specified posture, the surgical planning tool offers valuable information about the ergonomics and energy economy of the posture, essential to the long-term success of spinal deformity treatment.

Different steps were undertaken to verify and validate the model. Simulated correction was compared to actual postoperative correction using the radiographic indices. The developed model allowed to adequately represent actual surgical instrumentation with a difference of less than 4° for sagittal and coronal curves and 8 mm or less for SVA, which is below the reported variability for intra- and inter-observer measurement of radiographic indices (M. Gupta et al., 2016; Polly Jr et al., 1996), and below what is considered clinically important difference by many authors for the angle measurements (5°) (Shea et al., 1998). The loads supported by the screws were all below the threshold of the pullout force (Liljenqvist et al., 2001), meaning that the loads supported by the pedicle screws were of reasonable magnitude. The absolute values of the loads may not be validated in this study but demonstrating that they are of realistic magnitude is an important step in assessing the credibility of the model even though the conclusions drawn from this study are based on relative comparisons between the simulated scenarios. Furthermore, a sensitivity analysis was conducted to assess the impact on the loads supported by the instrumented spine of three parameters whose values were not precisely known. The analysis showed that a small variation of the PSO wedge angle or intervertebral stiffness had an impact on axial forces in the screws and bending moments in the rods, demonstrating that the model was well calibrated and sensitive enough to assess the effects of those parameters. However, the relative percentage difference between simulations of different degrees of sagittal correction was small and thus the derived interpretations based on relative comparisons of tested scenarios do not impact the conclusions of this study. Following the ASME standard « V&V 40 - 2018 » (ASME V&V 40, 2018), the undertaken steps allowed to ensure model credibility and trust in the conclusions drawn from this study.

The developed model and studies performed have various limitations inherent to any computational study. Firstly, mechanical properties of the intervertebral structures are a first order representation of the spine behavior, and do not incorporate the viscoelastic or stress relaxation properties of the discs and ligaments, which may imply an overestimation of the loads supported by the instrumentation. In addition, the spine flexibility of the tested cases was not precisely known, as lateral bending radiographs were not available. The estimations made affected the absolute values of the post-processed loads but not the conclusions of this study, as they were based on relative comparisons between the simulated scenarios. Another important simplification was the representation of the PSO with a hinge and bounded contacts between the superior and inferior faces of the remaining vertebral body parts. The simulated PSO represents a fusion at the site of

the osteotomy. This modeling choice allows to properly represent the resulting geometry and transmission of compressive forces between the resected parts but might not represent the subsequent instability of the spine near the level of the PSO in cases with pseudarthrosis, which could result in higher loads sustained by the instrumentation under various loading conditions. However, it has been demonstrated that mechanical failure of the instrumentation still happens with good fusion (Daniels et al., 2018) and the findings from this study allowed to assess in which cases instrumentation supported higher loads for different configurations of sagittal correction parameters. The PSO could eventually be modeled with a flexible link and a detailed contact between the superior and inferior parts of the vertebra to further assess how loads (especially shear) are sustained by the instrumentation and spine.

5.2 Interpretation of the biomechanical simulator approach planning of sagittal correction surgery

The developed computer aided biomechanical simulator represents an innovative approach for the planning of sagittal correction surgery, as compared to existing software such as Surgimap (Akbar et al., 2013; Langella et al., 2017), which only allows to assess the geometric correction of the spine. The graphical interface allows to easily plan the major steps of the surgery while the biomechanical simulation allows to assess the predicted postoperative alignment of the spine and loads sustained by the instrumented spine. In cases where the simulated postoperative alignment of the spine is not adequate, the user may go back to the planning steps of the biomechanical simulator and slightly adjust the parameters of the osteotomy, instrumented levels, or geometry of the rods and conduct another simulation of the surgery. Likewise, if the loads supported by the instrumentation are too high, parameters of the surgery may be adjusted to reduce the risks of mechanical failure. The use of 4-rod constructs may also be considered in cases where instrumentation is subject to higher loads to lower the risks of complications associated with this procedure. Once the spine has been reconstructed in 3D, the whole process of planning and simulating the surgery may be completed in less than 10 minutes on a personal computer, allowing a few different scenarios to be analyzed in a reasonable amount of time. Comparisons between different surgical scenarios may help to adopt the best surgical strategy. Figure 5.1 shows an example of three different scenarios of surgical planning for the same patient, realized in less than

15 minutes, along with the sagittal bending moments in the rods which are available after biomechanical simulation of the surgery.

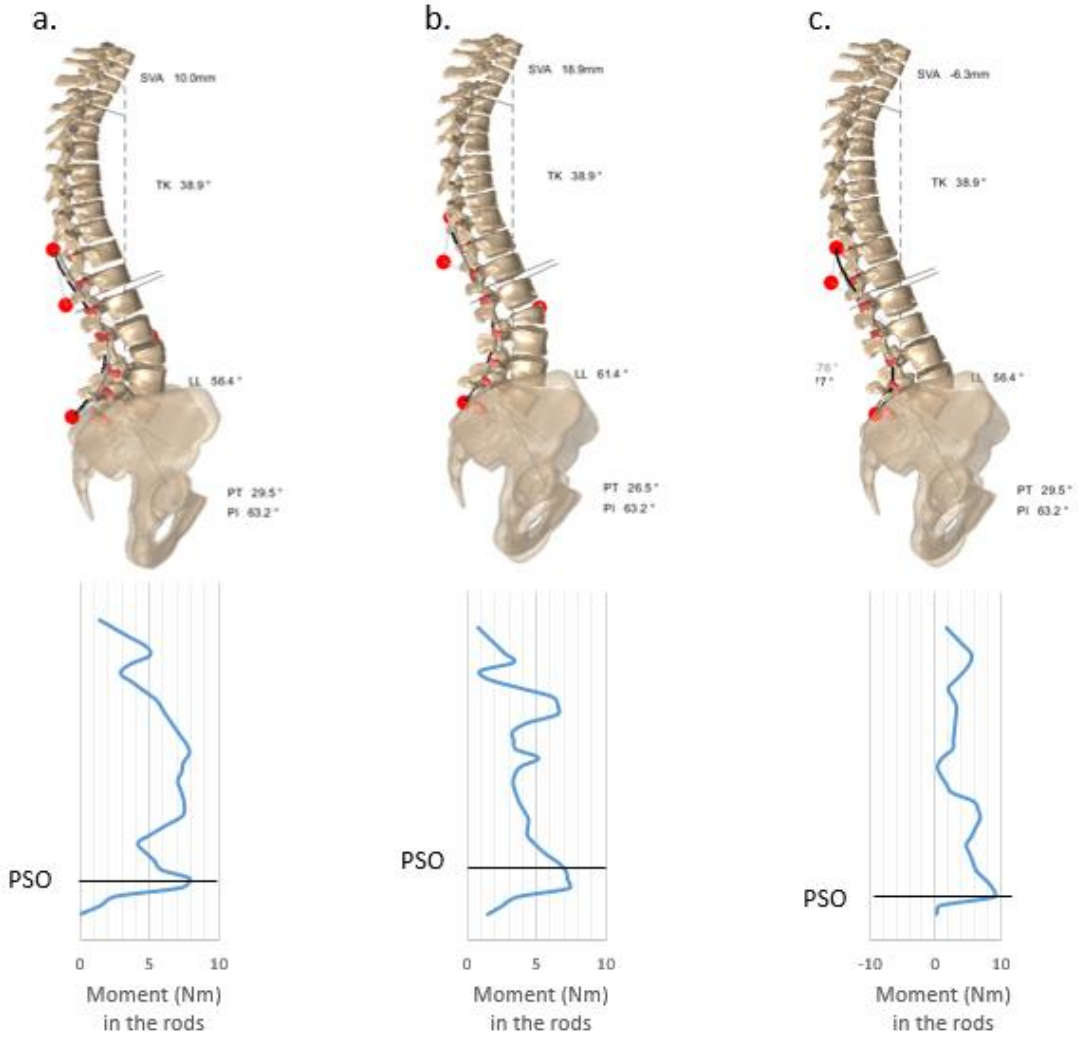

Figure 5.1: Different scenarios of surgical planning for the same patient (a) 25° PSO performed at L3, instrumented from T11 to S1. (b) 30° PSO performed at L2, instrumented from T10 to S1. (c) 25° PSO performed at L4, instrumented from T11 to S1.

The developed surgical planning tool distinguishes itself from the existing formulas (Y. J. Kim et al., 2006; V. Lafage et al., 2011; Ondra et al., 2006; Rose et al., 2009; Schwab et al., 2009), or computer aided graphical methods (Akbar et al., 2013) which are mainly based on geometrical methods to assist surgical planning or predict postoperative alignment of the spine in the sagittal plane. Firstly, the model of the spine including all the important sagittal plane indices allows a more in-depth analysis of the deformity as it can be assessed in 3D. Secondly, the interface offers

an extended surgical planning on a 3D model of the spine through the choice of osteotomies, implants and geometry of the rods. The user also has the possibility to virtually modify preoperative PT to an estimated postoperative value for the biomechanical simulation, which may be estimated using a formula developed to predict postoperative PT according to change in LL and TK (V. Lafage et al., 2011; Smith, Bess, et al., 2012). Multiple different surgical scenarios may be simulated to eventually find the most optimal one. This is the first method to include a biomechanical simulation of the surgical maneuvers in the context of sagittal balance correction. The loads shared between the spine and instrumentation influence postoperative alignment of the spine and are an important factor to consider while attempting to reduce the risks of mechanical failure. Finally, the rods geometry could eventually be exported from the simulation platform and the pre-bent curvature directly ordered from a provider, reducing the residual stresses in the rods coming from in-situ bending.

To simplify the planning process, the order in which the surgical maneuvers were simulated was predefined. In real surgical scenarios, surgeons may perform different maneuvers in a different order. For instance, some surgeons may anchor the rods distally first, which may influence how the loads are supported by the instrumentation. The developed simulator could easily by improved in the future to add supplementary features such as the definition of the order of surgical maneuvers. The modeling of the position of C7 during the closure of the PSO could also be refined. The reciprocal changes in the thoracic unfused segments is likely multifactorial and could be impacted by the number of unfused segments and age of the patient (V. Lafage, Ames, et al., 2012). Stiffness of the unfused segments and degree of sagittal correction may also play a role in the extent of reciprocal changes. Further work is required to assess how reciprocal changes are affected by those factors and to be able to better approximate postoperative SVA in the context of surgical planning. Finally, the biomechanical simulation occasionally requires fine tuning of the instrumentation parameters (such as the alignment of the screws one to another) or surgical maneuvers (insertion of the rods in the screw heads) to have proper convergence. For instance, a slight modification of the alignment of the pedicle screws or a modification of the number of screws into which the rod is simultaneously inserted may help the model to converge.

While considering the previously discussed limits, the developed biomechanical simulator represents an interesting proof of concept for the surgical planning of sagittal balance correction. The simulator could eventually be used in a teaching or training context to better understand and

predict postoperative alignment and how various sagittal correction parameters may influence the loads supported by the spine and instrumentation. Further work is required to use the simulator in the context of real surgical planning.

CHAPTER 6 CONCLUSIONS AND RECOMMENDATIONS

The first objective of this master project was to adapt a personalized multi-body biomechanical model integrated in a simulation platform to simulate the surgical correction of sagittal balance with osteotomy for ASD. The simulation platform offers an innovative graphical method for biomechanical planning of surgical instrumentation. Surgical planning can be completed in three easy steps and different surgical scenarios may be compared. By integrating the developed biomechanical model, the simulation platform is the first to allow analysis of predicted postoperative alignment based on surgical parameters and the loads in the instrumented spine in the context of sagittal balance correction. Risks of mechanical failure of the instrumentation may be compared for different surgical strategies. The biomechanical simulator presented in this work is an interesting proof of concept and further work is required to fully validate it and to further model reciprocal changes in the unfused segments.

The second objective of this project was to exploit the biomechanical model to evaluate the effects of the tested sagittal correction parameters on the distribution of forces and moments in the instrumented spine. The developed biomechanical model allowed to simulate real surgical corrections of sagittal balance with a difference of less then 4° for the sagittal and coronal curves and 8 mm for SVA. This study allowed to assess how different sagittal correction parameters (PSO resection angle, rod curvature, vertebral level of the PSO, and number of rods) affected the loads supported by the instrumentation and thus the risks of mechanical failure.

Through simulations of various degrees of sagittal correction (PSO wedge angle and rod contour), higher axial forces were supported by the screws and higher sagittal bending moments were supported by the rods at the PSO level for bigger sagittal correction. However, it is also important to consider the postoperative sagittal alignment. Higher loads may be sustained by the instrumented spine in under or over corrected cases, as the spine would be highly unbalanced. An optimal sagittal alignment would lead to reduced loads in the instrumented spine, when compared to an unbalanced spine. A PSO performed at a more caudal level resulted in higher sagittal bending moments in the segment of the rods next to the PSO level. Even though those sagittal correction parameters were shown to impact how the loads are shared in the instrumentation, surgeons may have to take into consideration other factors such as the severity of the spinal malalignment, previous fusion mass or vertebral level of the apex of the lumbar curve for an optimal correction. In this study, the use

of 4-rod constructs was shown to reduce the loads in the construct, which could reduce the risks of mechanical failure of the instrumentation, as they allowed to reduce the bending loads in the primary rods and the axial forces in the screws. No difference was found for the vertebral compression loads, suggesting that the strategy maximising anterior loads might be patient-specific.

In perspective, the simulation platform is an interesting proof of concept to help surgeons define patient-specific optimal surgical strategies and the knowledge gained through biomechanical simulations can help to better understand the different risk factors of mechanical complications after PSO. The developed model could be further refined to analyze the effects of other types of osteotomies like the vertebral column resection osteotomy or additional instrumentation such as cages. More cases with surgical instrumentation with PSO would be necessary to conduct a statistical analysis and more comprehensive validation.

BIBLIOGRAPHY

Aebi, M. (2005). The adult scoliosis. *European Spine Journal, 14*(10), 925-948.

Ailon, T., Scheer, J. K., Lafage, V., Schwab, F. J., Klineberg, E., Sciubba, D. M., . . . International Spine Study, G. (2016). Adult Spinal Deformity Surgeons Are Unable to Accurately Predict Postoperative Spinal Alignment Using Clinical Judgment Alone. *Spine Deform, 4*(4), 323-329. doi:10.1016/j.jspd.2016.02.003

Akbar, M., Terran, J., Ames, C. P., Lafage, V., & Schwab, F. (2013). Use of Surgimap Spine in sagittal plane analysis, osteotomy planning, and correction calculation. *Neurosurg Clin N Am, 24*(2), 163-172. doi:10.1016/j.nec.2012.12.007

Ames, C. P., Scheer, J. K., Lafage, V., Smith, J. S., Bess, S., Berven, S. H., . . . Daubs, M. D. (2016). Adult Spinal Deformity: Epidemiology, Health Impact, Evaluation, and Management. *Spine Deform, 4*(4), 310-322. doi:10.1016/j.jspd.2015.12.009

Arutyunyan, G. G., Angevine, P. D., & Berven, S. (2018). Cost-Effectiveness in Adult Spinal Deformity Surgery. *Neurosurgery*. doi:10.1093/neuros/nyx575

Asghar, J., Samdani, A. F., Pahys, J. M., D'andrea, L. P., Guille, J. T., Clements, D. H., . . . Group, H. S. (2009). Computed tomography evaluation of rotation correction in adolescent idiopathic scoliosis: a comparison of an all pedicle screw construct versus a hook-rod system. *Spine, 34*(8), 804-807.

ASME-V&V-40. (2018). Assessing Credibility of Computational Modeling Through Verification and Validation: Application to Medical Devices. New York: The American Society of Mechanical Engineers.

Aubin, C. E., Descrimes, J., Dansereau, J., Skalli, W., Lavaste, F., & Labelle, H. (1995). *Geometrical modeling of the spine and the thorax for the biomechanical analysis of scoliotic deformities using the finite element method.* Paper presented at the Annales de chirurgie.

Aubin, C. E., Labelle, H., Chevrefils, C., Desroches, G., Clin, J., & Eng, A. B. M. (2008). Preoperative planning simulator for spinal deformity surgeries. *Spine, 33*(20), 2143-2152.

Aubin, C. E., Petit, Y., Stokes, I., Poulin, F., Gardner-Morse, M., & Labelle, H. (2003). Biomechanical modeling of posterior instrumentation of the scoliotic spine. *Computer Methods in Biomechanics & Biomedical Engineering, 6*(1), 27-32.

Bakaloudis, G., Lolli, F., Di Silvestre, M., Greggi, T., Astolfi, S., Martikos, K., . . . Giacomini, S. (2011). Thoracic pedicle subtraction osteotomy in the treatment of severe pediatric deformities. *Eur Spine J, 20 Suppl 1*, S95-104. doi:10.1007/s00586-011-1749-y

Barrey, C., Perrin, G., Michel, F., Vital, J. M., & Obeid, I. (2014). Pedicle subtraction osteotomy in the lumbar spine: indications, technical aspects, results and complications. *Eur J Orthop Surg Traumatol, 24*(1), 21-30. doi:10.1007/s00590-014-1470-8

Barrey, C., Roussouly, P., Perrin, G., & Le Huec, J. C. (2011). Sagittal balance disorders in severe degenerative spine. Can we identify the compensatory mechanisms? *Eur Spine J, 20 Suppl 5*, 626-633. doi:10.1007/s00586-011-1930-3

Barton, C., Noshchenko, A., Patel, V., Cain, C., Kleck, C., & Burger, E. (2015). Risk factors for rod fracture after posterior correction of adult spinal deformity with osteotomy: a retrospective case-series. *Scoliosis, 10*, 30. doi:10.1186/s13013-015-0056-5

Barton, C., Noshchenko, A., Patel, V. V., Cain, C. M., Kleck, C., & Burger, E. L. (2017). Different types of mechanical complications after surgical correction of adult spine deformity with osteotomy. *World Journal of Meta-Analysis, 5*(6), 132-149.

Bergin, P. F., O'Brien, J. R., Matteini, L. E., Yu, W. D., & Kebaish, K. M. (2010). The use of spinal osteotomy in the treatment of spinal deformity. *Orthopedics, 33*(8), 586-594. doi:10.3928/01477447-20100625-22

Berjano, P., & Aebi, M. (2015). Pedicle subtraction osteotomies (PSO) in the lumbar spine for sagittal deformities. *Eur Spine J, 24 Suppl 1*, S49-57. doi:10.1007/s00586-014-3670-7

Berven, S. H., Kamper, S. J., Germscheid, N. M., Dahl, B., Shaffrey, C. I., Lenke, L. G., . . . Deformity, A. O. K. F. (2018). An international consensus on the appropriate evaluation and treatment for adults with spinal deformity. *Eur Spine J, 27*(3), 585-596. doi:10.1007/s00586-017-5241-1

Bess, S., Boachie-Adjei, O., Burton, D., Cunningham, M., Shaffrey, C., Shelokov, A., . . . Akbarnia, B. (2009). Pain and disability determine treatment modality for older patients with adult scoliosis, while deformity guides treatment for younger patients. *Spine, 34*(20), 2186-2190.

Bianco, R.-J., Arnoux, P.-J., Wagnac, E., Mac-Thiong, J.-M., & Aubin, C.-É. (2017). Minimizing Pedicle Screw Pullout Risks. *Clinical Spine Surgery, 30*(3), E226-E232.

Blondel, B., Schwab, F., Bess, S., Ames, C., Mummaneni, P. V., Hart, R., . . . Lafage, V. (2013). Posterior global malalignment after osteotomy for sagittal plane deformity: it happens and here is why. *Spine (Phila Pa 1976), 38*(7), E394-401. doi:10.1097/BRS.0b013e3182872415

Boyer, L. (2017). *Analyse biomécanique de techniques de dérotation vertébrale pour la correction 3D de la scoliose lors de la chirurgie d'instrumentation postérieure du rachis.* Polytechnique Montréal.

Bridwell, K. H. (2006). Decision making regarding Smith-Petersen vs. pedicle subtraction osteotomy vs. vertebral column resection for spinal deformity. *Spine, 31*(19S), S171-S178.

Bridwell, K. H., Lewis, S. J., Lenke, L. G., Baldus, C., & Blanke, K. (2003). Pedicle subtraction osteotomy for the treatment of fixed sagittal imbalance. *J Bone Joint Surg Am, 85*(3), 454-463.

Cammarata, M., Aubin, C. E., Wang, X., & Mac-Thiong, J. M. (2014). Biomechanical risk factors for proximal junctional kyphosis: a detailed numerical analysis of surgical instrumentation variables. *Spine (Phila Pa 1976), 39*(8), E500-507. doi:10.1097/BRS.0000000000000222

Charosky, S., Moreno, P., & Maxy, P. (2014). Instability and instrumentation failures after a PSO: a finite element analysis. *Eur Spine J, 23*(11), 2340-2349. doi:10.1007/s00586-014-3295-x

Cheriet, F., Laporte, C., Kadoury, S., Labelle, H., & Dansereau, J. (2007). A novel system for thE 3-D reconstruction of the human spine and rib cage from biplanar X-ray images. *IEEE Trans Biomed Eng, 54*(7), 1356-1358. doi:10.1109/TBME.2006.889205

Cho, K. J., Bridwell, K. H., Lenke, L. G., Berra, A., & Baldus, C. (2005). Comparison of Smith-Petersen versus pedicle subtraction osteotomy for the correction of fixed sagittal imbalance. *Spine, 30*(18), 2030-2037.

Daniels, A. H., DePasse, J. M., Durand, W., Hamilton, D. K., Passias, P., Kim, H. J., . . . International Spine Study, G. (2018). Rod Fracture After Apparently Solid Radiographic Fusion in Adult Spinal Deformity Patients. *World Neurosurg, 117*, e530-e537. doi:10.1016/j.wneu.2018.06.071

Delorme, S., Petit, Y., de Guise, J. A., Labelle, H., Aubin, C. E., & Dansereau, J. (2003). Assessment of the 3-d reconstruction and high-resolution geometrical modeling of the human skeletal trunk from 2-D radiographic images. *IEEE Trans Biomed Eng, 50*(8), 989-998. doi:10.1109/TBME.2003.814525

Deschênes, S., Charron, G., Beaudoin, G., Labelle, H., Dubois, J., Miron, M.-C., & Parent, S. (2010). Diagnostic imaging of spinal deformities: reducing patients radiation dose with a new slot-scanning X-ray imager. *Spine, 35*(9), 989-994.

Desrochers-Perrault, F., Aubin, C. E., Wang, X., & Schwend, R. M. (2014). Biomechanical analysis of iliac screw fixation in spinal deformity instrumentation. *Clin Biomech (Bristol, Avon), 29*(6), 614-621. doi:10.1016/j.clinbiomech.2014.04.016

Dickson, D. D., Lenke, L. G., Bridwell, K. H., & Koester, L. A. (2014). Risk factors for and assessment of symptomatic pseudarthrosis after lumbar pedicle subtraction osteotomy in adult spinal deformity. *Spine (Phila Pa 1976), 39*(15), 1190-1195. doi:10.1097/BRS.0000000000000380

Diebo, B. G., Lafage, V., Varghese, J. J., Gupta, M., Kim, H. J., Ames, C., . . . Obeid, I. (2017). After 9 years of 3-column osteotomies, are we doing better? Performance curve analysis of 573 surgeries with 2-year follow-up. *Neurosurgery, 83*(1), 69-75.

Diebo, B. G., Liu, S., Lafage, V., & Schwab, F. (2014). Osteotomies in the treatment of spinal deformities: indications, classification, and surgical planning. *European Journal of Orthopaedic Surgery & Traumatology, 24*(S1), 11-20. doi:10.1007/s00590-014-1471-7

Diebo, B. G., Varghese, J. J., Lafage, R., Schwab, F. J., & Lafage, V. (2015). Sagittal alignment of the spine: What do you need to know? *Clin Neurol Neurosurg, 139*, 295-301. doi:10.1016/j.clineuro.2015.10.024

Dorward, I. G., & Lenke, L. G. (2010). Osteotomies in the posterior-only treatment of complex adult spinal deformity: a comparative review. *Neurosurgical focus, 28*(3), E4.

Dubousset, J. (1994). Three-dimensional analysis of the scoliotic deformity. *The pediatric spine: principles and practice*.

Duval-Beaupere, G., & Robain, G. (1987). Visualization on full spine radiographs of the anatomical connections of the centres of the segmental body mass supported by each vertebra and measured in vivo. *International orthopaedics, 11*(3), 261-269.

Everett, C. R., & Patel, R. K. (2007). A systematic literature review of nonsurgical treatment in adult scoliosis. *Spine, 32*(19), S130-S134.

Ferrero, E., Liabaud, B., Henry, J. K., Ames, C. P., Kebaish, K., Mundis, G. M., . . . Lafage, V. (2017). Sagittal alignment and complications following lumbar 3-column osteotomy: does

the level of resection matter? *J Neurosurg Spine, 27*(5), 560-569. doi:10.3171/2017.3.SPINE16357

Fradet, L., Wang, X., Crandall, D., & Aubin, C. E. (2018). Biomechanical Analysis of Acute Proximal Junctional Failure After Surgical Instrumentation of Adult Spinal Deformity: The Impact of Proximal Implant Type, Osteotomy Procedures, and Lumbar Lordosis Restoration. *Spine Deform, 6*(5), 483-491. doi:10.1016/j.jspd.2018.02.007

Fu, K. M., Bess, S., Shaffrey, C. I., Smith, J. S., Lafage, V., Schwab, F., . . . International Spine Study, G. (2014). Patients with adult spinal deformity treated operatively report greater baseline pain and disability than patients treated nonoperatively; however, deformities differ between age groups. *Spine (Phila Pa 1976), 39*(17), 1401-1407. doi:10.1097/BRS.0000000000000414

Fujishiro, T., Boissiere, L., Cawley, D. T., Larrieu, D., Gille, O., Vital, J. M., . . . European Spine Study Group, E. (2018). Decision-making factors in the treatment of adult spinal deformity. *Eur Spine J*. doi:10.1007/s00586-018-5572-6

Gardner-Morse, M. G., & Stokes, I. A. F. (2004). Structural behavior of human lumbar spinal motion segments. *Journal of biomechanics, 37*(2), 205-212. doi:10.1016/j.jbiomech.2003.10.003

Glassman, S. D., Berven, S., Bridwell, K., Horton, W., & Dimar, J. R. (2005). Correlation of radiographic parameters and clinical symptoms in adult scoliosis. *Spine, 30*(6), 682-688.

Glassman, S. D., Bridwell, K., Dimar, J. R., Horton, W., Berven, S., & Schwab, F. (2005). The impact of positive sagittal balance in adult spinal deformity. *Spine, 30*(18), 2024-2029.

Gupta, M., Henry, J. K., Schwab, F., Klineberg, E., Smith, J. S., Gum, J., . . . International Spine Study, G. (2016). Dedicated Spine Measurement Software Quantifies Key Spino-Pelvic Parameters More Reliably Than Traditional Picture Archiving and Communication Systems Tools. *Spine (Phila Pa 1976), 41*(1), E22-E27. doi:10.1097/BRS.0000000000001216

Gupta, S., Eksi, M. S., Ames, C. P., Deviren, V., Durbin-Johnson, B., Smith, J. S., & Gupta, M. C. (2017). A novel 4-Rod technique offers potential to reduce rod breakage and pseudarthrosis in pedicle subtraction osteotomies for adult spinal deformity correction. *Operative Neurosurgery, 14*(4), 449-456.

Hallager, D. W., Gehrchen, M., Dahl, B., Harris, J. A., Gudipally, M., Jenkins, S., . . . Bucklen, B. S. (2016). Use of Supplemental Short Pre-Contoured Accessory Rods and Cobalt Chrome Alloy Posterior Rods Reduces Primary Rod Strain and Range of Motion Across the Pedicle Subtraction Osteotomy Level: An In Vitro Biomechanical Study. *Spine (Phila Pa 1976), 41*(7), E388-395. doi:10.1097/BRS.0000000000001282

Hasler, C. C. (2013). A brief overview of 100 years of history of surgical treatment for adolescent idiopathic scoliosis. *J Child Orthop, 7*(1), 57-62. doi:10.1007/s11832-012-0466-3

Hostin, R., Robinson, C., O'Brien, M., Ames, C., Schwab, F., Smith, J. S., . . . McCarthy, I. (2016). A Multicenter Comparison of Inpatient Resource Use for Adult Spinal Deformity Surgery. *Spine (Phila Pa 1976), 41*(7), 603-609. doi:10.1097/BRS.0000000000001280

Humbert, L., De Guise, J. A., Aubert, B., Godbout, B., & Skalli, W. (2009). 3D reconstruction of the spine from biplanar X-rays using parametric models based on transversal and longitudinal inferences. *Med Eng Phys, 31*(6), 681-687. doi:10.1016/j.medengphy.2009.01.003

Hyun, S. J., Lenke, L. G., Kim, Y. C., Koester, L. A., & Blanke, K. M. (2014). Comparison of standard 2-rod constructs to multiple-rod constructs for fixation across 3-column spinal osteotomies. *Spine (Phila Pa 1976), 39*(22), 1899-1904. doi:10.1097/BRS.0000000000000556

Januszewski, J., Beckman, J. M., Harris, J. E., Turner, A. W., Yen, C. P., & Uribe, J. S. (2017). Biomechanical study of rod stress after pedicle subtraction osteotomy versus anterior column reconstruction: A finite element study. *Surgical neurology international, 8*.

Kadoury, S., Cheriet, F., Beausejour, M., Stokes, I. A., Parent, S., & Labelle, H. (2009). A three-dimensional retrospective analysis of the evolution of spinal instrumentation for the correction of adolescent idiopathic scoliosis. *Eur Spine J, 18*(1), 23-37. doi:10.1007/s00586-008-0817-4

Kadoury, S., Cheriet, F., Laporte, C., & Labelle, H. (2007). A versatile 3D reconstruction system of the spine and pelvis for clinical assessment of spinal deformities. *Med Biol Eng Comput, 45*(6), 591-602. doi:10.1007/s11517-007-0182-1

Kiefer, A., Parnianpour, M., & Shirazi-Adl, A. (1997). Stability of the human spine in neutral postures. *European Spine Journal, 6*(1), 45-53.

Kim, Vaccaro, A., Whang, P., Kim, S. D., & Kim, S. H. (2013). *Lumbosacral and Pelvic Procedures*: CRC Press.

Kim, Y. J., Bridwell, K. H., Lenke, L. G., Rhim, S., & Cheh, G. (2006). An analysis of sagittal spinal alignment following long adult lumbar instrumentation and fusion to L5 or S1: can we predict ideal lumbar lordosis? *Spine, 31*(20), 2343-2352.

La Barbera, L., Brayda-Bruno, M., Liebsch, C., Villa, T., Luca, A., Galbusera, F., & Wilke, H. J. (2018). Biomechanical advantages of supplemental accessory and satellite rods with and without interbody cages implantation for the stabilization of pedicle subtraction osteotomy. *Eur Spine J, 27*(9), 2357-2366. doi:10.1007/s00586-018-5623-z

Lafage, R., Pesenti, S., Lafage, V., & Schwab, F. J. (2018). Self-learning computers for surgical planning and prediction of postoperative alignment. *Eur Spine J, 27*(Suppl 1), 123-128. doi:10.1007/s00586-018-5497-0

Lafage, R., Schwab, F., Challier, V., Henry, J. K., Gum, J., Smith, J., . . . International Spine Study, G. (2016). Defining Spino-Pelvic Alignment Thresholds: Should Operative Goals in Adult Spinal Deformity Surgery Account for Age? *Spine (Phila Pa 1976), 41*(1), 62-68. doi:10.1097/BRS.0000000000001171

Lafage, V., Ames, C., Schwab, F., Klineberg, E., Akbarnia, B., Smith, J., . . . International Spine Study, G. (2012). Changes in thoracic kyphosis negatively impact sagittal alignment after lumbar pedicle subtraction osteotomy: a comprehensive radiographic analysis. *Spine (Phila Pa 1976), 37*(3), E180-187. doi:10.1097/BRS.0b013e318225b926

Lafage, V., Bharucha, N. J., Schwab, F., Hart, R. A., Burton, D., Boachie-Adjei, O., . . . Gupta, M. (2012). Multicenter validation of a formula predicting postoperative spinopelvic alignment: Clinical article. *Journal of Neurosurgery: Spine, 16*(1), 15-21.

Lafage, V., Dubousset, J., Lavaste, F., & Skalli, W. (2004). 3D finite element simulation of Cotrel–Dubousset correction. *Computer Aided Surgery, 9*(1-2), 17-25.

Lafage, V., Schwab, F., Patel, A., Hawkinson, N., & Farcy, J.-P. (2009). Pelvic tilt and truncal inclination: two key radiographic parameters in the setting of adults with spinal deformity. *Spine, 34*(17), E599-E606.

Lafage, V., Schwab, F., Skalli, W., Hawkinson, N., Gagey, P.-M., Ondra, S., & Farcy, J.-P. (2008). Standing balance and sagittal plane spinal deformity: analysis of spinopelvic and gravity line parameters. *Spine, 33*(14), 1572-1578.

Lafage, V., Schwab, F., Vira, S., Patel, A., Ungar, B., & Farcy, J. P. (2011). Spino-pelvic parameters after surgery can be predicted: a preliminary formula and validation of standing alignment. *Spine (Phila Pa 1976), 36*(13), 1037-1045. doi:10.1097/BRS.0b013e3181eb9469

Langella, F., Villafane, J. H., Damilano, M., Cecchinato, R., Pejrona, M., Ismael, M., & Berjano, P. (2017). Predictive Accuracy of Surgimap Surgical Planning for Sagittal Imbalance: A Cohort Study. *Spine (Phila Pa 1976), 42*(22), E1297-E1304. doi:10.1097/BRS.0000000000002230

Laouissat, F., Sebaaly, A., Gehrchen, M., & Roussouly, P. (2018). Classification of normal sagittal spine alignment: refounding the Roussouly classification. *Eur Spine J, 27*(8), 2002-2011. doi:10.1007/s00586-017-5111-x

Le Huec, J. C., Aunoble, S., Philippe, L., & Nicolas, P. (2011). Pelvic parameters: origin and significance. *Eur Spine J, 20 Suppl 5*, 564-571. doi:10.1007/s00586-011-1940-1

Le Huec, J. C., Faundez, A., Dominguez, D., Hoffmeyer, P., & Aunoble, S. (2015). Evidence showing the relationship between sagittal balance and clinical outcomes in surgical treatment of degenerative spinal diseases: a literature review. *Int Orthop, 39*(1), 87-95. doi:10.1007/s00264-014-2516-6

Le Naveaux, F., Aubin, C. E., Larson, A. N., Polly, D. W., Jr., Baghdadi, Y. M., & Labelle, H. (2015). Implant distribution in surgically instrumented Lenke 1 adolescent idiopathic scoliosis: does it affect curve correction? *Spine (Phila Pa 1976), 40*(7), 462-468. doi:10.1097/BRS.0000000000000793

Le Naveaux, F., Larson, A. N., Labelle, H., Wang, X., & Aubin, C. E. (2016). How does implant distribution affect 3D correction and bone-screw forces in thoracic adolescent idiopathic scoliosis spinal instrumentation? *Clin Biomech (Bristol, Avon), 39*, 25-31. doi:10.1016/j.clinbiomech.2016.09.002

Leborgne, P., Skalli, W., Lecire, C., Dubousset, J., Zeller, R., & Lavaste, F. (1999). Simulation of CD surgery on a personalized finite element model: preliminary results. *Studies in Health Technology and Informatics*, 126-129.

Legaye, J., Duval-Beaupere, G., Hecquet, J., & Marty, C. (1998). Pelvic incidence: a fundamental pelvic parameter for three-dimensional regulation of spinal sagittal curves. *European Spine Journal, 7*(2), 99-103.

Lehman Jr, R. A., Polly Jr, D. W., Kuklo, T. R., Cunningham, B., Kirk, K. L., & Belmont Jr, P. J. (2003). Straight-forward versus anatomic trajectory technique of thoracic pedicle screw fixation: a biomechanical analysis. *Spine, 28*(18), 2058-2065.

Liljenqvist, U., Hackenberg, L., Link, T., & Halm, H. (2001). Pullout strength of pedicle screws versus pedicle and laminar hooks in the thoracic spine. *Acta orthopaedica belgica, 67*(2), 157-163.

Liu, H., Yang, C., Zheng, Z., Ding, W., Wang, J., Wang, H., & Li, S. (2015). Comparison of Smith-Petersen osteotomy and pedicle subtraction osteotomy for the correction of thoracolumbar kyphotic deformity in ankylosing spondylitis: a systematic review and meta-analysis. *Spine (Phila Pa 1976), 40*(8), 570-579. doi:10.1097/BRS.0000000000000815

Luca, A., Lovi, A., Galbusera, F., & Brayda-Bruno, M. (2014). Revision surgery after PSO failure with rod breakage: a comparison of different techniques. *Eur Spine J, 23 Suppl 6*, 610-615. doi:10.1007/s00586-014-3555-9

Luca, A., Ottardi, C., Sasso, M., Prosdocimo, L., La Barbera, L., Brayda-Bruno, M., . . . Villa, T. (2017). Instrumentation failure following pedicle subtraction osteotomy: the role of rod material, diameter, and multi-rod constructs. *Eur Spine J, 26*(3), 764-770. doi:10.1007/s00586-016-4859-8

Luque, E. R. (1982). Segmental spinal instrumentation for correction of scoliosis. *Clinical orthopaedics and related research*(163), 192-198.

Maier, S., Smith, J. S., Schwab, F., Obeid, I., Mundis, G., Klineberg, E., . . . International Spine Study, G. (2014). Revision Surgery After Three-Column Osteotomy in 335 Adult Spinal Deformity Patients: Inter-Center Variability and Risk Factors. *Spine (Phila Pa 1976)*. doi:10.1097/BRS.0000000000000304

Martino, J., Aubin, C. E., Labelle, H., Wang, X., & Parent, S. (2013). Biomechanical analysis of vertebral derotation techniques for the surgical correction of thoracic scoliosis. A numerical study through case simulations and a sensitivity analysis. *Spine (Phila Pa 1976), 38*(2), E73-83. doi:10.1097/BRS.0b013e31827a641e

Moal, B., Moal, O., Lafage, R., Schwab, F., Smith, J., Shaffrey, C., . . . International Spine Study, G. (2017). *Prediction of alignment after surgical treatment of adult spinal deformity with probabilistic principal component analysis.* Paper presented at the International Society for the Advancement of Spine Surgery, Florida, USA.

Moal, B., Schwab, F., Ames, C. P., Smith, J. S., Ryan, D., Mummaneni, P. V., . . . International Spine Study, G. (2014). Radiographic Outcomes of Adult Spinal Deformity Correction: A Critical Analysis of Variability and Failures Across Deformity Patterns. *Spine Deform, 2*(3), 219-225. doi:10.1016/j.jspd.2014.01.003

Mummaneni, P. V., Shaffrey, C. I., Lenke, L. G., Park, P., Wang, M. Y., La Marca, F., . . . Moal, B. (2014). The minimally invasive spinal deformity surgery algorithm: a reproducible rational framework for decision making in minimally invasive spinal deformity surgery. *Neurosurgical focus, 36*(5), E6.

Obeid, I., Hauger, O., Aunoble, S., Bourghli, A., Pellet, N., & Vital, J.-M. (2011). Global analysis of sagittal spinal alignment in major deformities: correlation between lack of lumbar lordosis and flexion of the knee. *European Spine Journal, 20*(5), 681.

Ondra, S. L., Marzouk, S., Koski, T., Silva, F., & Salehi, S. (2006). Mathematical calculation of pedicle subtraction osteotomy size to allow precision correction of fixed sagittal deformity. *Spine, 31*(25), E973-E979.

Ottardi, C., Galbusera, F., Luca, A., Prosdocimo, L., Sasso, M., Brayda-Bruno, M., & Villa, T. (2016). Finite element analysis of the lumbar destabilization following pedicle subtraction osteotomy. *Med Eng Phys, 38*(5), 506-509. doi:10.1016/j.medengphy.2016.02.002

Ottardi, C., Luca, A., & Galbusera, F. (2018). Sagittal Imbalance. 379-391. doi:10.1016/b978-0-12-812851-0.00021-5

Panjabi, M. M., & Brand, J. R. (1976). Mechanical properties of the human thoracic spine as shown by three-dimensional load-displacement curves. *The Journal of bone and joint surgery. American volume, 58*(5), 642-652.

Panjabi, M. M., Oxland, T., Yamamoto, I., & Crisco, J. (1994). Mechanical behavior of the human lumbar and lumbosacral spine as shown by three-dimensional load-displacement curves. *JBJS, 76*(3), 413-424.

Patwardhan, A. G., Havey, R. M., Meade, K. P., Lee, B., & Dunlap, B. (1999). A follower load increases the load-carrying capacity of the lumbar spine in compression. *Spine, 24*(10), 1003-1009.

Pearsall, D. J., Reid, J. G., & Livingston, L. A. (1996). Segmental inertial parameters of the human trunk as determined from computed tomography. *Annals of biomedical engineering, 24*(2), 198-210.

Petit, Y., Aubin, C.-É., & Labelle, H. (2004). Patient-specific mechanical properties of a flexible multi-body model of the scoliotic spine. *Medical and Biological Engineering and Computing, 42*(1), 55-60.

Polly Jr, D. W., Kilkelly, F. X., McHale, K. A., Asplund, L. M., Mulligan, M., & Chang, A. S. (1996). Measurement of lumbar lordosis: evaluation of intraobserver, interobserver, and technique variability. *Spine, 21*(13), 1530-1535.

Poulin, F., Aubin, C., Stokes, I., Gardner-Morse, M., & Labelle, H. (1998). *Modélisation biomécanique de l'instrumentation du rachis scoliotique à l'aide de mécanismes flexibles: étude de faisabilité.* Paper presented at the Annales de chirurgie.

Rohlmann, A., Zander, T., Rao, M., & Bergmann, G. (2009). Applying a follower load delivers realistic results for simulating standing. *J Biomech, 42*(10), 1520-1526. doi:10.1016/j.jbiomech.2009.03.048

Rose, P. S., Bridwell, K. H., Lenke, L. G., Cronen, G. A., Mulconrey, D. S., Buchowski, J. M., & Kim, Y. J. (2009). Role of pelvic incidence, thoracic kyphosis, and patient factors on sagittal plane correction following pedicle subtraction osteotomy. *Spine, 34*(8), 785-791.

Roussouly, P., Gollogly, S., Berthonnaud, E., & Dimnet, J. (2005). Classification of the normal variation in the sagittal alignment of the human lumbar spine and pelvis in the standing position. *Spine, 30*(3), 346-353.

Roussouly, P., & Nnadi, C. (2010). Sagittal plane deformity: an overview of interpretation and management. *Eur Spine J, 19*(11), 1824-1836. doi:10.1007/s00586-010-1476-9

Salvi, G. (2014). *Analyse biomécanique d'ostéotomies de Ponte et de soustraction pédiculaire pour la correction chirurgicale de déformations cyphotiques.* Master thesis. Polytechnique Montréal.

Salvi, G., Aubin, C. E., Le Naveaux, F., Wang, X., & Parent, S. (2016). Biomechanical analysis of Ponte and pedicle subtraction osteotomies for the surgical correction of kyphotic deformities. *Eur Spine J, 25*(8), 2452-2460. doi:10.1007/s00586-015-4279-1

Savage, J. W., & Patel, A. A. (2014). Fixed sagittal plane imbalance. *Global Spine J, 4*(4), 287-296. doi:10.1055/s-0034-1394126

Scheer, J. K., Tang, J. A., Smith, J. S., Klineberg, E., Hart, R. A., Mundis Jr, G. M., . . . Bess, S. (2013). Reoperation rates and impact on outcome in a large, prospective, multicenter, adult spinal deformity database: clinical article. *Journal of Neurosurgery: Spine, 19*(4), 464-470.

Schwab, F., Blondel, B., Bess, S., Hostin, R., Shaffrey, C. I., Smith, J. S., . . . International Spine Study, G. (2013). Radiographical spinopelvic parameters and disability in the setting of adult spinal deformity: a prospective multicenter analysis. *Spine (Phila Pa 1976), 38*(13), E803-812. doi:10.1097/BRS.0b013e318292b7b9

Schwab, F., Blondel, B., Chay, E., Demakakos, J., Lenke, L., Tropiano, P., . . . Glassman, S. (2014). The comprehensive anatomical spinal osteotomy classification. *Neurosurgery, 76*, S33-S41.

Schwab, F., Dubey, A., Gamez, L., El Fegoun, A. B., Hwang, K., Pagala, M., & Farcy, J.-P. (2005). Adult scoliosis: prevalence, SF-36, and nutritional parameters in an elderly volunteer population. *Spine, 30*(9), 1082-1085.

Schwab, F., Lafage, V., Boyce, R., Skalli, W., & Farcy, J. P. (2006). Gravity line analysis in adult volunteers: age-related correlation with spinal parameters, pelvic parameters, and foot position. *Spine (Phila Pa 1976), 31*(25), E959-967. doi:10.1097/01.brs.0000248126.96737.0f

Schwab, F., Lafage, V., Patel, A., & Farcy, J.-P. (2009). Sagittal plane considerations and the pelvis in the adult patient. *Spine, 34*(17), 1828-1833.

Schwab, F., Patel, A., Shaffrey, C. I., Smith, J. S., Farcy, J.-P., Boachie-Adjei, O., . . . Burton, D. C. (2012). Sagittal realignment failures following pedicle subtraction osteotomy surgery: are we doing enough? Clinical article. *Journal of Neurosurgery: Spine, 16*(6), 539-546.

Schwab, F., Ungar, B., Blondel, B., Buchowski, J., Coe, J., Deinlein, D., . . . Lafage, V. (2012). Scoliosis Research Society-Schwab adult spinal deformity classification: a validation study. *Spine (Phila Pa 1976), 37*(12), 1077-1082. doi:10.1097/BRS.0b013e31823e15e2

Shea, K. G., Stevens, P. M., Nelson, M., Smith, J. T., Masters, K. S., & Yandow, S. (1998). A comparison of manual versus computer-assisted radiographic measurement: intraobserver measurement variability for Cobb angles. *Spine, 23*(5), 551-555.

Singh, M. K., Ibrahimi, D. M., Shaffrey, C. I., & Smith, J. S. (2015). Pedicle Subtraction Osteotomy. In Y. Wang, O. Boachie-Adjei, & L. Lenke (Eds.), *Spinal Osteotomy* (pp. 89-109). Dordrecht: Springer Netherlands.

Smith-Petersen, M., Larson, C. B., & Aufranc, O. E. (1945). Osteotomy of the spine for correction of flexion deformity in rheumatoid arthritis. *JBJS, 27*(1), 1-11.

Smith, J. S., Bess, S., Shaffrey, C. I., Burton, D. C., Hart, R. A., Hostin, R., . . . International Spine Study, G. (2012). Dynamic changes of the pelvis and spine are key to predicting postoperative sagittal alignment after pedicle subtraction osteotomy: a critical analysis of preoperative planning techniques. *Spine (Phila Pa 1976), 37*(10), 845-853. doi:10.1097/BRS.0b013e31823b0892

Smith, J. S., Klineberg, E., Lafage, V., Shaffrey, C. I., Schwab, F., Lafage, R., . . . International Spine Study, G. (2016). Prospective multicenter assessment of perioperative and minimum 2-year postoperative complication rates associated with adult spinal deformity surgery. *J Neurosurg Spine, 25*(1), 1-14. doi:10.3171/2015.11.SPINE151036

Smith, J. S., Sansur, C. A., Donaldson, W. F., 3rd, Perra, J. H., Mudiyam, R., Choma, T. J., . . . Shaffrey, C. I. (2011). Short-term morbidity and mortality associated with correction of thoracolumbar fixed sagittal plane deformity: a report from the Scoliosis Research Society Morbidity and Mortality Committee. *Spine (Phila Pa 1976), 36*(12), 958-964. doi:10.1097/BRS.0b013e3181eabb26

Smith, J. S., Shaffrey, C. I., Ames, C. P., Demakakos, J., Fu, K.-M. G., Keshavarzi, S., . . . Bess, S. (2012). Assessment of Symptomatic Rod Fracture After Posterior Instrumented Fusion for Adult Spinal Deformity. *Neurosurgery, 71*(4), 862-868. doi:10.1227/NEU.0b013e3182672aab

Smith, J. S., Shaffrey, C. I., Klineberg, E., Lafage, V., Schwab, F., Lafage, R., . . . Group, o. b. o. t. I. S. S. (2017). Complication rates associated with 3-column osteotomy in 82 adult spinal deformity patients: retrospective review of a prospectively collected multicenter consecutive series with 2-year follow-up. *J Neurosurg Spine, 27*(4), 1-14. doi:10.3171/2016.10.SPINE16849

Smith, J. S., Shaffrey, E., Klineberg, E., Shaffrey, C. I., Lafage, V., Schwab, F. J., . . . Fu, K.-M. G. (2014). Prospective multicenter assessment of risk factors for rod fracture following surgery for adult spinal deformity: Clinical article. *Journal of Neurosurgery: Spine, 21*(6), 994-1003.

Soroceanu, A., Diebo, B. G., Burton, D., Smith, J. S., Deviren, V., Shaffrey, C., . . . International Spine Study, G. (2015). Radiographical and Implant-Related Complications in Adult Spinal Deformity Surgery: Incidence, Patient Risk Factors, and Impact on Health-Related Quality of Life. *Spine (Phila Pa 1976), 40*(18), 1414-1421. doi:10.1097/BRS.0000000000001020

Steinmetz, M. P., & Benzel, E. C. (2016). *Benzel's Spine Surgery E-Book: Techniques, Complication Avoidance, and Management*: Elsevier Health Sciences.

Stokes, I. A. (1994). Three-Dimensional Terminology of Spinal Deformity. *Spine, 19*(2), 236-248.

Suk, S.-I., Kim, W.-J., Lee, S.-M., Kim, J.-H., & Chung, E.-R. (2001). Thoracic pedicle screw fixation in spinal deformities: are they really safe? *Spine, 26*(18), 2049-2057.

Takahashi, T., Kainth, D., Marette, S., & Polly, D. (2017). Alphabet Soup: Sagittal Balance Correction Osteotomies of the Spine-What Radiologists Should Know. *AJNR Am J Neuroradiol*. doi:10.3174/ajnr.A5444

Tang, J. A., Leasure, J. M., Smith, J. S., Buckley, J. M., Kondrashov, D., & Ames, C. P. (2013). Effect of severity of rod contour on posterior rod failure in the setting of lumbar pedicle subtraction osteotomy (PSO): a biomechanical study. *Neurosurgery, 72*(2), 276-282; discussion 283. doi:10.1227/NEU.0b013e31827ba066

Thomasen, E. (1985). Vertebral osteotomy for correction of kyphosis in ankylosing spondylitis. *Clinical orthopaedics and related research*(194), 142-152.

Vialle, R., Levassor, N., Rillardon, L., Templier, A., Skalli, W., & Guigui, P. (2005). Radiographic analysis of the sagittal alignment and balance of the spine in asymptomatic subjects. *J Bone Joint Surg Am, 87*(2), 260-267. doi:10.2106/JBJS.D.02043

Vosoughi, A. S., Joukar, A., Kiapour, A., Parajuli, D., Agarwal, A. K., Goel, V. K., & Zavatsky, J. (2018). Optimal Satellite Rod Constructs to Mitigate Rod Failure Following Pedicle Subtraction Osteotomy (PSO): A Finite Element Study. *Spine J*. doi:10.1016/j.spinee.2018.11.003

Waldrop, R., Cheng, J., Devin, C., McGirt, M., Fehlings, M., & Berven, S. (2015). The burden of spinal disorders in the elderly. *Neurosurgery, 77*(suppl_1), S46-S50.

Wang, C., Bell, K., McClincy, M., Jacobs, L., Dede, O., Roach, J., & Bosch, P. (2015). Biomechanical comparison of ponte osteotomy and discectomy. *Spine (Phila Pa 1976), 40*(3), E141-145. doi:10.1097/BRS.0000000000000697

Wang, X., Aubin, C. E., Crandall, D., & Labelle, H. (2011). Biomechanical comparison of force levels in spinal instrumentation using monoaxial versus multi degree of freedom postloading pedicle screws 3DX. *Spine (Phila Pa 1976), 36*(2), E95-E104. doi:10.1097/BRS.0b013e3181f07cca

Wang, X., Aubin, C. E., Crandall, D., Parent, S., & Labelle, H. (2012). Biomechanical analysis of 4 types of pedicle screws for scoliotic spine instrumentation 3DX. *Spine (Phila Pa 1976), 37*(14), E823-835. doi:10.1097/BRS.0b013e31824b7154

Wang, X., Boyer, L., Le Naveaux, F., Schwend, R. M., & Aubin, C. E. (2016). How does differential rod contouring contribute to 3-dimensional correction and affect the bone-screw forces in adolescent idiopathic scoliosis instrumentation? *Clin Biomech (Bristol, Avon), 39*, 115-121. doi:10.1016/j.clinbiomech.2016.10.002

Wenger, D. R., Carollo, J. J., Wilkerson, J. J., Wauters, K., & Herring, J. A. (1982). Laboratory testing of segmental spinal instrumentation versus traditional Harrington instrumentation for scoliosis treatment. *Spine, 7*(3), 265-269.

APPENDIX A – BIOMECHANICAL SIMULATOR FOR THE SURGICAL CORRECTION OF SAGITTAL BALANCE IN ADULT SPINAL DEFORMITY

A numerical platform for surgical planning of sagittal balance with osteotomy for ASD was developed integrating the patient-specific multi-body biomechanical model of the spine presented in section 4.1 and was coded under Matlab (R2015b, The MathWorks, Inc., Natick, MA, USA).

The numerical platform was used to define the main steps of the surgical planning, as well as to simulate different configurations of osteotomies and instrumentation to relatively assess and compare different surgical strategies.

Biomechanical surgical planning simulator

Patient specific 3D anatomical landmarks and the geometric model of the vertebrae and pelvis (cf. section 4.3.1) were imported into the simulation platform, allowing a 3D visualization of the spine and pelvis. Sagittal and coronal radiographs are displayed next to the 3D model. The main sagittal plane indices are automatically calculated from 3D anatomical landmarks and are shown on the reconstructed spine and pelvis (Figure A.1).

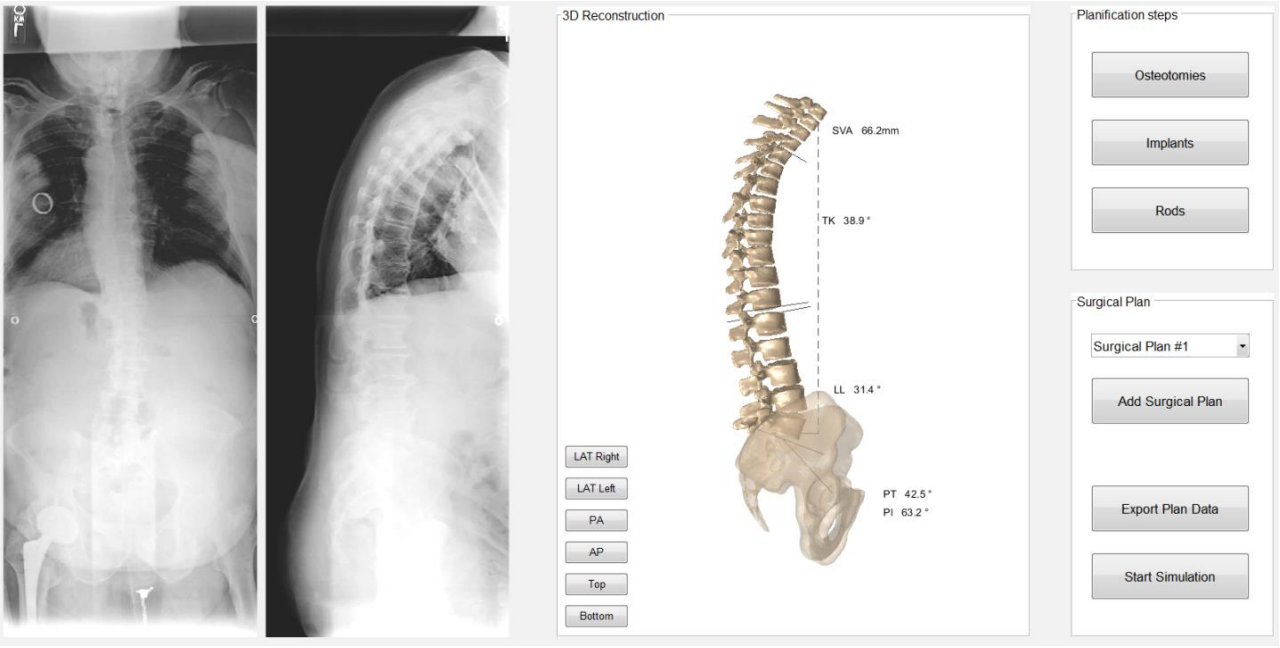

Figure A.1: Main window of the simulation platform

Surgical planning consists of three major steps:

- Planning of spinal osteotomies;
- Defining implants location along the spine;
- Defining rods geometry and properties.

The platform allows to define many surgical scenarios to further analyze the simulated 3D correction of the deformity and forces sustained by the spine and instrumentation.

Spinal osteotomies and pelvic orientation

This step consists of selecting the osteotomy level by clicking on a vertebra directly on the 3D reconstruction of the spine and selecting the type of osteotomy as well as the osteotomy resection angle (Figure A.2).

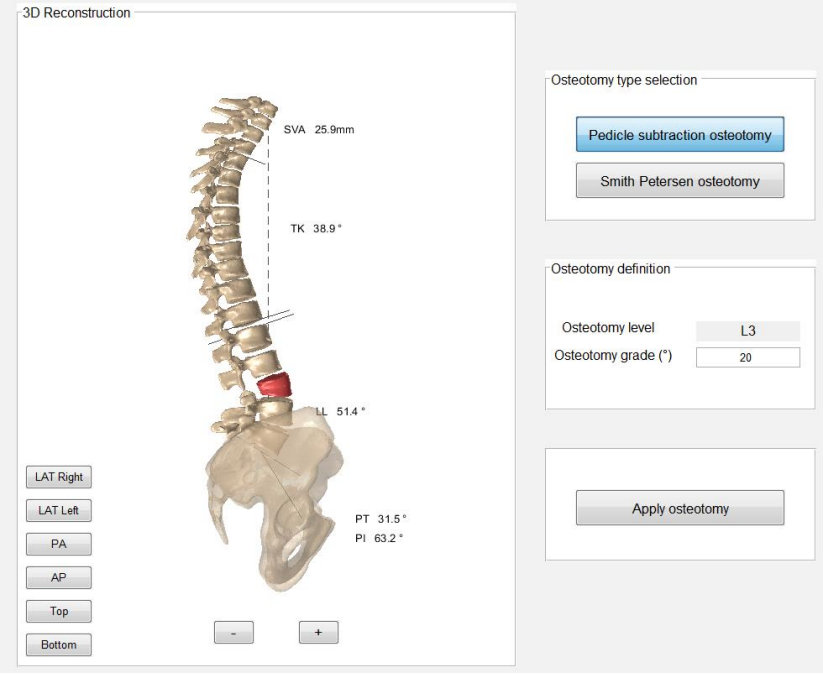

Figure A.2: Osteotomy window of the simulation platform

Resulting geometric changes can be visualized on the 3D model of the spine with sagittal plane indices updated with the new spinal alignment, to help users assess the potential correction. The 3D anatomical landmarks and vertebra geometric models are updated in the biomechanical model.

For the PSO, a local rotation is done at the most anterior part of the vertebral body, at midpoint between the upper and lower vertebral endplates (Figure A.3).

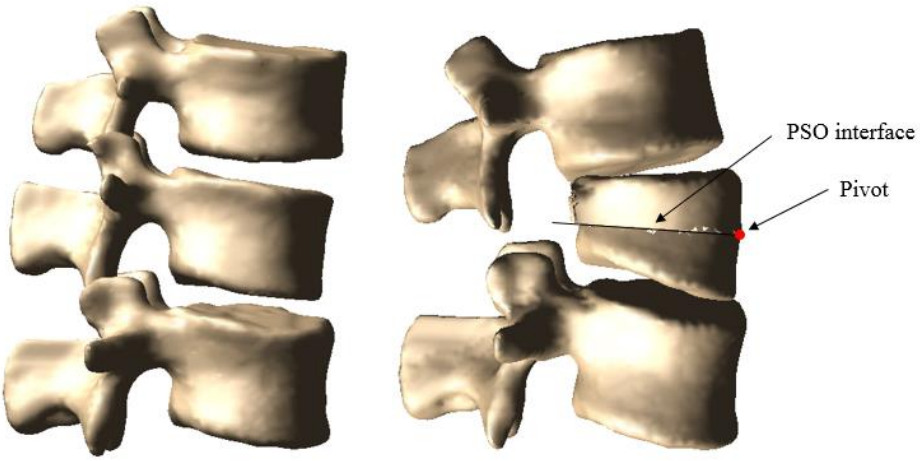

Figure A.3: Geometric model of the vertebra before (left) and after (right) PSO

The user has the possibility to modify the PT to assess its effect on the global sagittal correction after the PSO and instrumentation.

Implants

The second step of surgical planning is the definition of implants. This step allows the user to define the type and side of implants for every vertebral level (Figure A.4). 3D geometric models of different types of implants are imported into the simulation platform. In this study, multi-axial screws were used for all patients but other kinds of implants may be used in future studies. By selecting the multi-axial screw, as well as the vertebral level and side, the 3D geometric model can be recorded so that its position and orientation correspond to the straight forward trajectory. Each implant model is then shown on the 3D reconstruction of the spine to appreciate its position and to further help define the rods geometry in the last surgical planning step.

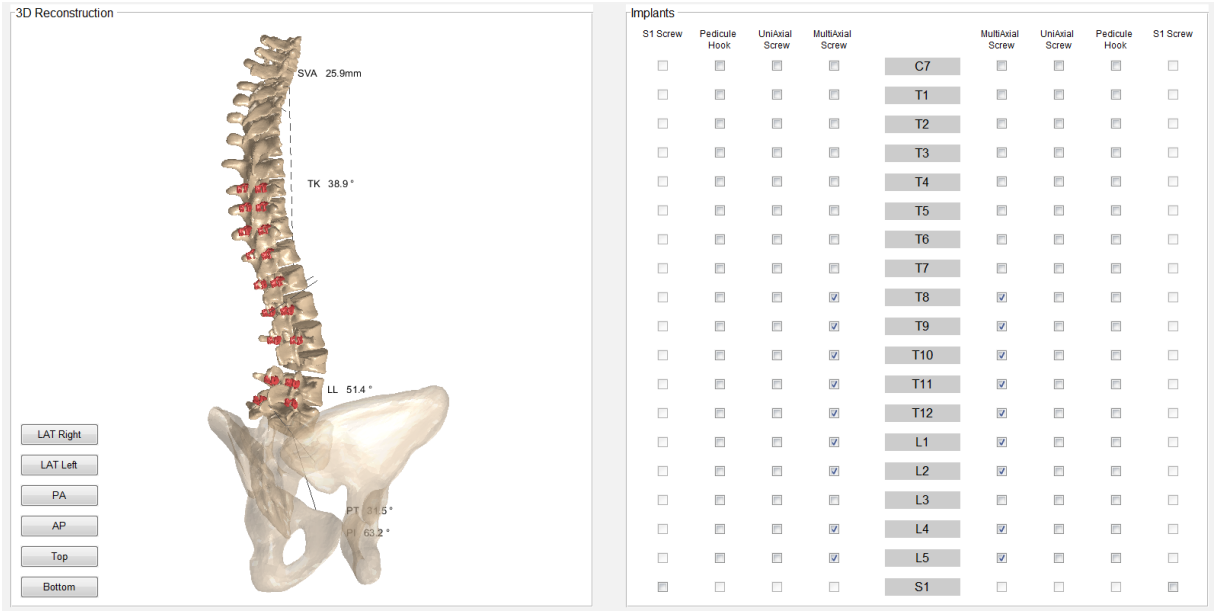

Figure A.4: Implant window of the simulation platform

Rods

The last step consists in defining the geometry, diameter and material of the rods (Figure A.5). The 3D geometry of the rods is modeled by a cubic Bézier curve, with 4 control points represented by red dots. The first and forth control points allow the user to define the position of the proximal and distal ends of the rod, and the two intermediate control points allow to define the initial and ending slope, as well as to contouring of thoracic and lumbar sections of the rods. The user can adjust the position of the control points in the sagittal and coronal planes, using a click and drag method. Rod contouring angles are displayed next to the Bézier curve on the 3D reconstruction. The 3D model can be rotated to help the user defining the instrumentation planning. Different rod materials and diameters can be selected using a drop-down menu. Rods characteristics rigidity are translated in the biomechanical model for the simulation of the surgical instrumentation.

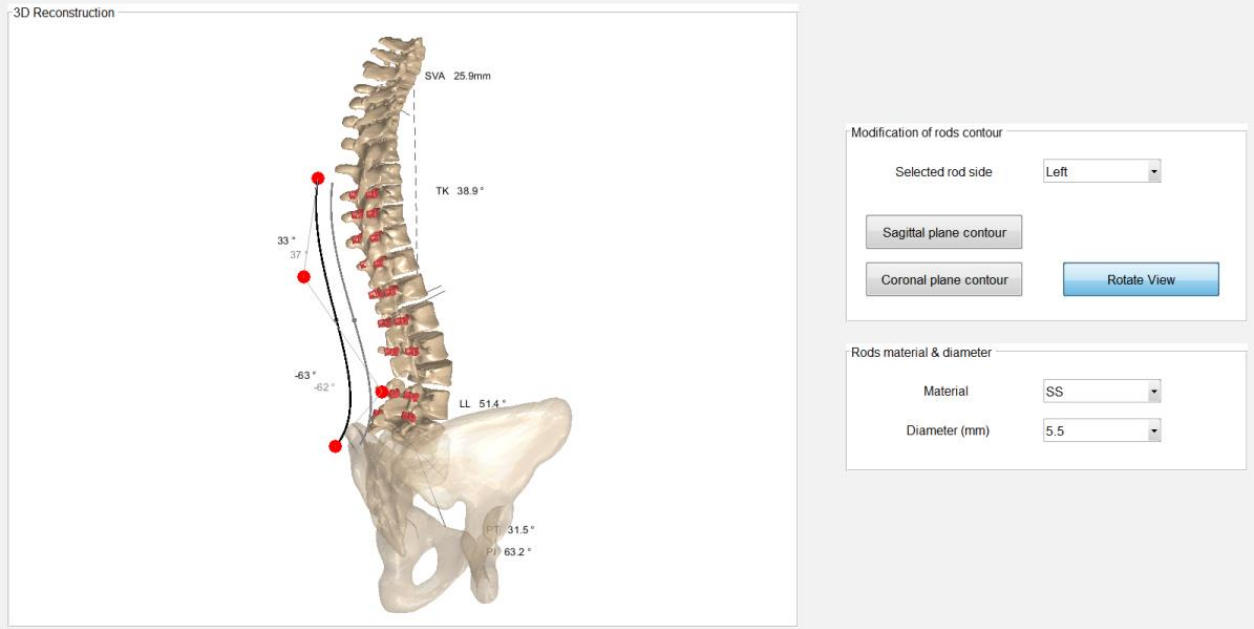

Figure A.5: Rods definition window of the simulation platform

Biomechanical modeling and analysis of the surgical planning

After completion of the preceding surgical planning steps, data related to the osteotomies, implants and rods are formatted and exported in files format readable Adams/View, (Version MD Adams 2017, MSC Software Corporation, Santa Ana, CA, USA) software to generate the personalized multi-body model of the patient and surgical correction simulation, similarly as what presented in section 4.1.

The resulting correction and post-processed spine alignment, deformed rods and loads in the spine and instrumentation are then exported back in the numerical platform and results can be reviewed by the user (Figure A.6). Forces and moments sustained by intervertebral discs, at the vertebra-implant interface and in the rods can be analyzed within the platform. For intervertebral discs, their reference frames are aligned with the upper plate of their respective vertebra, which allows to analyze compression and shear forces. For the screws, reference frames are aligned with their longitudinal axis, which allows to analyze axial forces. For the rods, reference frames are aligned with their respective rod segment, which allows to analyze bending moments.

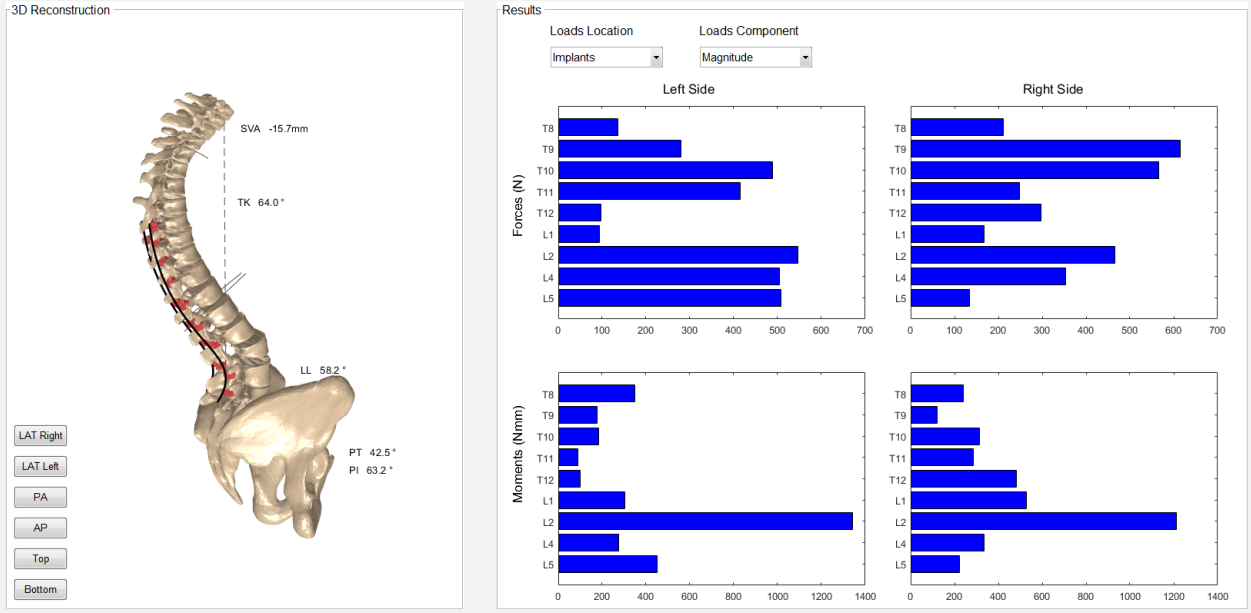

Figure A.6: Window of the analysis of the results of the biomechanical simulation. Axial forces in the screws, bending moments in the rods and vertebral compression loads may be analyzed, amongst other variables.